The Canadian Journal of Chemical Engineering

formerly

CANADIAN JOURNAL OF TECHNOLOGY

CONTENTS

Published by
THE CHEMICAL INSTITUTE OF CANADA
OTTAWA CANADA

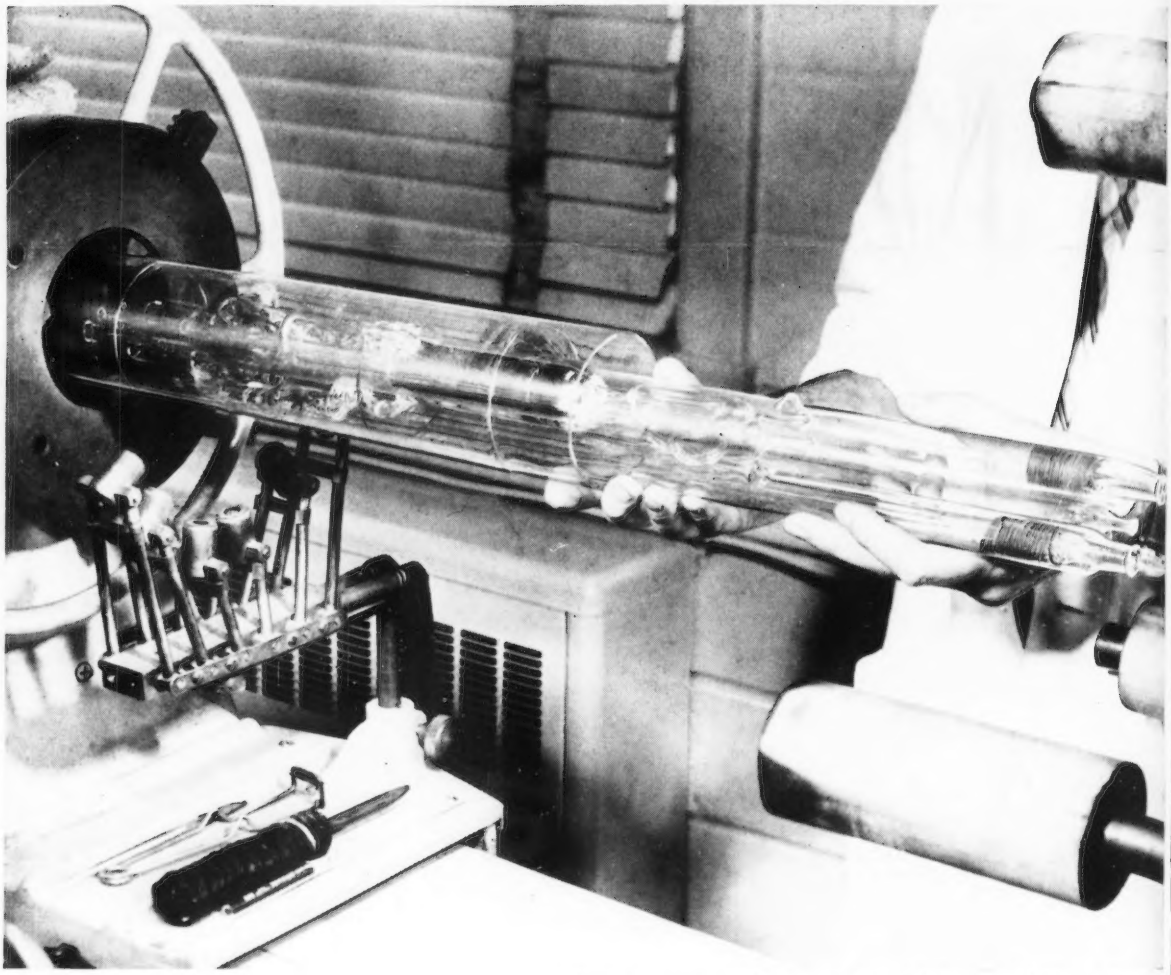

Photograph taken at C-I-L Central Research Laboratory, McMasterville, Que.

POLYMERIC PRECISION

This is an ebulliometer—being assembled by the master glass-blower on his own lathe at our Central Research Laboratory.

The ebulliometer uses two vapor lift pumps such as those found in electric coffee percolators. One circulates a polymer solution while the other circulates boiling solvent—each liquid stream is directed over a temperature detector so sensitive that a difference of one-millionth of 1°C. may be sensed. This device allows the measurement of high molecular weights related to the physical properties of polymers.

Such C-I-L research contributes to higher standards of performance in the plastics industry . . . to new and better plastic products . . . and—through better technical service—to greater success in the application of these new materials to modern living.

C-I-L **CANADIAN INDUSTRIES LIMITED**

Serving Canadians Through Chemistry

Agricultural Chemicals • Ammunition • Coated Fabrics • Industrial Chemicals • Commercial Explosives • Paints • Plastics • Textile Fibres

The Canadian Journal of Chemical Engineering

formerly

Canadian Journal of Technology

Published by The Chemical Institute of Canada

VOLUME 39 | DECEMBER, 1961 | NUMBER 6

Authorized as second class mail, Post Office Department, Ottawa, and for payment of postage in cash. Postage paid at Ottawa. Printed in Canada.

Manuscripts for publication should be submitted to the Editor: Dr. A. Cholette, Faculty of Science, Laval University, Boulevard de l'Entente, Quebec, Que. (Instructions to authors are on the next page).

Editorial, Production and Circulation Offices: 48 Rideau Street, Ottawa 2, Ont.

Advertising Office: C. N. McCuaig, manager of advertising sales, *The Canadian Journal of Chemical Engineering*, Room 601, 217 Bay Street, Toronto, Ont. Telephone—EMpire 3-3871.

Plates and Advertising Copy: Send to *The Canadian Journal of Chemical Engineering*, 48 Rideau Street, Ottawa 2, Ont.

Subscription Rates: In Canada—$6.00 per year and $1.25 per single copy; U.S. and U.K.—$7.00, Foreign—$7.50.

Change of Address: Advise Circulation Department in advance of change of address, providing old as well as new address. Enclose address label if possible.

The Canadian Journal of Chemical Engineering is published by The Chemical Institute of Canada every two months.

The Canadian Journal of Chemical Engineering

INSTRUCTIONS TO AUTHORS

Manuscript Requirements for Articles

1. The manuscript should be in English or French.
2. The original and two copies of the manuscript should be supplied. These are to be on 8½ x 11 inch sheets, typewritten, and double spaced. Each page should be numbered.
3. Symbols should conform to American Standards Association. An abridged set of acceptable symbols is found in the third edition of Perry's Chemical Engineers' Handbook. Greek letters and subscripts and superscripts should be carefully made.
4. Abstracts of not more than 200 words in English indicating the scope of the work and the principal findings should accompany all technical papers.
5. References should be listed in the order in which they occur in the paper, after the text, using the form shown here: "Othmer, D. F., Jacobs, Jr., J. J., and Levy, J. F., Ind. Eng. Chem. **34**, 286 (1942). Abbreviations of journal names should conform to the "List of Periodicals Abstracted by Chemical Abstracts". Abbreviations of the common journals are to be found in Perry's Handbook also. All references should be carefully checked with the original article.
6. Tables should be numbered in Arabic numerals. They should have brief descriptive titles and should be appended to the paper. Column headings should be brief. Tables should contain a minimum of descriptive material.
7. All figures should be numbered from 1 up, in Arabic numerals. Drawings should be carefully made with India ink on white drawing paper or tracing linen. All lines should be of sufficient thickness to reproduce well, especially if the figure is to be reduced. Letters and numerals should be carefully and neatly made, with a stencil. Generally speaking, originals should not be more than twice the size of the desired reproduction; final engravings being 3¼ in. or 7 in. wide depending on whether one column or two is used. For further details ask the Editor for the Guide for Drawings.
8. Photographs should be made on glossy paper with strong contrasts. Photographs or groups of photographs should not be larger than three times the size of the desired reproduction.
9. All tables and figures should be referred to in the text.

Submission of Manuscripts

1. The three copies of the manuscript, including figures and tables, should be sent directly to:
   DR. A. CHOLETTE, editor,
   The Canadian Journal of Chemical Engineering,
   Faculty of Science, Laval University,
   Boulevard de l'Entente,
   Quebec, Que.
2. The authors addresses and titles should be submitted with the manuscript.
3. The author may suggest names of reviewers for his article, but the selection of the reviewers will be the responsibility of the editor. Each paper or article is to be reviewed by two chemical engineers familiar with the topic. Reviewers will remain anonymous.
4. All correspondence regarding reviews should be directed to the editor.

Reprints

1. At least 50 free "tear sheets" of each paper will be supplied.
2. Additional reprints may be purchased at cost. An estimated cost of reprints, with an attached order form, will be sent to the author with the galley proofs.
3. Orders for reprints must be made before the paper has appeared in the Journal.

Communications, Letters and Notes to the Editor

Short papers, as described below, will be considered for publication in this Journal. Their total length should be such that they will not occupy more than one page of the Journal.

Communications

A communication is a prompt preliminary report of observations made which are judged to be sufficiently important to warrant expedited publication. It usually calls for a more expanded paper in which the original matter is republished with more details.

Letters

A letter consists of comments or remarks submitted by readers or authors in connection with previously published material. It may deal with various forms of discussion arising out of a publication or it may simply report and correct inadvertent errors.

Notes

A note is a short paper which describes a piece of work not sufficiently important or complete to make it worth a full article. It may refer to a study or piece of research which, while it is not finished and may not be finished, offers interesting aspects or facts. As in the case of an article a note is a final publication.

* * *

Treatment of Uranium Leach Plant Solutions by Liquid-Liquid Extraction to Produce High Purity Uranium Products[1]

R. SIMARD[2], *A. J. GILMORE*[2], *V. M. McNAMARA*[2], *H. W. PARSONS*[2] *and H. W. SMITH*[2]

Three liquid-liquid extraction processes were tested in continuous equipment, on bench scale, to determine their relative merits in the purification of uranium as found in ion exchange eluates of various Canadian leach plants. Tri-n-butyl phosphate and dibutyl butylphosphonate were used as extractants on nitrate eluates. A tertiary amine was used in the case of sulphuric acid eluates. Optimum conditions for high recovery and low reagent costs were established, and the adaptability of the processes to existing leach plants is discussed. The suitability of the ammonium diuranate product as a source of ceramic-grade UO_2 was also investigated. Suggested changes to the adopted flowsheets are given, for further testing on a pilot plant scale.

Status of Canadian Uranium Industry

The uranium industry is now well established in Canada and the processes used in the production of leach plant concentrates and reactor-grade oxide or metal are well known to the metallurgist. This paper will refer at times to details of the production flowsheets, and it will be useful at this time to define where the present work fits in the uranium picture.

All Canadian uranium leach plants, with the exception of the Eldorado plant at Beaverlodge, Saskatchewan, use sulphuric acid leaching followed by ion exchange. (The Eldorado plant has adopted the sodium carbonate leach process). A typical sulphuric acid leach plant flowsheet showing the important steps of the process is shown in Figure 1; since the main topics of this paper are associated with the last three operations, a few comments on these may be of interest.

Recovery and concentration of uranium from acid sulphate solutions by stationary or moving-bed anion exchange resins is both efficient as a process and cheap in terms of the overall cost. Resin life is measured in years, while basic chemicals used account for only 10 to 15 cents in the cost per pound of uranium recovered. The concentration ratio may be as high as 20 to 1 when nitrate elution and moving-bed columns are used.(1) Precipitation in most plants is in two stages. In the first stage, lime added to pH 3.0 to 3.5 precipitates most of the iron and sulphate, and, in the second stage, magnesia, caustic soda, or ammonia recovers a diuranate relatively free of iron, thorium, phosphates and halides. This second product is dried and then shipped in drums to a customs refinery or exported to other countries — mainly to the U.S.A. and Britain, and, in minor quantities, to Germany and Japan.

In the refinery,(2) as shown in Figure 2, the precipitate is dissolved in nitric acid and the uranyl nitrate is extracted with 25% tri-n-butyl phosphate (TBP) in kerosene; the extract is scrubbed and finally stripped with water. This water strip, at this point, is either evaporated to recover uranium trioxide or neutralized to precipitate ammonium diuranate (ADU). Depending on the demand for uranium hexafluoride as a feed to the isotope separation plant or for natural uranium metal, the trioxide is processed accordingly. Recent developments(3) in the use of sintered uranium dioxide as a reactor fuel have emphasized the ammonium diuranate route.

An alternate route for the production of the hexafluoride from leach plant concentrate has been developed in the U.S.A. whereby direct hydrofluorination of the concentrate, followed by fluorination and distillation, can produce a suitable feed to the isotope plant.

Short-cuts to Refined Uranium

Looking back at the leach plant, where operating costs are constantly being reduced by improved maintenance, by refine-

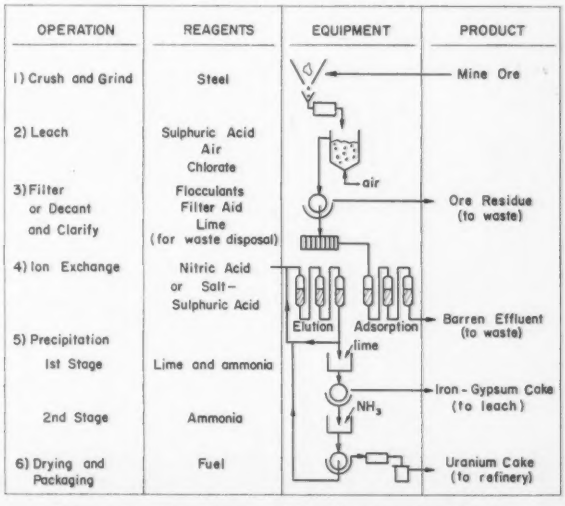

Figure 1—Uranium acid leach plant flowsheet.

[1]*Manuscript received March 27; accepted July 28; 1961.*
[2]*Extraction Metallurgy Division, Mines Branch, Department of Mines and Technical Surveys, Ottawa, Ont.*
Based on a paper presented to the Joint C.I.C.-A.I.Ch.E. Chemical Engineering Conference, Cleveland, Ohio, May 7-10, 1961.

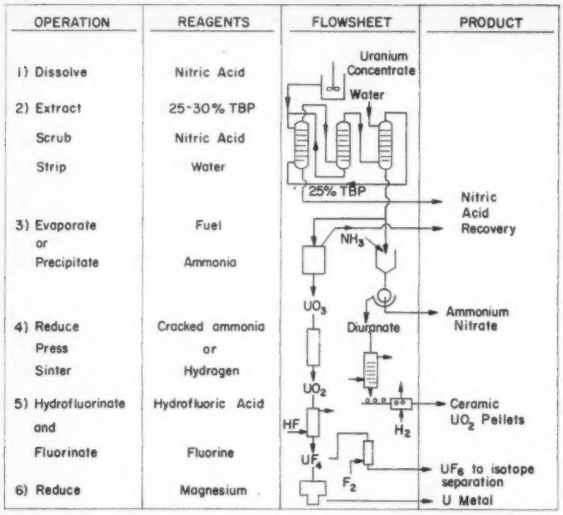

Figure 2—Uranium refining and fabrication flowsheet.

ment in control, or by recycling some waste products, it is apparent that a simplification can also be achieved by by-passing the precipitation, drying and packaging steps and refining the uranium directly from ion exchange eluates. The merging of plant and refinery to produce "reactor grade" ammonium diuranate was the object of some laboratory and pilot plant studies at the Mines Branch. The feasibility, cost and adaptability of three liquid-liquid extraction processes, as applied to ion exchange eluates, were the main concern in these investigations.

Adaptation of Liquid-Liquid Extraction

Liquid-liquid extraction of uranium from acid solutions has been developed and applied in many countries in the last ten years, to a point where it would be difficult to review in detail. In the United States, the research groups that have pioneered this research, under USAEC contracts, include the Dow Chemical Co. in California, the Union Carbide Nuclear Company at Oak Ridge, Tennessee, and the E. I. du Pont de Nemours and Company at the Savannah River Laboratory, S.C.

The tri-n-butyl phosphate (TBP) refining process was one of the first to achieve success in this field and has now attained a high degree of efficiency. Data are available from operating refineries to predict that the process could possibly be applied to the direct treatment of nitrate eluates from ion exchange circuits as shown in Figure 3. The mechanism of extraction is favored by high nitric acid concentration (3 normal) and depressed by the presence of the sulphate ion. Since eluates as produced in leach plants contain essentially 0.3 to 0.4 HNO_3

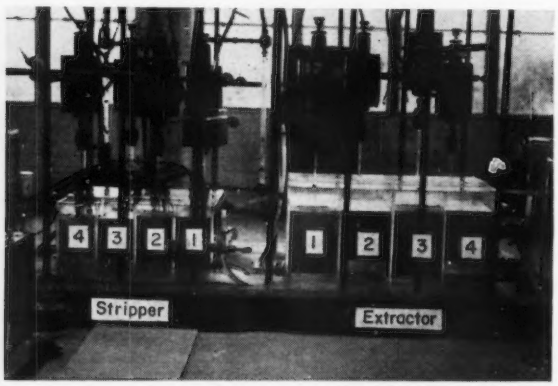

Figure 4—Four stage mixer-settlers.

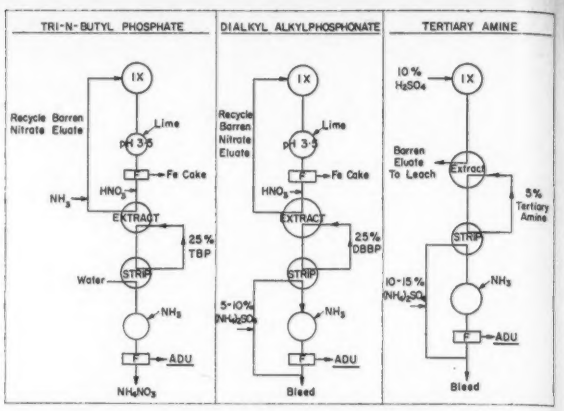

Figure 3 — Proposed flowsheets for refining of uranium from ion exchange eluates by liquid-liquid extraction.

and 0.3 to 0.6 N SO_4, these concentrations would not be as favourable to equilibrium as those obtained from the dissolution of uranium concentrates in nitric acid. These factors and their effect on possible uranium loading in a countercurrent circuit would require further study. The ultimate effect on the purity of the product could best be determined by continuous testing in liquid-liquid extraction apparatus.

A second possibility can also be considered where TBP is replaced by a dialkyl alkylphosphonate[4] with a more favorable extraction coefficient. Some kerosene-soluble phosphonates are commercially available at this time and the more suitable compounds could be chosen on the basis of low water-solubility, high capacity and lower cost. Available data on their behavior were limited and little or no work had been reported to predict whether water or other solutions could be used for stripping in a practical countercurrent system.

A third possibility appeared in the adoption of sulphuric acid elution[5] of uranium from anion exchange resins in place of nitrate or chloride solutions. This would allow the use of liquid anion exchangers, such as the tertiary amines, for re-extraction. These highly selective extractants[6] of the uranyl sulphate anion complex are now used in many leach plants in place of resins.[7]

Ammonium diuranate (ADU) has been shown to be one of the more suitable forms of uranium for the fabrication of high-density dioxide pellets. The present investigation was therefore concerned with the suitability of the ADU which would be produced from the proposed flowsheets of Figure 3, in a continuous bench-scale circuit.

EQUIPMENT

Since 1948 the Mines Branch has been active in the development of leaching, ion exchange and liquid-liquid extraction as applied to Canadian uranium and thorium ores. The research facilities include a small pilot plant section where a liquid-liquid extraction and stripping unit was used in this study. This unit will be described briefly in the following paragraphs.

Two four-stage countercurrent mixer-settlers, as shown in Figure 4, were constructed from ¼-in. Plexiglas. The extractor section is a rectangular tank 16-in. × 12-in. high. Each stage is composed of a mixing chamber (3-in. × 4-in.) in which the aqueous phase is introduced from the previous stage through a bottom weir and a ⅝-in. draught pipe extending from a false-bottom plate set at one inch from the bottom. The organic phase enters over a weir from the opposite side. Mixing is done with a three-blade, 2-in. diameter marine impeller with upward thrust, driven by a variable speed motor. The impeller acts as a pump for the aqueous phase which must move against a ⅛-in. level differential from stage to stage. The organic phase flows by gravity from weir to weir, each weir being ⅛-in. lower than the preceding one. This arrangement dispenses with the use of interstage pumps or airlifts. The mixer compartment connects

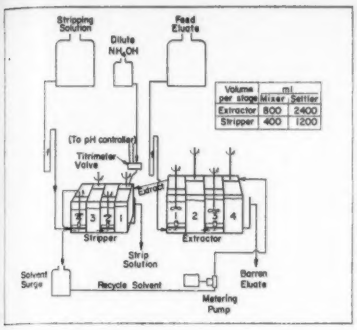

Figure 5 — Bench-scale mixer-settler circuit.

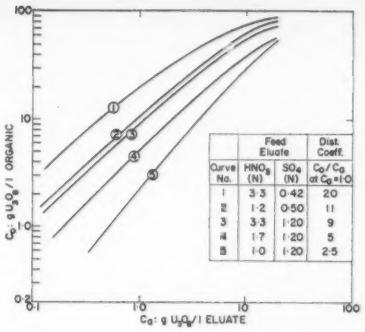

Figure 6—Uranium extraction equilibria 25% *TBP* vs nitrate eluates.

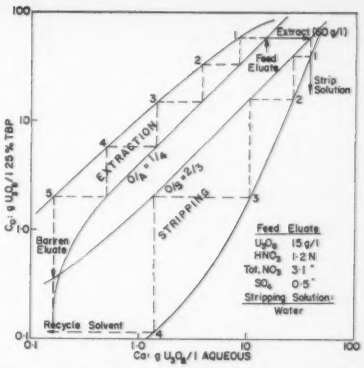

Figure 7—25% *TBP*-uranium extraction and stripping in mixer-settler circuit.

with the settler through a vertical slot (4-in. × 3/8-in.) and around an L-shaped baffle. This allows internal recycling of the organic phase so that the mixing ratio may be kept at a much higher value (O/A = 2/1) than the actual flow ratio. The O/A flow ratio is set by the requirements of the system, which must achieve high recoveries at or near saturation of the organic phase. The extract from this section overflows directly to a stripper of the same design but reduced to half the mixing volume and half the settling area; the overall dimensions in this case are 13-in. × 9-in. × 6-in. high.

Accessories to these two units include a solvent metering pump (rated at 25 to 700 ml./min.) to recycle the solvent, and flowmeters to control the eluate and strip solution flowrates. For pH control of the strip solution, an automatic pH recorder-controller and a titrimeter valve were used on the first stage mixer compartment, while the second, third and fourth stages were controlled manually.

For precipitation of ammonium diuranate from the strip solution, a continuous circuit was assembled from a two-litre mixing tank equipped with heating mantle, mechanical stirrer and pH electrodes. Metered streams of solution and ammonia gas were fed near the bottom of this tank, while the slurry overflowed to a surge tank and hence to a vacuum stationary filter.

Procedure

Source of Materials

Drum quantities of ion exchange nitrate eluates were obtained on request from two leach plants in Elliot Lake, Ontario. The solvents were prepared from commercially available tri-n-butyl phosphate (TBP), dibutyl butylphosphonate (DBBP) and di-2 ethylhexyl 2-ethylhexyl phosphonate (DEEP), all of which were supplied by the Electric Reduction Co. of Canada Limited, Toronto, Ontario.

For the study of the sulphuric acid elution-amine extraction process, the eluate was produced at the Mines Branch during a pilot plant leaching operation. Sufficient leach filtrate was obtained to carry out 20 cycles of adsorption and elution on two four-inch diameter ion exchange resin columns. The sulphuric acid eluate collected from this investigation was used as feed to the liquid-liquid extraction circuit. The solvent chosen for this work was a tri-capryl amine (TCA) supplied by General Mills, Inc., Kankakee, Illinois, under the trade name Alamine 336. This amine is produced commercially and has had wide acceptance in acid leach plants — for example, at the Eldorado Port Radium leach plant from 1958 to 1960. Previous studies by the authors on sodium hydroxide-sodium sulphate stripping of amine extracts[8] had indicated certain advantages over the chloride, nitrate or carbonate stripping procedures. For this reason it was felt that, for the production of ADU, an ammonium hydroxide ammonium sulphate strip should be investigated in the present circuit.

The kerosene diluent used in all three flowsheets was obtained from the Shell Oil Co. of Canada Limited, and is the same refined, high-flash-point (140°F.) diluent as used in the Eldorado refinery at Port Hope, Ontario.

Operating Conditions

The circuit, as shown in Figure 5, was operated for periods of six to seven solvent replacement (20 litres), samples were taken of the equilibrated aqueous phase at each stage of extraction and stripping, together with samples of the solvent extract and recycle. A composite barren eluate from each run was also used to determine soluble and entrained solvent losses. For the amine studies, an amine determination of the solvent was also done by a standard acid-base titration.

Dilution of the TBP and dialkyl phosphonates to 25% v/v in kerosene was chosen on the basis of calculations which had shown that in order to obtain high recoveries (99+%) in a practical number of stages, say four or five, such a concentration would be necessary. The amine was diluted to 5% v/v and this dilution was dictated by the problem of phase separation and stripping at higher amine concentration. The diluted amine was modified with n-decyl alcohol (3% v/v) to further improve phase separation and prevent third phase formation.

RESULTS AND OBSERVATIONS

Equilibria and Stage Calculations

Tri-n-butyl Phosphate

A series of seven continuous runs was completed at various nitrate and sulphate levels on one feed eluate. Equilibria as obtained from the mixer-settlers are presented graphically in Figure 6, which emphasizes the counteracting effects of the two variables on the distribution coefficient (Co/Ca). At 3.3 N HNO_3 the coefficient was depressed from 20 to 9 by an increase of the sulphate from 0.42 to 1.2 N. By controlling the sulphate at 0.5 N in the lime precipitation step, a coefficient of 11 was obtained with a feed eluate at 1.2 N HNO_3.

The data of curve 2 from Figure 6 were transferred to Figure 7 for a graphical calculation of the number of stages required to lower the uranium content to an acceptable value for recycling ion exchange barren eluates. A value of 0.1 g U_3O_8/1 is the maximum allowable for efficient elution. It will be seen that a minimum of five stages are needed with a feed eluate analyzing 15 g U_3O_8/1. The O/A flow ratio of 1/4 was chosen to limit the number of stages to a practical value. In order to approach saturation of the solvent (80 g U_3O_8/1), a much larger number of stages would be needed.

Stripping is much less of a problem. A high uranium concentration in the strip would be preferred were the solution to be evaporated. In this study, since uranium was to be recovered by ammonia precipitation and the concentration was not of first importance, the O/S flow ratio was set higher at 2/3 to reduce the number of stages needed for near complete stripping.

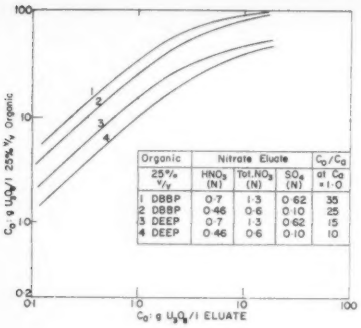

Figure 8—Batch extraction equilibria 25% *v/v* dialkyl alkylphosphonates vs nitrate eluates.

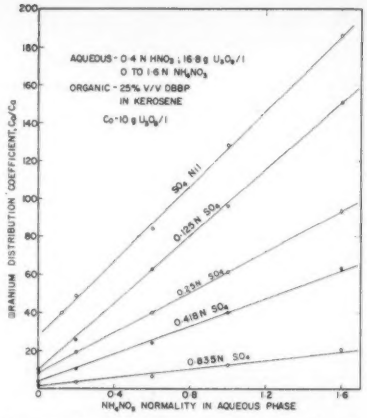

Figure 9 — Effect of nitrate and sulphate on uranium distribution coefficient using 25% *v/v DBBP*.

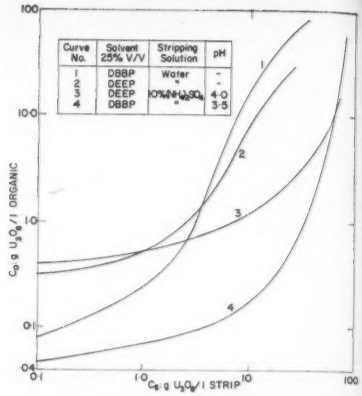

Figure 10—Batch stripping equilibria 25% dialkyl alkylphosphonates.

Dialkyl Alkylphosphonates

Because of the limited data on uranium extraction at low nitric acid concentration, the work was directed first to some equilibration tests in separatory funnels. 25% v/v solutions o DBBP and DEEP in kerosene, conditioned with nitric acid solution at the same normality as the eluate, were then equilibrated with leach plant eluates at two nitrate and two sulphate levels. The results shown in Figure 8 indicate that for equal concentrations by volume, DBBP is more effective. Saturation capacity is almost double, while the extraction coefficient (Co/Ca) at low concentration is 2½ times higher. It must be noted, of course, that the molar concentration of each solvent is 1 M and 0.6 M for DBBP and DEEP respectively. Later equilibration tests with synthetic eluates and 25% DBBP emphasized the effect of the total nitrate and sulphate ion concentrations at a constant acidity of 0.4 N HNO_3. The data are presented in Figure 9, which can be used as a guide in the choice of nitrate and sulphate levels to be used in practice.

The batch stripping equilibria of Figure 10 were obtained with water alone and with ammonium sulphate as a complexing agent. Whereas water was a relatively poor stripping agent, a 10% w/v solution of ammonium sulphate adjusted to pH 3.5 to 4.0 gave stripping coefficients (Cs/Co) ranging from 10 to 100 for DBBP and 1 to 10 for DEEP.

On the basis of the above results and its higher rate of phase separation, the 25% DBBP solvent was chosen for continuous testing in the countercurrent mixer-settler circuit.

A series of nine runs on three sources of eluate was completed with 25% DBBP. Results of a typical run are presented graphically on the McCabe-Thiele diagram of Figure 11. In contrast with the TBP uranyl nitrate system, efficient recovery was obtained in four stages at a nitric acid level of 0.4 N HNO_3. Extract loadings ranged from 85 to 95 g U_3O_8/1. On stripping with 8% w/v ammonium sulphate with the pH of the first stage at 3.5, a recycle solvent containing 0.2 to 0.3 g U_3O_8/1 was obtained in four stages. The second, third and fourth stages did not require pH control; when the stripping feed solution was adjusted at pH 6.5, the pH of these stages was slightly below the point of uranium precipitation. The presence of 0.35 N ammonium nitrate in the aqueous phase resulted from the recycling of 50% of the barren strip, which had been done in order to reduce the ammonium sulphate consumption. The nitrate ion depresses the stripping coefficient, and results showed that equivalent stripping was obtained with 5% ammonium sulphate at zero nitrate.

Tri-capryl Amine

The feed eluate was produced from the elution of the pilot plant ion exchange columns, with 10% H_2SO_4. The maximum uranium concentration obtainable was 8 g U_3O_8/1 in 0.9 N sulphuric acid. This solution was fed continuously to the extraction circuit in a series of fifteen runs. Extraction and stripping equilibria of a typical run are shown in Figure 12.

In this system, in contrast with the preceding two, uranium concentration in both phases is much lower as dictated by elution results and by extraction equilibria. From the data of Figure 12 it can be seen that if the barren eluate is to be recycled to leaching, three extraction stages will be sufficient. In the stripping section, where a pinch is noticeable in the stage diagram, the uranium recycled to the extraction circuit will be a minimum of 0.1 g U_3O_8/1 of recycle solvent; this is tolerable in view of the relatively high distribution coefficient in the third or fourth stage of extraction. Also emphasized in Figure 12 is the need for close pH control at each stage of stripping. A pH slightly below the point of uranium precipitation was maintained in order to take advantage of the improved stripping coefficient at the higher pH.

Precipitation

The strip solutions collected from the liquid-liquid extraction circuit were used to produce ammonium diuranate (ADU). Batch and continuous precipitation tests with gaseous ammonia were done to study the effects of pH, temperature, and ammonia gas dilution on filtering, washing, and subsequent reduction and sintering to UO_2.

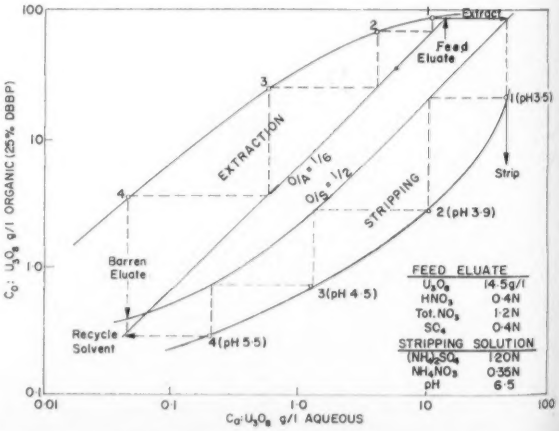

Figure 11—25% *DBBP*-uranium extraction and stripping equilibria in mixer-settler circuit.

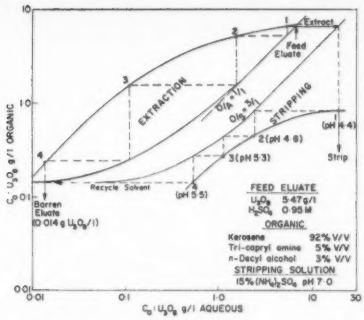

Figure 12—5% tri-capryl amine-uranium extraction and stripping operating equilibria in mixer-settler circuit.

With the TBP strip solution, where the sulphate ion is absent, optimum conditions for good filterability and high final density of the UO_2 pellets were defined as follows:

pH of precipitation	7.0-7.5
Temperature	40-60°C.
Retention time	20-30 min.
Gas dilution	None
Drying temperature	110°C.

Under these conditions sound UO_2 pellets with densities of 10.5 to 10.7 were produced.

Batch precipitation of phosphonate and amine strip solutions with high sulphate content produced a coarse ADU containing 10 to 15% SO_4. This had been experienced in leach plants where ammonia is used to precipitate uranium from the eluates. With continuous precipitation at a pH of 7.0 to 7.5, this was avoided. On the other hand, the product was very fine and difficult to filter and wash. This difficulty was minimized by higher temperature and by the dilution of the ammonia with nitrogen. The optimum conditions were defined as follows:

pH	7.0-7.5
Temperature	60°C. or above
Retention time	10-20 min.
$\%NH_3$ in N_2	25 to 35%

Uranium dioxide pellets, having reproducible densities of 10.6 to 10.7, were obtained from this ADU.

Analyses of ADU Products

Chemical and spectrographic analyses of the ADU products are shown in Table 1. For comparison, the analyses of a typical leach plant ion exchange product and the specifications of the ADU product from the TBP refinery are included. In terms of "nuclear grade" purity, the leach plant IX product is relatively high in iron, thorium, calcium, boron, molybdenum, and rare earths. Of these, iron and calcium are easily removed by any one of the three processes. Thorium is effectively reduced to specification level, except in the case of TBP, in which a low degree of saturation in the extract will allow extraction of some thorium with the uranium. In the amine process which is an anion exchange reaction, thorium is essentially rejected, but molybdenum, even in small concentrations, is extracted. Boron, a high neutron absorber, is reduced below specification. Lanthanide rare earths were also reduced below specification with DBBP; results are lacking for TBP and TCA.

At this point it must be stressed that the significance of these analyses in terms of "nuclear grade" purity can only be determined by carrying out neutron absorption tests and in-reactor evaluations on the sintered dioxide pellets.

Solvent Losses

Entrained and soluble solvent losses in the barren eluate were low per pound of recovered uranium and will represent a negligible item in the overall reagent cost. With DBBP the

TABLE 1

CHEMICAL AND SPECTROGRAPHIC ANALYSES OF ADU PRODUCTS

	Source				
	Leach Plant IX	TBP from IX	DBBP from IX	TCA from IX	Refinery Specifications (max.)
Chemical					
U_3O_8, %	80.0	88.0	85.5	88.4	86
NH_3 ,,	3.0	1.8	2.8	2.2	–
NO_3 ,,	–	0.2	–	–	–
SO_4 ,,	1.5	–	1.8	2.1	–
PO_4 ,,	0.2	–	–	–	–
Ca ,,	0.5	–	–	–	–
Fe ,,	0.5	–	–	–	–
Th, p.p.m.	500	100	27	16	50
Mo ,,	100	–	5	30	1
B ,,	–	–	<0.1	<0.1	0.2
$[RE]_2O_3$,,	400	–	<5	34	–
Spectrographic					
Ag, p.p.m.	–	–	<0.1	–	1.0
B ,,	5–10	0.1	<0.1	<0.1	0.2
Cd ,,	<1	<1	<0.1	<5	0.2
Co ,,	<10	<10	<10	<10	–
Cr ,,	–	<5	–	<5	10
Cu ,,	<10	–	7	20	10
Fe ,,	1750	30	<17	75	35
Mn ,,	<10	<10	<1	<10	5
Mo ,,	20–100	<10	6	200	1
Ni ,,	<20	<2	<2	<2	15
P ,,	<300	–	10	–	50
Si ,,	150	–	15	–	–
Y ,,	<50	<10	<10	–	–
Dy ,,	220	–	0.06	–	0.1
Gd ,,	10	–	0.06	–	0.05

TABLE 2

COMPARISON OF REAGENT COSTS FOR REFINING URANIUM FROM ION EXCHANGE ELUATES

Process	Reagent			Cost, $/lb. U_3O_8
	Type	Price ($/lb.)	Consumption (lb./lb. U_3O_8)	
TBP	HNO_3	0.07	2.5	0.175
	NH_3	0.045	0.7	0.031
	Total			0.206
DBBP	HNO_3	0.07	0.04	0.003
	NH_3	0.045	0.01	0.0004
	$(NH_4)_2SO_4$	0.020	1.2	0.024
	Total			0.0274
TCA	H_2SO_4	0.012	2.0	+0.024
	Lime	0.01	−1.5	−0.015
	HNO_3	0.07	−1.7	−0.119
	Total		(savings)	−0.110

loss was 0.006 lb./lb. U_3O_8, while with TCA it was too low to determine within the 100 solvent cycles completed in the circuit. Loss of TBP was not determined.

Reagent Consumption and Costs

A list of the reagent consumptions and costs in producing a refined ADU by the three processes is presented in Table 2. These are over and above the cost of producing the current leach plant ADU ("yellow cake") by the two-stage precipitation of nitrate eluates. In the case of TBP, the eluate after lime neutralization is reacidified to 1.0 N HNO_3 and the barren eluate is neutralized again with ammonia to 0.4 N HNO_3 before recycling to elution. For DBBP, the only reagents involved will be the ammonium sulphate for stripping, plus the small amount of nitric acid extracted which must be neutralized with ammonia during stripping. In the TCA process the sulphuric acid is recycled to leaching except for the amount adsorbed on the resin and in the extract; this acid replaces the total nitric acid and lime consumed by the present nitrate elution process and is shown as a negative cost, i.e., savings.

DISCUSSION

On the basis of purity of product, the dibutyl butylphosphonate (DBBP) process will be preferred. It is also more readily adaptable to acid leach plant flowsheets, in which either all of the eluate or only a portion can be treated without disrupting current procedure. If acidified sodium chloride elution is in use, a change can be readily made to nitrate elution without any change in the equipment.

The tri-capryl amine (TCA) process does have some good points. First, the need for recycling the "royal barren" or uranium bleed in the first fractions of the barren effluent will be eliminated when sulphuric acid elution is used. Secondly, the elution is done in an open circuit, which eliminates possible build-up of impurities. Thirdly, where nitrate elution presents a problem of waste disposal because of the very low permissible nitrate level in natural streams, the sulphuric acid elution would be an easy solution. Lastly, there is a saving in reagent costs but at the expense of a longer elution cycle. As noted previously, molybdenum in the final product could be a major problem with certain ores. In such a case, an ammonium chloride strip in place of the proposed sulphate strip would be more selective for uranium, as suggested by the literature;[9] this would have to be confirmed for individual cases.

The tri-n-butyl phosphate (TBP) process presents a major increase in cost and would not be competitive with current refinery costs. The purity of the product would be improved by phosphate complexing of the thorium.

CONCLUSION

Three proposed flowsheets for refining uranium from ion exchange eluates have been studied sufficiently in continuous bench scale equipment to assess their feasibility. As shown in Table 2, the dibutyl butylphosphonate extraction process will produce a nuclear grade ammonium diuranate at an additional reagent cost of three cents per pound of uranium. The amine process affords a saving of eleven cents in reagents but may not be as readily adaptable; it will require further testing to assure its success in individual cases. The TBP process applied to nitrate eluates is not competitive with the same process applied to the chemical precipitate. The work has therefore established that a nuclear grade uranium product can be produced in the uranium leach plant at a relatively low cost and with little change in the existing flowsheet.

References

(1) Maltby, P. D. R., Trans. I.M.M., **69,** 95-109 (1959).

(2) Burger, J. C., and Jardine, J. McN. Canadian Refinery Practice in the Production of Uranium Trioxide by Solvent Extraction with Tributyl Phosphate. Paper 228, Second UN International Conference on the Peaceful Uses of Atomic Energy, Geneva, Switzerland, Volume 4, pp. 319 (1958).

(3) Anon. An Outline of the Activities of Atomic Energy of Canada Limited and Some of the ABC's of Nuclear Power. A.E.C.L. Publication 962, Chalk River, Ontario (1959).

(4) Siddall, T. H. Ind. Eng. Chem., **51,** 41-44 (1959).

(5) Petrov, H. G. Solvent Extraction of Uranium from Sulphuric Acid Eluates. Topical Report WIN-28, National Lead Co., Winchester, Mass. March (1956).

(6) Brown, K. B., Coleman, C. F., Crouse, D. J., Blake, C. A., and Ryon, A. D. Solvent Extraction Processing of Uranium and Thorium Ores, Paper 509, Second UN International Conference on the Peaceful Uses of Atomic Energy, Geneva, Switzerland. Volume 3, pp. 472-487 (1958).

(7) Bellingham, A. I. The Application of Solvent Extraction to the Recovery of Uranium from El Sherana Ore. Paper 1, Symposium on Hydrometallurgy, A.I.M.M., Adelaide, Australia. February (1960).

(8) Bellingham, A. I., and Simard, R. Can. J. of Chem. Engr., **37,** 113-116 (1959).

(9) Crouse, D. J. Controlled pH Stripping of Uranium from Amines. Report No. ORNL 2941, Oak Ridge National Laboratory, Oak Ridge, Tennessee. June (1960).

* * *

Photography in Bubble and Drop Research[1]

R. C. KINTNER[2], T. J. HORTON[3], R. E. GRAUMANN[4] and S. AMBERKAR[5]

Methods of photographing bubbles and drops moving in a liquid field are described. Shape, size, terminal velocity, local semi-vectorial velocities, size distribution and high speed phenomena such as coalescence and breakup can be advantageously investigated by photographic methods. Recommended combinations of lights, reflectors, diffusers, screens, films, and *f*-stop values are given. Applications of particle trace and interrupted particle trace photography are described.

Both still and motion picture photography have been extremely useful in capturing bubble and drop phenomena in a form of record which often reduces the personal factor inherent in observations. Such photographic records must be interpreted with considerable reservation. For example, a large air bubble rising in a cylindrical tube may appear to exhibit a ledge along the periphery of its spherical cap shape[1,2]. A still photograph made with a high speed electronic flash will show no such ledge but a disturbed, wavy periphery. Only when a high speed motion picture camera is used and the results viewed in slow motion on a screen can the situation be resolved. The edge of the bubble is a fluttering, wavy ribbon which appears as a ledge due to hysteresis of the eye. The steady state ledge can be formed, but only on a large bubble in a viscous (over 25cp) liquid. Photography has aided in the resolution of many such phenomena, usually by the acquisition of qualitative information.

The principle uses of photography in bubble and drop investigations have been to record the shapes of dispersed particles[3–12] and the velocities at which they travel[3–5,7,8,10,13–15]. With a reference scale in the scene, drop and bubble sizes may be quantitatively determined[2,13]. By adding a dye to one phase, the boundary layer separation can be shown[16,17]. By taking advantage of various light transmission disturbances the flow patterns in the field fluid can be studied. Such disturbances include the photoviscosity effect in glycerol[18], bi-refringence due to fine solids such as bentonite[19], differences in concentration[20], and changes in refractive index due to temperature gradients[16]. Stroboscopic and other multiple image techniques[7,8,10,13,15] permit one to learn if phenomena be at steady state and to measure velocity of travel. High speed motion picture techniques permit observation of the nature and progress of such fast phenomena as bubble or drop formation[8,21–23], coalescence[24,25] or breakup. Much has been learned of boiling phenomena by the use of such cameras[22,23]. They also permit close views with sufficient time for observation without other elaborate apparatus[26,27]. A summary of readily available pertinent articles is given in Table 1.

Shape and Eccentricity

Rising gas bubbles are easily photographed[3–5,12,13,19–23]. If two-dimensional shape alone is desired, any camera with a double or triple extension bellows and almost any film may be used. Backlighting is best and an electronic flash unit will produce a short duration light of sufficient intensity to give excellent results. A good home built unit of high power can be built for a fraction of the cost of a commercially sold one. If good images of the surface of the bubble are desired, a "slave" unit top light should be added. When photo flood lamps are used, the exposure time must be of the order of 0.001 second. This means, of course, either a fast film or a very strong light must be employed. One may assume that a large gas bubble, travelling at 30 cm./sec. is to be photographed on 4 × 5 cut film. If the image on the film may be allowed to move by 0.1 mm. and the bubble is to be photographed at full natural size, the time of exposure is but 1/3000 of a second. Electronic flash units are more economical over extended service than photoflood lamps. Judicious use of reflectors such as white

TABLE 1

+ USES OF PHOTOGRAPHY IN BUBBLE AND DROP RESEARCH

Still photographs to show shape, eccentricity, boundary layers, etc.	3-9, 11-13, 16-20, 26, 27, 29, 34, 35
Size and shape by shadowgraph	13, 14, 30
Velocity by multiple image on still photographs	8, 13
Velocity by dark field trace	29, 31-33, 36
Velocity by motion pictures	3-5, 14, 37, 38
Drop internal velocity pattern by dark field trace	18, 29, 34, 35
Strobolume methods	7, 8, 10, 15
Velocities by interrupted trace	32, 36
Shapes and qualitative action by motion pictures	3, 5, 8, 17, 21, 26, 27, 29, 34, 37, 39
General qualitative and quantitative action by high speed motion pictures	8, 15, 17, 21-24, 26, 27, 36, 37, 39

[1]*Manuscript received February 12; accepted July 27, 1961.*
[2]*Department of Chemical Engineering, Illinois Institute of Technology, Chicago, Illinois, U.S.A.*
[3]*Universal Oil Products Company, Riverdale, Illinois, U.S.A.*
[4]*Amoco Chemicals Company, Whiting, Indiana, U.S.A.*
[5]*Eugene Dietzgen Company, Chicago, Illinois, U.S.A.*
Based on a paper presented to the Joint C.I.C.-A.I.Ch.E. Chemical Engineering Conference, Cleveland, Ohio, May 7-10, 1961.

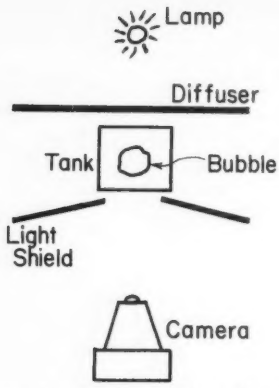

Figure 1 — Photography with back lighting.

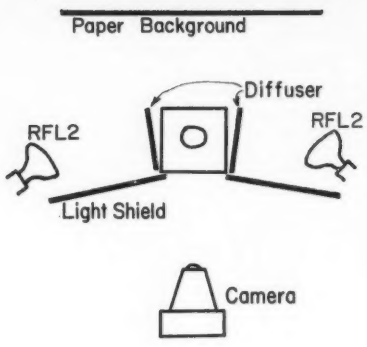

Figure 2 — Photography with side lighting.

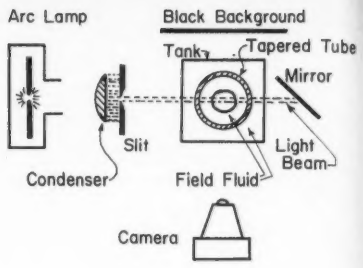

Figure 3—Side lighting with a collimated beam.

cardboard, aluminum foil, and glass mirrors can greatly aid in good pictures with a single light source. Cardboard shields must be used to protect the lens from unwanted direct rays from the lamps or from reflecting surfaces. A good arrangement is shown in Figure 1. When the dispersed particles must move in a vertical cylindrical vessel, lighting must be supplied from such a direction that images of the light sources will not enter the camera lens by reflection from the cylindrical tubes.

Liquid drops moving in a liquid medium are more difficult to photograph due to the much smaller differences in densities and refractive indices[7]. The simplest solution is to dye the drop to produce high contrast[7,17]. Calco Oil Red N-1700 is excellent and seems entirely devoid of interfacial activity characteristics, the presence of which cannot be determined by surface tension measurements alone. A combination of side and back lighting has been found best. A tan or light brown reflecting background gives good results with panchromatic films such as Eastman Tri-X or Ansco Super Hypan. A good arrangement for both still and motion pictures is shown in Figure 2. The background paper must be far enough away from the container to avoid shadows. Some photographers prefer no close background of any kind. If a dye is used in the drop liquid, color photography can be made superior to black and white. Garner and Tayeban[20] used back lighting with a tungsten lamp and fast shutter speed to produce excellent photographs of the boundary separation and wake of slow moving drops of benzyl alcohol in water.

Drop Size Distribution

One may photograph the dispersed droplets in a fluid field, enlarge the photograph and laboriously arrive at a drop size distribution. Care must be taken to avoid photographing drops adhering to a wall. The collimated flat beam illumination shown in Figure 3 is the best insurance against erroneous results. By this method only freely suspended drops are illuminated.

Velocity Measurements

Three kinds of velocities must be considered in bubble and drop research. True vectorial velocities cannot be photographed. Semi-vectorial velocities can be used to plot velocity fields and true vectorial velocities may then be obtained from these by a process of graphical differentiation. The most commonly measured velocity is the "gross terminal velocity", obtained by measuring the time necessary for a particle to fall (or rise) through a measured vertical distance. The distance must be long enough that all cyclic phenomena such as oscillation[2,7,9,28] will be repeated many times. Several photographic methods have been developed for such determinations[3–5,8,10,13,15].

Velocity by Multiple Image

The strobolume[7,8,10,15] is a useful device for short distance and time determinations. About six images can be obtained on a single piece of film. Local variations in velocity can be detected and stages in short cycle phenomena can be observed. One can also devise[13] a technique whereby the camera shutter can be operated at exact time intervals by a cam and microswitch arrangement. The wear on the camera is excessive and this method is not recommended.

Particle Trace Methods

Darkfield particle trace photography can yield much information on local velocities[29–36]. Particles of carefully de-greased aluminum powder, resin[31], clay or other materials are suspended in the continuous phase and a strong flat beam of light is sent through the field at a right angle to the line along which the camera is aimed. A timing device such as a motor-driven arm must be included in the photograph in order to measure the short elapsed time corresponding to the streak of reflected light. The time of exposure of a camera shutter is not sufficiently dependable for such work. A typical arrangement is shown in Figure 3.

Velocities Inside Drops

The flow pattern in the interior of a moving drop has been qualitatively recorded many times by both still and motion picture photography[8,18,34,35,37,38]. Garner and Haycock[37] have recently published a very meticulous set of quantitative measurements of the velocity distribution inside a falling drop, using a motion picture technique. In all these cases, the camera and lights were placed on a platform and allowed to fall at the same speed as the falling drop, the rate of fall of the platform being controlled by a hydraulic cylinder.

By using an unmarked rotameter tube with the larger end up, a species of "water tunnel" was recently used to carry on a limited study of the circulation inside drops[29]. An 84% glycerine solution was pumped upward through the rotameter tube. The fluid velocity was slower at the top than at the bottom and, at some point in the tube, its speed could be made to exactly match the fall velocity of a drop of measured size which was introduced at the top of the system. With this apparatus the drop could be held at one point for an hour or more for observation. A flow diagram is given in Figure 4.

The photographic arrangement is shown in Figure 3. Light from a carbon arc is led thru a condensing lens and an adjustable vertical slit, thus producing a flat beam of light to illuminate a narrow cross section of the drop. A square plastic tank was placed around the rotameter tube to minimize distortion and keep the light beam sharp. The space between tank and tube was filled with 84% glycerine. The camera was set on a support at 90° to the light beam and a black cardboard background was provided. Degreased aluminum particles appeared in the photographs as tiny light blips and their progress recorded by dark field particle trace photography.

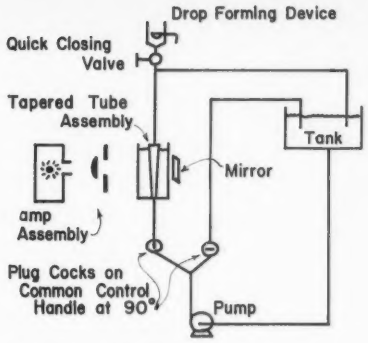

Figure 4—Flow diagram of tapered tube system.

The camera used was a 4 × 5 Speed Graphic with a triple extension bellows and an f4.7 lens in a Compur shutter. Film used was Ansco's Super Hypan with a rated ASA speed number of 400. By overdeveloping methods, its effective speed number was doubled to 800. A typical photograph is shown in Figure 5. Several such photographs were obtained in the course of each experimental run, the total number of such negatives being about 500.

The problem then becomes one of interpreting the streaks shown in the photographs in terms of circulation velocities. Garner and Haycock used organic mixtures having the same index of refraction as the surrounding glycerine mixture but this limits the range of variables involved. In the present system rays of light reflected from the various aluminum particles traveling along the streamlines inside the drop as a result of circulation pass through the interface of the drop and field fluid, through the glass of the tapered tube, and finally through the plastic of the box surrounding the tapered tube assembly. There is a difference of index of refraction between the drop fluid and the field fluid, and this difference presents the most serious error in the interpretation of photographs. A method of coping with this problem on a mass production basis is presented below.

The assumptions involved in this development are the following:

(1) The curve generated by the intersection of a plane passed through the vertical axis of the drop can be expressed in equation form.

(2) The drop is symmetrical about its vertical axis.

(3) The pencil of rays reflected from the aluminum particle which impinges upon the lens of the camera can be approximated by a single ray ("average" ray) passing through the drop interface and moving thence in a direction normal to the plane of the sheet of light passing through the drop.

Figure 6—Drop not centered in tube.

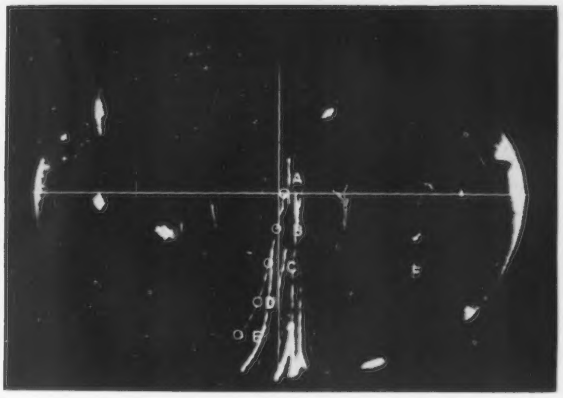

Figure 5—Trace photograph of drop.

(4) The lens of the camera lies along a line normal to the plane of the sheet of light, and which intersects the major and minor axes of the drop.

(5) The distortion of the hardware about the drop is negligible.

The first assumption seems justified although its actual realization in practice may be quite difficult.

If the drop is centered in the tapered tube, and if the tapered tube is perfectly vertical, the second assumption is justified with respect to the photographs of the drop obtained. Whether or not the drop vertical axis lay along the tapered tube axis could be checked in this equipment by suspending a drop of about 0.8 cubic centimeters volume, the density of which differed from that of the field fluid by about 0.1 gram per cubic centimeter, in the tapered tube and observing the drop's symmetry about the vertical axis from two directions. A drop photographed in the tapered tube which had been thrown out of adjustment for the purpose is shown in Figure 6. This figure also shows the possibility of photography of non-symmetrical drops in this apparatus by purposefully causing the tapered tube to be out of adjustment.

The third assumption greatly simplifies the treatment of the drop data and is necessary for this reason. The error introduced by this assumption is seen to be quite small, as the direction of the "average" ray considered below differs from that of the direction of the true "average" ray by a very small quantity.

The fourth assumption can be realized by proper design of the equipment. Note that because of this assumption, the position of the drop in the tapered tube cannot be allowed to vary in a vertical direction.

The fifth assumption is justified on the basis of a photograph of a spherical ball suspended in the tapered tube under nonflow conditions. Photographs of spherical balls of different sizes taken in the course of the work show an equally small amount

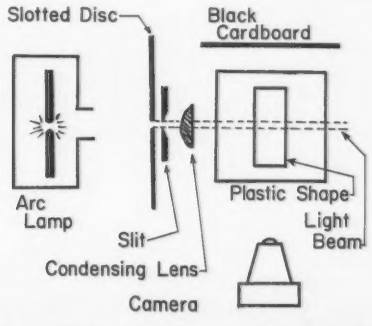

Figure 7—Interrupted trace photography.

of distortion caused by the optical system of the tapered tube and the plastic box surrounding it.

The problem is one of finding the actual location of the aluminum powder trace shown on the drop photograph with respect to the geometry of the system. A graphical method is available, but is somewhat tedious and does not lend itself to the processing of large amounts of data. A more direct analytical method based on the above assumptions is also available, and a modification of this method which does lend itself to the processing of large amounts of data is discussed below.

Snell's law of refraction is familiar from the study of optics. It is:

$$n_1 \sin\alpha_1 = n_2 \sin\alpha_2 \quad \ldots\ldots(1)$$

This must be applied in the plane of the normal to the lens surface (at the point of intersection of the ray with the surface) and the ray. It is seen that a method of solution could be to find the equation of the surface of the drop, find the normal to it at the point of intersection, and proceed to the determination of the deviation from the apparent position of the aluminum particle by the application of trigonometry. An illustration of this is shown below assuming that the curve generated by the intersection of the plane of the sheet of light with the drop interface is that of an ellipse.

It is found in practice that the curve of the drop interface (as obtained above) seems to follow one equation above and another equation below its major axis. If these equations are both those of ellipses:

$$\frac{x^2}{a_1^2} + \frac{y^2}{b_1^2} = 1 \quad \ldots\ldots(2)$$

$$\frac{x^2}{a_2^2} + \frac{y^2}{b_2^2} = 1 \quad \ldots\ldots(3)$$

respectively, it is seen that:

$$a_1 = a_2 \qquad b_1 \neq b_2 \quad \ldots\ldots(4)$$

for the drops in this work.

Consider the upper ellipse given by Equation (2), which is the equation given by the simultaneous solution of:

$$\frac{x^2}{a_1^2} + \frac{y^2}{b_1^2} + \frac{z^2}{c_1^2} = 1 \quad \ldots\ldots(5)$$

and:

$$z = 0 \quad \ldots\ldots(6)$$

In the case of drops symmetrical about the vertical axis (oblate spheriods), $c_1 = a_1$ so that

$$\frac{x^2}{a_1^2} + \frac{y^2}{b_1^2} + \frac{z^2}{a_1^2} = 1 \quad \ldots\ldots(7)$$

The apparent position of the trace is available from the photograph in question. The actual physical dimension of the major and minor axes of the drop is also available from the photograph and a knowledge of the width of the tapered tube at the position of the drop. Let the length of the major axis be taken as two units, so that $a = 1$.

Then:

$$x^2 + \frac{y^2}{b_1^2} + z^2 = 1 \quad \ldots\ldots(8)$$

The values of x_1 and y_1 are available from the photograph. They must be substituted into Equation(8) to obtain the value of z_1, so that

$$x_1^2 + \frac{y_1^2}{b_1^2} + z_1^2 = 1 \quad \ldots\ldots(9)$$

The equation of a plane tangent to the surface of the drop at the point of its intersection with the light ray from the particle is:

$$(x - x_1)\left(\frac{\partial f}{\partial x}\right)_1 + (y - y_1)\left(\frac{\partial f}{\partial y}\right)_1 + (z - z_1)\left(\frac{\partial f}{\partial z}\right)_1 = 1 \ldots(10)$$

and the direction of the normal to the surface of the drop at this point is given by:

$$\left(\frac{\partial f}{\partial x}\right)_1, \left(\frac{\partial f}{\partial y}\right)_1, \left(\frac{\partial f}{\partial z}\right)_1 \quad \ldots\ldots(11)$$

where:

$$f = x_1^2 + \frac{y_1^2}{b_1^2} + z_1^2 - 1 \quad \ldots\ldots(12)$$

Thus the direction of the normal is:

$$(2x_1), \left(\frac{2y_1}{b_1^2}\right), (2z_1) \text{ or } (x_1), \left(\frac{y_1}{b_1^2}\right), (z_1) \quad \ldots\ldots(13)$$

The angle between the line corresponding to the path of the ray from the drop interface to the camera lens is given by:

$$\alpha_1 = \text{arc sin} \frac{\sqrt{x_1^2 + \frac{y_1^2}{b_1^4}}}{\sqrt{x_1^2 + \frac{y_1^2}{b_1^4} + z^2}} \quad \ldots\ldots(14)$$

This is substituted into Equation (1) so that:

$$\alpha_2 = \text{arc sin} \frac{n_1}{n_2} \sin\alpha_1 \quad \ldots\ldots(15)$$

Now:

$$\alpha_3 = \alpha_1 - \alpha_2 \quad \ldots\ldots(16)$$

and:

$$z_1 \tan\alpha_3 = d \quad \ldots\ldots(17)$$

The direction of "d" on the photograph is given by:

$$\tan\rho = \frac{y_1}{b_1^2 x_1} \quad \ldots\ldots(18)$$

In this way several points on the trace can be selected and the actual position of the points plotted on the photograph. The length of the trace can be found by means of calipers, and the velocity of the particle which caused the trace determined. Final calculation of results awaits only the availability of time on a digital computer to complete the thousands of such solutions necessary.

Interrupted Trace Methods

If a slotted metal disc, driven at a known exact speed by a synchronous motor, be inserted between the condensing lens and the subject, the slots in the disc will enable stroboscopic photography of the light streaks[30–33,36]. If a narrow slot be followed by a wide one and a space be provided between such a pair and the succeeding one, a dot-dash image will be formed[32,36]. The number of such images must be the same for every sequence if the particles are travelling in the beam[36]. A lesser number of dot-dash pairs indicates that the particle was travelling across the beam and the data must be rejected as invalid. The known rotational speed of the spinning interruper disc provides the time measurement.

Flow Around a Cylinder

A large gas bubble will rise through a liquid in a shape which has been described as a spherical cap[2–5,12]. The front surface is a portion of a perfect sphere[3] and the rear area a disturbed but relatively flat or somewhat concave one. A very large liquid drop falling through a viscous liquid would possess a definitely crescent-shaped vertical cross section[26]. The profile of the frontal surface of the rising bubble was determined by Davies and Taylor[3] and an idealized geometric shape described by Rosenberg[4].

The vertical cross section of the idealized spherical cap will, when described in but two dimensions, be a circular segmental cylinder. Such cylindrical shapes were made of plastic and pulled upward[36] through water in a rectangular plastic tank

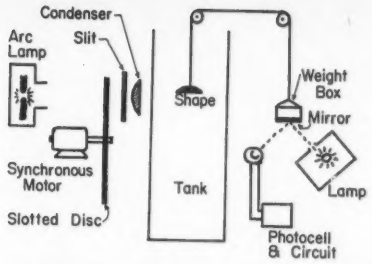

Figure 8—Elevation of interrupted trace apparatus.

as shown diagrammatically in Figures 7 and 8. The light from a carbon arc was led through a spinning disc interrupter, an adjustable slit and a condensing lens to the tank. This produced a flat plane of light to permit a two-dimensional field of illumination. Thus, a system of dark field, interrupted streak photography was made possible. Much of the equipment had been used by previous workers in mixing investigations[32,33].

The light interrupting apparatus consisted of a rotating slotted disc shown in Figure 9 of metal driven by a synchronous motor operating at 1700 r.p.m. Two slots were provided. One was a 5° cut out and the second, located ¼ of the circumference away, was 30° in width. The spinning disc was located in front of the adjustable slit. The exposure times are regulated by the width of the slits and the width of the light beam by the adjustable slit.

The camera used was a 4 × 5 Speed Graphic with 127 mm., f-4.7 Ektar lens. The full lens opening was needed, using Eastman Tri-X cut film. The shutter speed of the camera was set to permit at least two revolutions (dot-dash images) of the rotating disc. The still pictures were supplemented with high speed (300 pps) motion pictures using a Fastax WF-3 camera. The arc lamp was then operated on direct current to avoid the fluctuations in light inherent in AC supply. The interrupter disc was not used for motion pictures.

The still camera shutter was automatically triggered by means of a photoelectric cell and circuit. A light beam was reflected from a mirror on the bottom of the weight pan so that the shutter would be opened while the rising cylindrical shape was in the field of view, as shown in Figure 10.

To obtain velocity values, the negatives were placed in a photoenlarger and projected on to a piece of graph paper. Each clearly discernible sequence of particle images was traced on the paper along with the base of the lowest image of the shape. After the images had been traced, both the horizontal and vertical

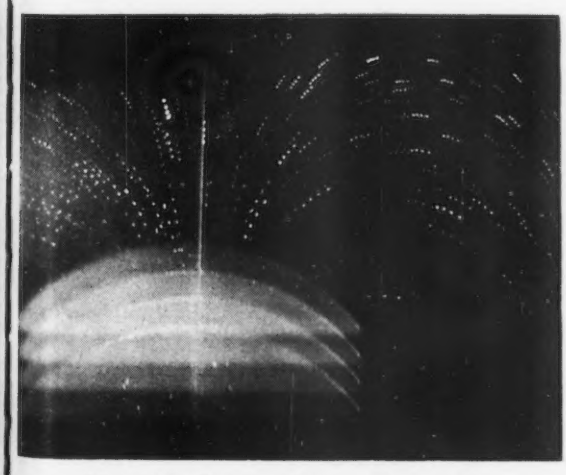

Figure 10—Interrupted trace photograph.

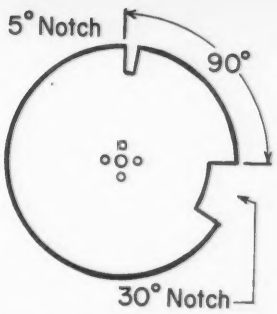

Figure 9—The interrupter disc.

distances between successive dashes were measured and positioned relative to the center of the base line of the shape. Horizontal and vertical velocity components could then be determined by means of the time elapsed during one interruption cycle. By keeping the geometry of both photography and enlargement constant, the results of a considerable number of repetitive runs could be plotted on a single sheet of graph paper. By moving the reference center of the graph paper from the center of one shape base line to that of the next, the velocities may be converted to those relative to the shape. As originally photographed they are relative to the tank and other stationary parts (Figures 11 and 12).

The number of dot-dash images must correspond to the number of images of the moving shape in each photograph. If a lesser number of traces was recorded, the particle was moving across the flat light beam and that trace was ignored. If more than a very few such invalid traces be recorded, the whole experiment must be rejected and the cause of the action found.

The method described permits the determination of local velocities without the great expense of a "water tunnel". The results can be related to the usual dimensionless groups or can be interpreted in terms of the hydrodynamics of moving submerged bodies.

Velocity by Motion Pictures

Davies and Taylor[3] measured the gross terminal velocity of rising air bubbles by means of a periscope arrangement somewhat like that shown in Figure 13. The framing rate of the motion picture camera measures the time interval between the image of the bubble as it passes the lower mark and, later, the upper one. Calibration is, of course, necessary.

Rosenberg[4] and Haberman and Morton[5] used the progression of the bubble image across succeeding frames of 35 mm. motion picture film to determine velocity of rise.

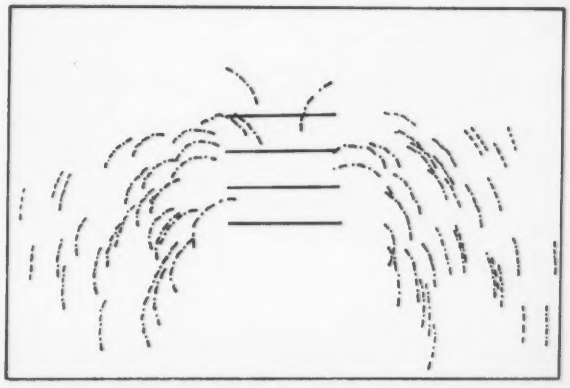

Figure 11—Particle traces around a cylindrical cap shape.

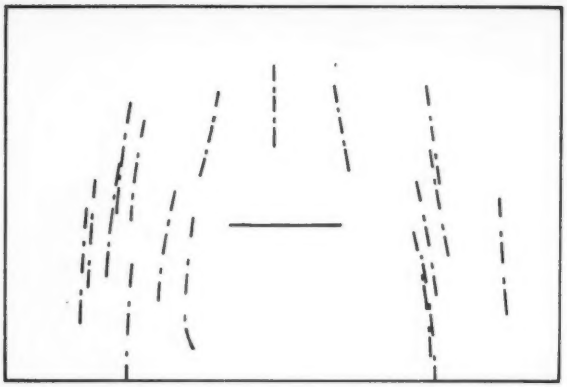

Figure 12—Observer moves with cylinder.

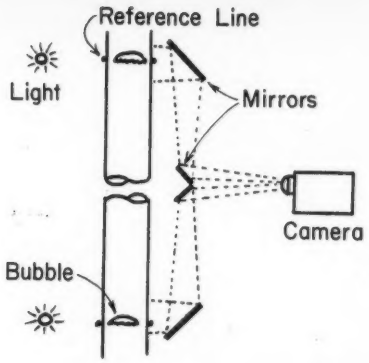

Figure 13—Velocity by split field photography.

The gross terminal velocity of a single drop moving alone in a liquid field is easily measured by any of several techniques with an error of less than 4%. The velocity of a single drop moving in a stream of such drops is more difficult. The usual method is to divide a volumetric holdup by a volumetric flow rate to obtain a residence time. This is then used with a vertical distance to obtain an average velocity of rise or fall. A technique for measuring the velocity of each individual drop in a rain of such drops by the use of ordinary (up to 64 p.p.s.) motion pictures is presented[14].

The containing tube with its rain of falling drops was in the center of the scene, a 0.01 sec. electric timer at the left and a panel on which to record pertinent data at the right as shown in Figure 14. A scale was provided at the rear of the vertical tube. The whole was then calibrated for geometry and distortion.

The camera used was a Kodak K-100 with a 25 mm. lens. Eastman Tri-X Reversal, 16 mm., film was used. Illumination was by three 375-watt reflector floods on the main subject and a small spot on the stopwatch. Any of the popular photocell light meters and a good camera stand completed the equipment needed. The background was a tan cardboard.

A good editing machine in which single frames can be observed is a necessity. One simply records the position of the drop as it enters the view together with the corresponding reading of the stopwatch. The drop is followed visually as film is slowly fed through the viewer until a second pair of readings may be taken. The gross terminal velocity is then $\Delta h/\Delta t$. A knowledge of the range of velocities and some information on their distribution can be obtained.

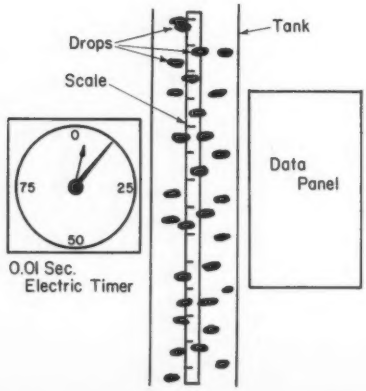

Figure 14—Arrangement of apparatus before camera.

There are some obvious deficiencies in the method. One does not know the front-to-back position of the droplet and a velocity vs. diameter distribution is tenuous. This has now been remedied by the use of side-lighted, dark field methods illustrated in Figure 3. Even 64 p.p.s. is not fast enough for systems of high density difference in which the drops fall at high velocities. The authors are fortunate in having a Fastax camera to extend their range. Reflector spot lamps are needed for such camera speeds.

The results of the studies in which the method is used are part of a series on drop velocities in tanks.

High Speed Motion Pictures

Motion picture cameras employing a shutter system by which the film is stopped, a picture taken and the film then moved forward into position for the next picture are generally limited to 64 p.p.s. When projected at 16 p.p.s., the motion is slowed by a factor of four. In cameras capable of higher framing rates, the film moves through at constant speed and framing is accomplished by other mechanisms. One of these is the rotating prism type, the most commonly used ones having speeds of about 200 to 8000 p.p.s.

While such cameras have many uses, they are chiefly employed to produce slow-motion movies. Such fast phenomena as partial coalescence and boiling[22] can be more clearly understood by observation of the details of the action. Even 4000 p.p.s. was found to be somewhat slow to fully observe the early stages of bubble growth during boiling. Circulation patterns inside falling drops[8] and the collapse of steam bubbles in water[39] have been determined by such methods. The frequency and amplitude of drop oscillations and rupture can also be taken from such films.

If one wishes to take motion pictures of fast moving drops with the drop filling the field of view, he can use the falling camera technique[8,18,34,35,37]. A second method is to tilt the camera, keeping the droplet in view as it falls. A telescopic lens and very small stop (about f-22) are necessary to have both close up view and a sufficient depth of field to keep the image in focus. High speed (150 to 500 p.p.s.) cameras permit one to attain the same result in a more satisfactory manner[2,26,27].

Acknowledgement

Research using some of the techniques described above was supported in part by the National Science Foundation and by the Esso Educational Foundation.

Nomenclature

a,b,c = half axes of ellipsoid
d = Equation (17)
f = Equation (12)
h = height
n = index of refraction of liquid
t = time
x,y,z = coordinates of ellipsoid with origin at center of symmetry
α,ρ = angles

References

(1) Ladyzhensky, R. M., J. Appl. Chem. (U.S.S.R.), **27,** 22 (1954).

(2) Uno, S., and Kintner, R. C., A.I.Ch.E. Journal, **2,** 420 (1956).

(3) Davies, R. M., and Taylor, G. I., Proc. Royal Soc., **A200,** 375 (1950).

(4) Rosenberg, B., TMB Rep. 727 (1950).

(5) Haberman, W. L., and Morton, R. K., TMB Rep. 802 (1953).

(6) Keith, F. W., Jr., and Hixon, A. N., Ind. Eng. Chem., **47,** 258 (1955).

(7) Licht, W., and Narasimhamurty, G. S. R., A.I.Ch.E. Journal, **1,** 366 (1955).

(8) Johnson, A. I., and Braida, L., Can. J. Chem. Eng., **35,** 165 (1957).

(9) Klee, A. J., and Treybal, R. E., A.I.Ch.E. Journal, **2,** 244 (1956).

(10) Korchinski, I. J. O., Thesis, Univ. of Toronto (1956).

(11) Jennings, H. V., Rev. Sci. Insts., **28,** 774 (1957).

(12) Azim, S., Thesis, Ill. Inst. Tech. (1957).

(13) Allawala, M. A., Thesis, Ill. Inst. Tech. (1952).

(14) Amberkar, S., Thesis, Ill. Inst. Tech. (1960).

(15) Calderbank, P. H., and Korchinski, I. J. O., Chem. Eng. Sci., **6,** 65 (1956).

(16) Elzinga, E. R., and Banchero, J. T., A.I.Ch.E. Journal, **7,** 394 (1961).

(17) Garner, F. H., Trans. Inst. Chem. Engrs. (London), **28,** 88 (1950).

(18) Spells, K. E., Proc. Phys. Soc., **65B,** 541 (1952).

(19) Hughes, R. R., Ind. Eng. Chem., **49,** 947 (1957).

(20) Garner, F. H., and Tayeban, M., Anales Real Soc. Espan. Fis. y Quim. (Madrid), **LVI-B,** 479 (1960).

(21) Spells, K. E., and Bakowski, S., Trans. Inst. Chem. Engrs. (London), **28,** 38 (1950).

(22) Westwater, J. W., Chem. Eng. Progr., **55,** 49 (1959).

(23) Chun, K., Thesis, Ill. Inst. Tech. (1956).

(24) Charles, G. E., and Mason, S. G., J. Colloid. Sci., **15,** 105 (1960).

(25) Groothius, H., and Zuiderweg, F. J., Chem. Eng. Sci., **12,** 288 (1960).

(26) Fararoui, A., Thesis, Ill. Inst. Tech. (1960).

(27) Mhatre, M. V., and Kintner, R. C., Ind. Eng. Chem., **51,** 865 (1959).

(28) Hu, S., and Kintner, R. C., A.I.Ch.E. Journal, **1,** 42 (1955).

(29) Horton, T. J., Thesis, Ill. Inst. Tech. (1960).

(30) Kessie, R. W., Thesis, Ill. Inst. Tech. (1955).

(31) Metzner, A. B., and Taylor, J. S., A.I.Ch.E. Journal, **6,** 109 (1960).

(32) Neilsen, H. J., Thesis, Ill. Inst. Tech. (1958).

(33) Sachs, J. P., and Rushton, J. H., Chem. Eng. Prog., **50,** 597 (1954).

(34) Savic, P., Natl. Council Can., Mech. Eng. Rep. MT22 (1953).

(35) McPhail, D. C., 4th AGARD Gen. Assembly, 73 NATO Memo AG14/P5 (1954).

(36) Graumann, R., Thesis, Ill. Inst. Tech. (1959).

(37) Garner, F. H., and Haycock, P. J., Proc. Royal Soc., **A252,** 457 (1959).

(38) Garner, F. H., Skelland, A. H. P., and Haycock, P. J., Nature, **173,** 1239 (1954).

(39) Levenspiel, O., Ind. Eng. Chem., **51,** 787 (1959).

★ ★ ★

Diffusion Coefficients for the Liquid System: Ethanol-Water

F. A. L. DULLIEN[2] *and L. W. SHEMILT*[3]

Measurements of the liquid diffusion coefficients over the complete range of compositions of the ethanol-water system at 25°C. have been carried out using the porous diaphragm technique with a magnetically-stirred and modified cell. Both the integral and differential coefficients agree very closely with the values reported by Hammond and Stokes, although an improved method of calculating the differential coefficients has been used. The limiting values at 0 and 100% concentrations differ somewhat from those previously reported. By means of an experimental investigation the work of Smith and Storrow on the same system has been shown to be in error. Analytical errors in calibration have been reduced to a probable error of ± 0.1%, although there is an average deviation of ± 2% for all experimental points relative to the best line drawn through them. The diffusion coefficients based on concentration as a driving force, show a minimum at 25 mole % ethanol, corresponding to the minimum for the relative decrease in volume on mixing and the maximum for the viscosity-composition curve. For the dimensionless Schmidt number, a very sharp peaking to a value of 7500 occurs at the same composition.

Although the diaphragm cell technique for measuring diffusion coefficients in liquid systems has been widely used, only very few measurements in binary non-electrolyte systems have been made. This apparent neglect has been not only due to the difficulty of constructing a satisfactory cell for use with most organic liquids, but, of more importance, to the lack of an acceptable general procedure for computing the true differential values from the measured integral diffusion coefficients. To obtain practically differential diffusion coefficients directly by using small concentration differences in the diffusion experiments, extreme analytical precision is necessary because of the multiplying effects of the mathematical treatment. Some doubt has been cast on the method, also, in the recent competent review article by Johnson and Babb[1]. Their criticism was based on the fact that the diffusion coefficients in the ethanol-water system as obtained by Smith and Storrow[2] and by Hammond and Stokes[3] differ by as much as 100%. The pairs of investigators considered their results accurate to three and one per cent respectively, and were not able to explain the discrepancy between their measurements.

[1]*Manuscript received December 8, 1960; accepted September 5, 1961.*
[2]*Assistant Professor, Department of Chemical Engineering, Oklahoma State University, Stillwater, Oklahoma, U.S.A.*
[3]*Professor, Department of Chemical Engineering, The University of New Brunswick, Fredericton, N.B.*

It was considered fruitful, therefore, to re-investigate the ethanol-water system again, and if possible to provide a modified diaphragm cell design and methods suitable for rigorous calculation of differential diffusion coefficients. The equations necessary for the latter, involving the general case for systems where volume changes occur on mixing, have been reported elsewhere[4,5]. The re-evaluation of the diffusion coefficients for the ethanol-water system at 25°C. is presented here.

Investigation of Previous Diffusion Cells

The diffusion cell used by Smith and Storrow[2] is shown schematically in Figure 1, and is somewhat different from the classical design of Northrop and Anson[6] which provided the essential basis for the cells used by Stokes[7] and in this work. In Figure 1, A is a glass tube ending in a sealed male ground glass joint C; D is the half-cell containing the solution richer in alcohol; E is the sintered glass diaphragm; F are magnetic stirrers; G is a large test tube serving as the other half cell; and B is a vented rubber stopper.

Smith and Storrow used aqueous KCl solutions for calibration, determining the concentration changes in the upper half-cell conductometrically. In their experiments to establish the lower limit of satisfactory stirring rates, they found very much lower values (3 r.p.m.) than Stokes[7] (25 r.p.m.). The most likely explanation for this disagreement is to be found in the different geometry of the types of cells used by these investigators. Experiments carried out in the course of the present work have established that with cells of geometry similar to those used by Stokes, there are significant concentration gradients inside the bulk of the liquids in the cell-compartments at stirring rates of about 10 to 15 r.p.m. At higher rates these non-homogeneities cease to exist. In the shorter type of cell-compartment, containing the conductivity electrodes, as used by Smith and Storrow, it is reasonable to expect that the concentration gradients in the bulk of the liquids are wiped out at lower rates of stirring. However, the electrodes, that incidentally served also as baffles in the calibration runs, were absent in the ethanol-water experiments which might have resulted in inadequate stirring in this latter case.

The seal, essentially a ground glass stopper, used by Smith and Storrow for the upper half of their cell was also investigated[8] by using, in the first instance, the simple apparatus in Figure 2. *B* is a U-tube plugged at one end with a ground glass stopper *C* and fitted with a piece of narrow capillary *E* at the other end to prevent both evaporation and the development of vacuum. *A* is a jacket and *D* is a rubber stopper.

B was filled with over 90% alcohol, *C* was inserted, the edges of *C* and all the interior of *A* were dried, and small amounts of water were pipetted into the bottom of *A*. *D* was placed in position. The meniscus in the right arm of *B* was

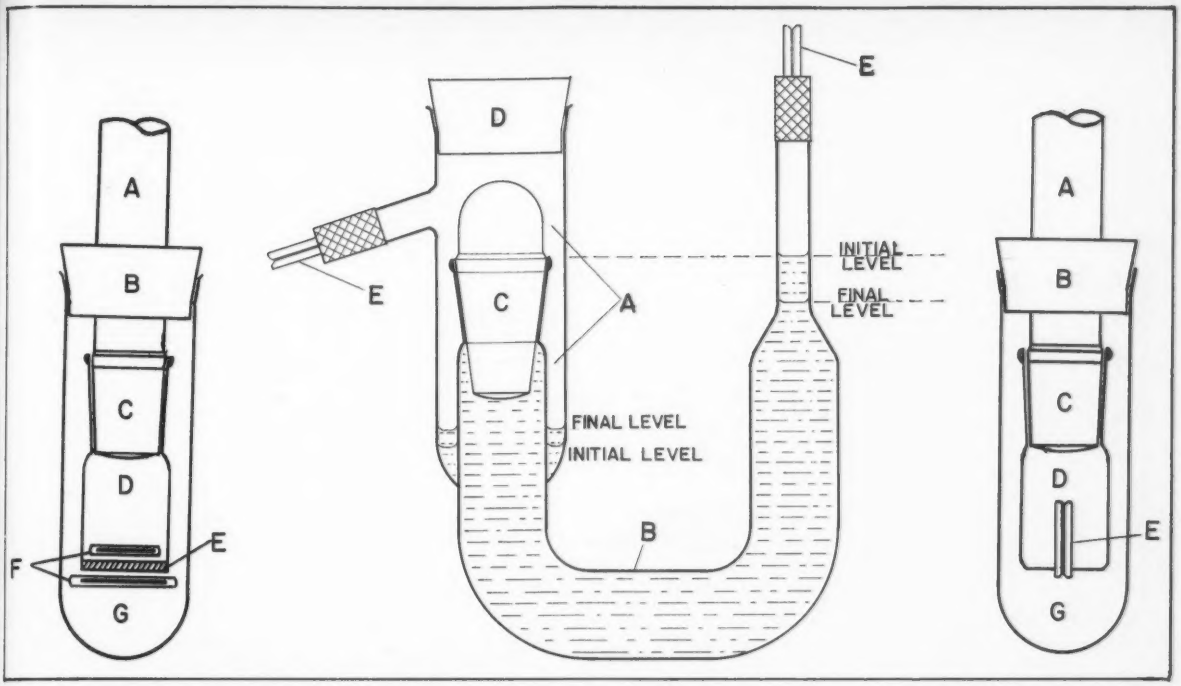

Figure 1—Sketch of diaphragm diffusion cell used by Smith and Storrow.

Figure 2—Apparatus used to investigate distillation through ground glass joint.

Figure 3—Apparatus used in pseudo diffusion experiments.

observed to move downwards while the meniscus in *A* was moving upwards. This process was observed for several days, when the liquid in *A*, orignially pure water, had increased its volume by several times the original value. This experiment was repeated several times although occasionally the process observed would not start, or apparently stopped after proceeding so far. The ground glass stopper *C* was always inserted very firmly to prevent ordinary leakage through the joint. The mechanism of this distillation effect has not been elucidated further, although it was observed that whenever the distillation was in progress, the edges of the joint, originally dry, were seen to be moist.

An attempt to measure the magnitude of the distillation effect under conditions similar to those used by Smith and Storrow required a cell, Figure 3, that differed from the one used by the above authors only in that the sintered glass disk has been replaced by a short piece of narrow capillary *E*. This permitted bulk flow from *G* into *D* in case part of the liquid were removed from *D* via distillation through *C*. Other things being equal, the diffusional transport through *E* is about one millionth of that through a sintered glass disk and hence is completely negligible. This cell was accommodated, along with another reference-cell of the same construction, but not containing any ground glass joint in a constant temperature bath maintained at 25 ± 0.1°C.

D was filled with alcohol solution, *C* inserted, the outside of the cell dried carefully, about 30 ml. of water placed in *G*, and *B* placed in position. The reference cell was treated in the same way.

Runs of 14 to 89 hours duration were carried out, and at their conclusion samples were taken from *G* using a hypodermic needle that was inserted through *B* and served the purpose of venting *G* throughout the runs. Analysis by refractive index was carried out. The reference cell containing no ground glass joint exhibited negligible transference, but significant changes were found to occur in the other cell and were judged to be due to distillation through the joint.

Several runs at the low concentration differences used by Smith and Storrow[2] in their experiments showed that the distillation effect might have accounted for about 10 and 15% respectively, of the values they obtained for the diffusivity. This indicates a strong possibility that the higher values of the diffusivities obtained by these authors are a consequence of mass transfer through the ground glass joint used in their apparatus.

Apparatus and Procedures

A. Equipment

The diaphragm cell as designed and used in the present experiments is shown in Figure 4. In this design the use of rubber stoppers and lubricated or unusually well-fitting ground glass parts has been eliminated. *B* is filled and emptied through two narrow (0.5 mm. i.d.) capillaries, *E* and *D*, fitted near the ends with "polythene valves" made from short pieces of polythene tubing and commercial screwclips. These valves showed no detectable leakage of water under a vacuum of about 20 mm. Hg. *F* is "fine grade" sintered glass diaphragm. *G* are iron-in-polythene stirrers. *A* is the top half-cell sealed with a Teflon stopcock. The two capillary side-arms *D* and *E* are situated on the same side of the cell although for the sake of clarity Figure 4 shows them on opposite sides and set further from the cell-body than in actuality. About the level of "*A*" the side-arms are reinforced with a few windings of plastic insulating tape.

A multiple unit was designed to accommodate six cells arranged with their centres on the corners of a regular hexagon (Figure 5).

The body of each cell is surrounded by a brass sleeve *D* containing four slots *S* for aiding circulation of the bath liquid. The cells are supported on a piece of cork placed in the sealed bottom of the brass tube, and by cork wedges on the sides. On the outside of the bottom of the brass sleeve there are two pegs, the one in the centre a little longer than the other one.

The sleeves are held in position by bottom supports *C*, consisting of short pieces of brass rods soldered on a brass base

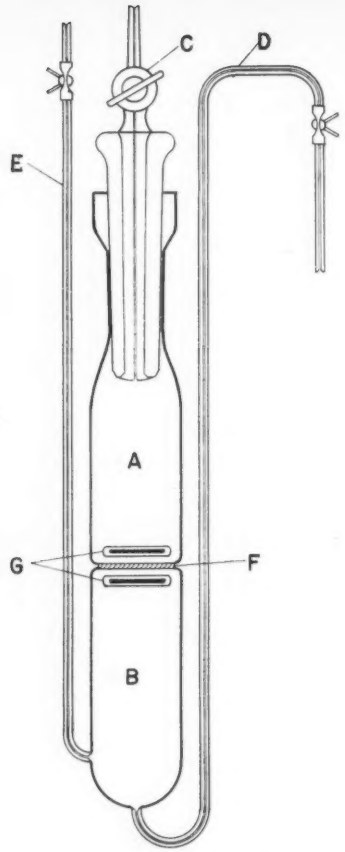

Figure 4—Diaphragm cell.

plate *B* in a hexagonal arrangement. There are two holes through each support matching the two pegs on the bottom of the sleeves holding the cells.

All stirring is achieved by a pair of rotating magnets *M* arranged around each cell with the poles level with the diaphragms. The magnets are standing upright mounted on pinions *E*, driven by a central drive *F*, and rotating in bearings provided by circular holes in a large disc made of "Tufnol" (linen-laminated phenolformaldehyde resin) sheet *G* which is supported centrally by a pillar *A* consisting of a large brass tube soldered on the base plate *B*. In the centre of this pillar there is a foot-bearing in which the axle *H* of the centre gear rotates. The latter is driven by a variable speed motor. The battery of six cells assembled outside the bath is shown in Figure 6.

The constant temperature bath containing thin paraffin oil, was maintained at 25°C. measured with a standardized thermometer, and the temperature was found constant within ±0.01°C. inside the cells.

B. Diffusion Experiments

The cells were calibrated using 0.1*N*. aqueous *KCl* solutions made with *B*. & *A*. Reagent Special grade of *KCl* and high quality distilled water. (Specific conductivity 2×10^{-6} mho. cm.$^{-1}$). All the solutions were carefully degassed prior to introduction into the cells. The *KCl* solutions were degassed by boiling, and the aqueous ethanol mixtures by freezing and subsequent thawing under vacuum. The solutions were introduced into *B* via *D* (Figure 4). Air was removed from the sintered glass diaphragms by boiling the solutions in *B* under vacuum. Subsequently the cell was placed in the bath, and after temperature equilibration the other solution was introduced into *A*. After two to three hours the solution in *A* was pipetted out,

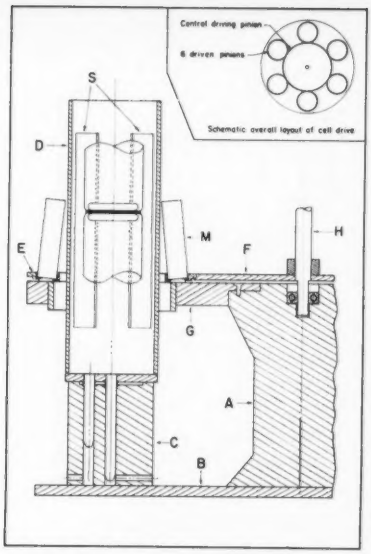

Figure 5—Cell support and stirring device in section.

A was rinsed and finally filled with fresh solution from the same stock. In the case of the calibration runs the liquid in *A* initially was always distilled water. The liquid displaced in the seal around the ground glass plug served to prevent evaporation of the liquid in *A* through the joint. During the diffusion period, stirring was carried out at high rates (about 100 r.p.m.). After several days of diffusion the contents of *A* were pipetted out, and the contents of *B* were blown out through *D*, by applying dried compressed air at *E*. The first few mls. were discarded, and the remainder kept for analysis.

C. Analyses

The aqueous *KCl* solutions were analyzed by a modification of the procedure recommended by McBain and Dawson[9], i.e., of evaporating the solutions to dryness and weighing the residues. By careful operation the accuracy (±0.02 mg.) of the semi-micro "gram-atic" analytical balance was fully exploited. The change in buoyancy on the weighing bottles from the time of weighing the empty bottles to the time of weighing the residues was noted by weighing a "standard bottle" each time. The true weight of the potassium chloride residue, m_R, was computed by the following formula:

$$m_R = \left(\frac{m_{B+R}}{M_1} - \frac{m_B}{M_2} \right) M, \quad \ldots\ldots\ldots\ldots\ldots\ldots (1)$$

where

m_{B+R} = apparent weight of the bottle plus residue,
m_B = apparent weight of the bottle,
M = weight of standard bottle corrected to vacuo,
M_1 = apparent weight of standard bottle at time of weighing the residue,
M_2 = apparent weight of standard bottle at time of weighing empty bottle.

Three parallel determinations of each sample were made. The probable error of the determinations was found to be $\pm 2 \times 10^{-5}$ g. which is about an order of magnitude better than the precision claimed by McBain.

The aqueous alcohol solutions were analyzed by density using 10 ml. Sprengel pycnometers modified by drawing out the tip of one of the arms to a capillary of about 0.1 mm. i.d., and part of the other arm to less than 1 mm. i.d. In the latter section a mark was engraved. The atmospheric density was determined by weighing a previously calibrated standard tare

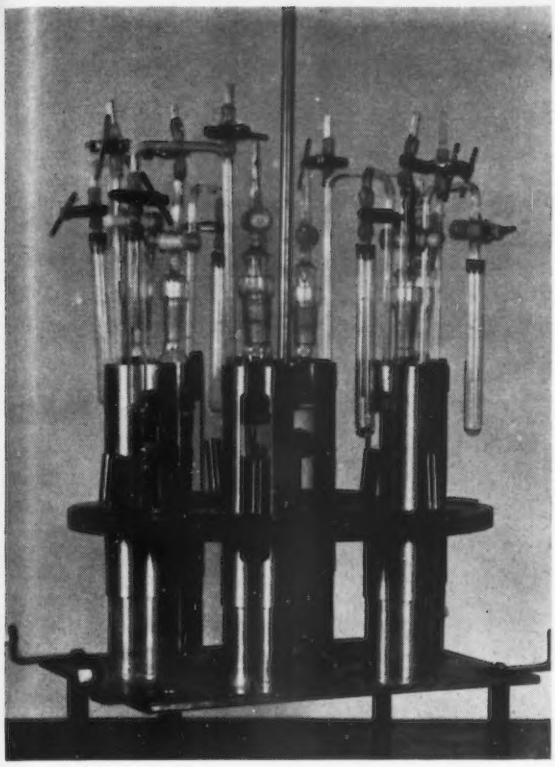

Figure 6—Battery of six diaphragm cells.

along with each pycnometer. This standard tare was prepared by sealing off the neck of a 100 ml. flask. Each sample was subjected to at least two density determinations. The probable error of the individual determinations was estimated to be $\pm 1 \times 10^{-5}$ g./ml. The accepted density data of the U.S. National Bureau of Standards[10] were used.

The commercial absolute ethanol used was treated with activated charcoal and fractionated at a reflux ratio of 10:1 in a 3 ft. glass column, packed with glass helices. Its purity was checked by density (0.79140 at 20°C. for 99.35% by weight) by accurately preparing a series of dilutions and comparing their compositions as found on the basis of the measured densities with the calculated ones.

The volumes of the cell-compartments and the pore volumes of the diaphragms were determined volumetrically, using degassed distilled water.

Results and Discussion

The analytical results for two calibration runs, Runs 7 and 8, using aqueous *KCl* solutions are given in Table 1* for five cells, and one confirming result for Cell 1.

The cell-compartment volumes are given in Table 2*. Each value is the mean of at least three determinations. The pore volume for the diaphragm was found to be approximately 0.3 ml. in all cases.

The cell constants, β, were calculated by the well-known simple logarithmic formula

$$ln \frac{\Delta C_o}{\Delta C_f} = \beta \cdot \theta \cdot \overline{D} \quad \ldots\ldots\ldots\ldots\ldots\ldots\ldots\ldots (2)$$

*Tables 1, 2, 3, 4, and 5 of this paper have been deposited as Document No. 6908 with the ADI Auxiliary Publications Project, Photoduplication Service, Library of Congress, Washington 25, D.C. A copy may be obtained by citing the Document No. and by remitting $1.25 for Photoprints, or $1.25 for 35 mm. microfilm. Advance payment is required. Make cheques or money orders payable to: Chief, Photoduplication Service, Library of Congress.

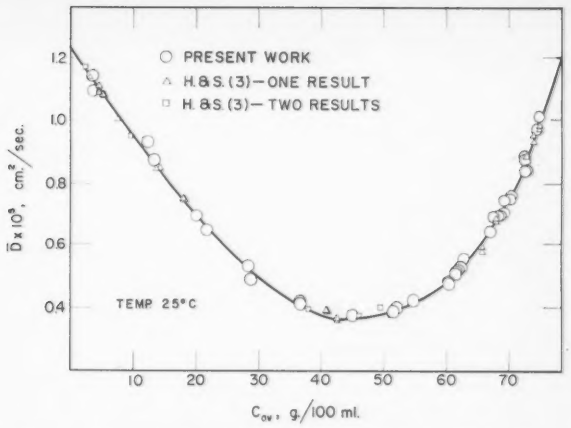

Figure 7—Integral diffusivity vs. mean concentration for ethanol-water system.

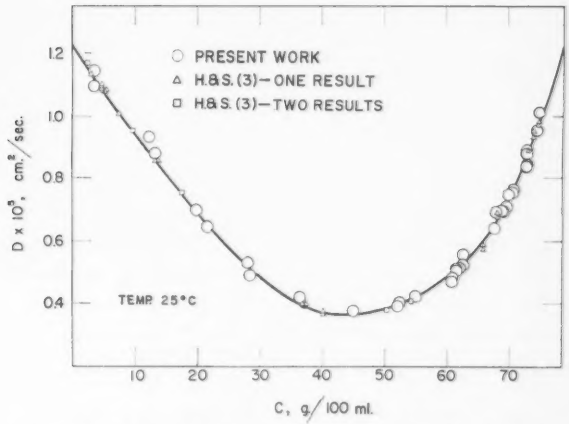

Figure 8—True diffusivity vs. concentration for ethanol-water system.

where $$\beta = \frac{A}{L}\left(\frac{1}{V'} + \frac{1}{V''}\right), \text{ cm.}^{-3},$$

$$\Delta C_o = C_o' - C_o'',$$

$$\Delta C_f = C_f' - C_f'',$$

The values of $\overline{D}$ recommended by Stokes[7] were used. The results are given in Table 3*.

The ethanol concentrations obtained in the runs with the ethanol-water mixtures at 25°C. are shown in Table 4*. The densities used to calculate the concentration values were the mean of at least two parallel determinations (exceptions: runs 4/1 and 5/1).. For the column "Cell/Run" the first number refers to the cell, the second to the run in chronological order. Two experiments with the same number "run" represent parallel experiments. As is apparent from the table, the solution richer in alcohol was contained in the upper half-cell in the majority of runs. Owing to the volume changes taking place in the open compartment of the cell the initial concentration in the lower compartment had to be computed by two material balances: one overall balance, and one on either component. The necessity for trial-and-error solution has been eliminated by a simple device described elsewhere[11]. With the exception of runs 5/1, 4/4, 1/6 and 6/7 the upper half-cell was open in all diffusion experiments.

From the data in Table 4 the integral diffusivities were computed by Equation (2). Although Equation (2) has been

derived on the assumption of constant solution volumes it has been shown elsewhere[5,11] that under the conditions of the present experiments the correction necessitated by the volume changes taking place on diffusion is negligible. The present measurements were found to be in excellent agreement with those of Hammond and Stokes[3]. The two sets of data are plotted in Figure 7 as integral diffusion coefficients against the mean concentration.

To obtain the true differential values, Hammond and Stokes used the method of least squares after dividing the whole concentration range into three regions and making rather arbitrary assumptions concerning the degree of the power series used to describe the individual regions.

It appeared much more straightforward to use a graphical method very similar to the one used earlier by Stokes[7] which he thought unusable in the present case owing to "the great change of the diffusion coefficient with concentration, together with the lack of any theoretical limiting values at the end of the concentration range"[3]. It is obvious, however, that the method of least squares does not supply the theoretical limiting values of the diffusivities but only constitutes a particular way of extrapolating to the limiting concentrations.

Plotting the combined data obtained in the present work and those of Hammond and Stokes against the mole fraction showed a linear relationship near the two ends of the concentration range. Hence, the limiting values of D could be obtained by linear extrapolation on this graph. These additional points were used to construct the best-fitting curve through the measured integral diffusivities as shown in Figure 7. Integral diffusivities were calculated by tabular integration for each run listed in Table 4 using the well-known formula

$$\bar{D} = \frac{1}{\bar{C}' - \bar{C}''} \int_{\bar{C}''}^{\bar{C}'} D dC, \quad \ldots\ldots\ldots\ldots\ldots\ldots (3)$$

where the bar over the concentrations denotes the mean of the initial and final values. Next, the concentrations corresponding to the calculated integral diffusivities were read from Figure 7 and the measured integral diffusivities were replotted against the new concentrations in Figure 8 to give the true or differential diffusivity-concentration relationship. The very small change as compared with Figure 7 clearly indicates that a second approximation was not necessary and also refutes the argument by Hammond and Stokes concerning the difficulty of using the graphical procedure because of the very sharp change of diffusivity with concentration. In any case, it is not the rate of change of the diffusivity with concentration, but the degree of curvature of the $\bar{D}$ vs. C curve that can increase the labour involved in the approximations. If the curve is linear, the measured integral diffusivities are rigorously equal to the differential values at the mean concentrations of the experiments. So far as the uncertainty introduced by the use of the extrapolated limiting values is concerned it should be noted that, fortunately, their effect on the rest of the values as obtained in the graphical procedure decreases rapidly as one moves away from the limiting compositions.

Partly owing to the difference in the computational method and partly due to the larger number of data considered in the present work, the resulting D vs. C relationship is somewhat different from the one obtained by Hammond and Stokes. The diffusivity values interpolated on the curve shown in Figure 8 have been tabulated and are shown together with the corresponding figures obtained by Hammond and Stokes in Table 5*.

It is to be noted that the limiting values reported in this work as 1.220 at each end of the concentration range compare to the Hammond and Stokes values of 1.240 and 1.132 for 0% and 100% ethanol respectively. The difference is due to the additional amount of data available and the improved method of extrapolation described above. As a result it is considered that the end values of 1.220 and 1.220 represent the best available.

*See footnote for Table 1.

In view of the close agreement between the present results and the data obtained by Hammond and Stokes, on the one hand, and the very significant disagreement between the above two sources and the measurements by Smith and Storrow, on the other, it seems most likely that there was some systematic source of error present in the experiments of the latter researchers. The fact that they carried out experiments at various temperatures without any apparent intersection of the resulting lines gives support to the contention that their source of error must have been systematic. One such possible source of error is that distillation can occur through a wetted ground glass joint as discussed above.

Careful and rigorous examination of the sources of error and the effects on the calculated results have been made. It has been found that the most probable error of a single diffusivity value, based on the analytical error, is about $\pm 0.4\%$. It has also been found, however, that the average deviation of the experimental points from the best line drawn through them (see Figure 7) is $\pm 2\%$. In the case of the calibration runs, the average deviation from the mean of the individual determinations of the cell constant is equal to the most probable error as calculated from the analytical error ($\pm 0.1\%$).

There are several possible sources of error that might account for the increased scatter of the alcohol experiments. One of them undoubtedly is the fact that the thermal expansion coefficient of the alcohol solutions is considerably larger than that of pure water. Consequently, equal irregularities in bath temperatures give rise to greater bulk flow through the porous diaphragm, this way or the other, with the ethanol solutions. Another possible source of error is relative loss of ethanol on sampling owing to its high volatility. A further source of error is the fact that the diaphragms were not in perfectly horizontal position which, under the effect of larger density difference, could have caused some flow through the diaphragm. All these sources of error could be reduced by making refinements in the experimental technique.

It appears that these sources of error played a less important role in the experiments of Hammond and Stokes. The scatter of their data seems to be determined primarily by the analytical errors. This may be concluded from the fact that their parallel determinations agree much better in the range of low and medium alcohol concentrations, where the experiments were done under conditions of considerably greater concentration differences than in the case of the more concentrated solutions.

Since, in the present work, there was no detectable trend in the results of re-runs, it is safe to conclude that the values of the cell constants did not decrease significantly in the course of the experiments. Also, Cell No. 1 had been used in about a dozen runs before completing the calibration with the *KCl* solutions without any noticeable trend in the values obtained for its cell constant.

Inspection of the figures will show that the minimum of the diffusivity-composition function is at a composition corresponding to three molecules of water and one molecule of ethanol, or very nearly so. The exact alcohol concentration corresponding to this molal ratio is 0.423 g./ml. at 25°C.

It is of some interest to note that if the relative decrease in volume on mixing is computed from the very accurate density data, it is found that this function also has a minimum at the same composition.

The viscosity-composition function also has a maximum at this composition and the shape of the curve of reciprocal viscosity vs. composition is also very similar to the corresponding diffusivity curve. A notable difference, however, is that the viscosity of pure ethanol is some 25% higher than that of pure water.

The fact that the above three functions have a maximum or minimum at a composition corresponding to three molecules of water and one molecule of ethanol suggests that at this composition the ethanol-water system is in a state of maximum stability or minimum energy. Whether or not such complexes also exist at compositions different from $x = 0.25$ is a question that should

be decided by methods of investigation more suited to this type of problem than diffusivity measurements. At the same time, when dD/dC is plotted against C the resulting plot consists of two branches intersecting at the composition corresponding to the hypothetical complex, indicating that the diffusivity is a function of a different degree of the ethanol concentration on the two sides of the minimum. Furthermore, when the diffusivity is replotted against the mole fraction of the hypothetical complex, the plot consists of two almost perfectly symmetrical halves on the two sides of the minimum, with the diffusivity changing only a few percent from pure complex to about 0.5 mole fraction of complex in both directions. It seems reasonably certain, however, that when approaching pure water or pure ethanol other modes of association become more stable, resulting in a rapid change in the value of diffusivity. The number of different sorts of possible associations in the ethanol-water system being enormously large, no explanation seems possible, at the present time, of the peculiar fact that the values of the diffusivity at the two ends of the concentration range are practically identical.

Further interest in terms of using these diffusivity data in mass transfer calculations arises in the calculation of the Schmidt number (dimensionless group, $\mu/\rho.D$) for the ethanol system. Using the diffusivity values in Table 5, with accepted data for viscosity and density, at 25°C., it is found that the Schmidt number has values of 736 and 1144 for the 0% and 100% concentrations respectively, but shows a remarkable sharp peak of about 7500 at 25 mole percent ethanol. A similar result is obtained if the activity-based diffusion coefficient is used. This is defined (4) as:

$$D' = D \cdot \frac{\partial \, ln \, a_A}{\partial \, ln \, \omega_A} \qquad \ldots\ldots\ldots\ldots\ldots\ldots\ldots\ldots (4)$$

and for mass transfer purposes is highly preferable since it is based on chemical potential as the driving force rather than concentration. Calculation of $\mu/\rho.D$ provides the same terminal values, and the same sharp peaking occurs at 25 mole percent, this time at a value of approximately 2200. As indicated previously, the postulate of a complex is tentatively advanced, but further elucidation in terms of molecular theory will be required.

Acknowledgement

We thank the National Research Council of Canada for a grant-in-aid, and the Eldorado Mining and Refining Company, and Canadian Industries Limited, for the grants of fellowships (to F. A. L. D.) and financial support.

Nomenclature

a_A = activity of component A
A = area of diffusion, cm.^{2}
C = concentration, in gms./ml. (or units as shown)
D = differential or true diffusion coefficient or diffusivity, cm.^{2} sec.$^{-1}$
D' = activity-based diffusion coefficient defined by Equation (4)
$\overline{D}$ = integral diffusion coefficient, cm.^{2} sec.$^{-1}$
L = length of diffusion path in diaphragm, cm.
m = weight, gms.
M = weight of standard item, gms.
V = volume of cell compartment, c.c.'s
β = cell constant
θ = time, seconds
μ = viscosity, poises
ρ = density, gms./c.c.
ω_A = mass fraction of component A
o, f (subscript) = quantities evaluated at initial and final conditions
$', ''$ (superscript) = quantity pertaining to closed and open half-cell, respectively

References

(1) Johnson, P. A., and Babb., A. L., Chem. Rev., **56,** 387 (1956).
(2) Smith, I. E., and Storrow, J. A., J. Appl. Chem. (London) **2,** 225 (1952).
(3) Hammond, B. R., and Stokes, R. H., Trans. Faraday Soc., **49,** 890 (1953).
(4) Dullien, F. A. L., and Shemilt, L. W., Nature, **187,** 767 (1960).
(5) Dullien, F. A. L., and Shemilt, L. W., Accepted for publication Trans. Faraday Soc.
(6) Northrop, J. H., and Anson, M. L., J. Gen. Physiol., **12,** 543 (1929).
(7) Stokes, R. H., J. Am. Chem. Soc., **72,** 763 (1950).
(8) Crossland, R. W., B.A.Sc. Thesis, Univ. of B.C. (1960).
(9) McBain, J. W., and Dawson, C. R., Proc., Roy. Soc. (London), **A-148,** 32, 1935.
(10) National Bureau of Standards, Circular No. 19, (1913).
(11) Dullien, F. A. L., Ph.D. Thesis, Univ. of B.C. (1960).

★ ★ ★

Concurrent Two-Phase Upward Flow of Air and Water Through an Open Vertical Tube and Through an Annulus[1]

CECIL O. CARTER[2] and R. L. HUNTINGTON[3]

The concurrent vertical upward flow of air and water has been made at various rates and ratios of air to water in a 2⅛-in. x 20 ft. open transparent Tenite tube as well as in a 1 5/16-in. x 2⅛-in. annulus. Pressure drops and in-place ratios of gas to liquid have also been observed in order to correlate such data with corresponding flow types and patterns. Motion pictures taken at normal and especially those at high-speed have made it possible to see flow mechanisms indistinguishable to the naked eye.

There are many industrial operations in which gases and liquids flow vertically upward through open tubes as well as annuli. Although these operations have taken place for more than a century, it has been only within the past two decades that extensive laboratory studies have been made in iron pipe as well as clear plastic and glass tubing[1,2,3,4,5,6,7,8,9,10].

The visual studies which have been carried out in tubing ranging from ½-in. up to 2-in. in size have thrown much light on the various flow types which probably take place in deep wells, as well as in plant processing equipment.

A search of the literature revealed the fact that little, if any, visual studies had been made in annuli, hence the decision to compare the performance in an annulus with comparable flow rates and gas-liquid ratios in an open tube along with the added feature of taking slow-motion movies in both flow channels.

Description of Apparatus

In Figure 1, it can be seen that the apparatus is somewhat similar to the type of flow assembly which has been used by previous investigators with provisions to take such measurements as:

(1) Flow rates of both gas and liquid phases.
(2) Shut-in ratios of liquid to gas.
(3) Pressure drops over the flow section.

Discussion of Experimental Results

Open 2-in. Tube

In Figure 2, it is seen that the pressure drop decreases as the mass velocity of the air increases up to a rate of 5 lb./sec./ft.[2] of open tubing for a low water rate of 10 lbs./sec./ft.[2] For higher liquid rates, the pressure drops also decrease to minima at slightly higher air rates. To the left of these minima the flow type is primarily that of slugging. At very low air rates not shown on the graph, bubbles with occasional bullet-shaped pistons work their way slowly upward through the liquid. In this region of extremely low air flow rates, it was difficult to maintain steady-state conditions from the standpoint of pressure drop as well as flow rates of air and water. With no air or water flow the pressure drop would, of course, be the liquid head of water standing in the pipe, or 62.4 lbs./ft.[2]/ft. of liquid height, or with air only 0.076 lbs./ft.[2]/ft.

To the right of the minima, spray flow sets in with frothy annular rings of air-water bubbles and droplets moving at relatively slow rates along the walls of the pipe. In the central spray of water droplets, the velocity was much faster. These visual observations were clearly perceptible only through the showing of slow-motion movies resulting from high-photography at 800 frames/sec. When shown on the screen, the motion was slowed down to 24/800 or 1/33 of normal motion.

Flow through the 2⅛-in. x 1 5/16-in. Annulus

In Figure 3, it is easy to see that the pressure drop curves sweep through minima, however, at lower air mass velocities than those encountered in the open 2⅛-in. tube with slugging to the left and spray-annular flow to the right. With a larger wetted-wall area per unit area of cross-sectional flow, one would expect a lesser tendency for slugging in annuli. It is to be observed, however, that the minima for pressure drop drift toward the left with increasing water rates rather than to the

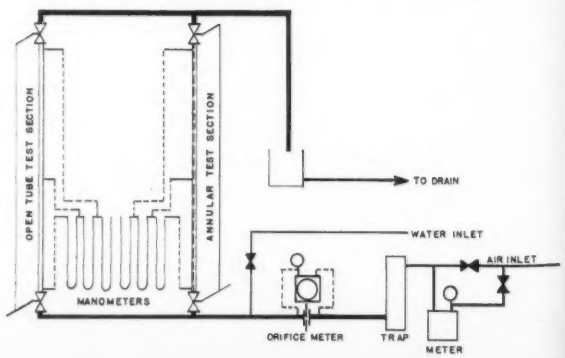

Figure 1—Flow diagram of test apparatus.

[1]*Manuscript received February 15; accepted July 12, 1961.*
[2]*Phillips Petroleum Company, Borger, Texas, U.S.A.*
[3]*School of Chemical Engineering, College of Engineering, University of Oklahoma, Norman, Oklahoma, U.S.A.*
Based on a paper presented at the National Meeting, American Institute of Chemical Engineers, Tulsa, Oklahoma, September, 1960.
Contribution from the College of Engineering, University of Oklahoma, Norman, Oklahoma, U.S.A.

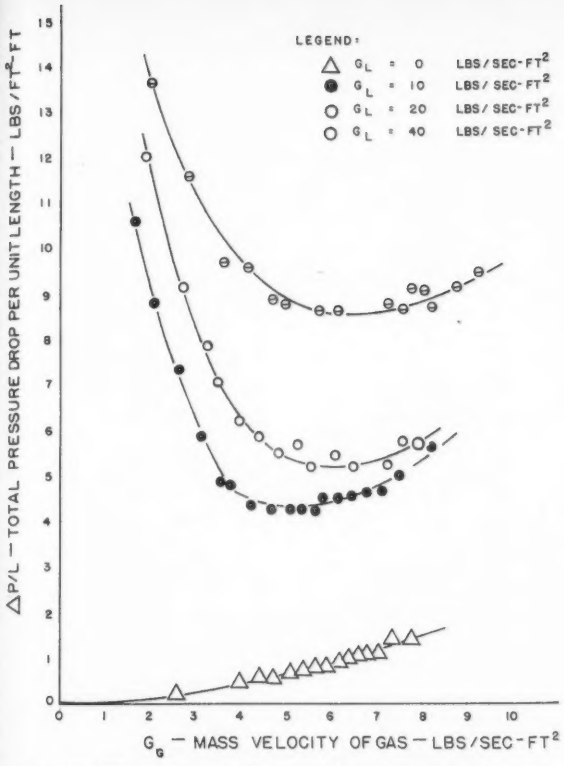

Figure 2—Flow of air and water through the 2⅛-in. open tube.

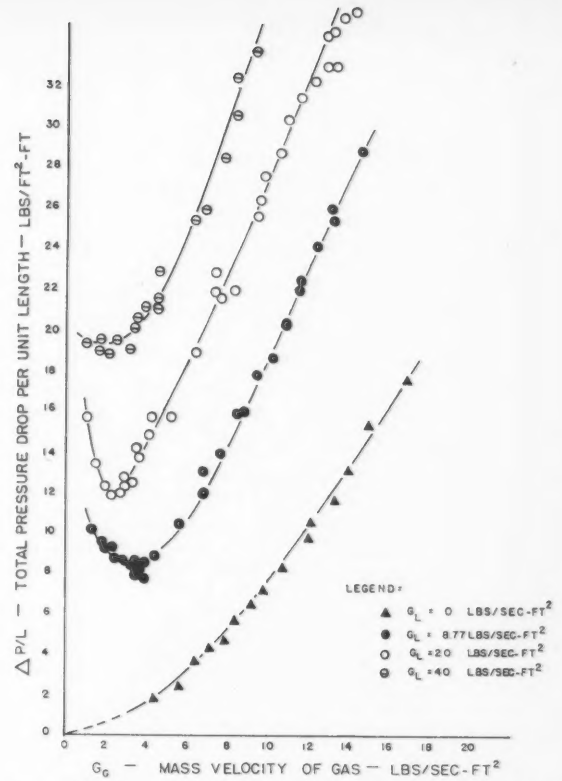

Figure 3—Flow of air and water through the 2⅛-in. x 1 5/16-in. annulus.

right as was the case with the open tube. No satisfactory explanation can be given as yet for this reversal in trend.

The higher pressure drops in the annulus over those in the open tube with the same cross-sectional area can be accounted for from the mean hydraulic radius, namely the cross-sectional area divided by the total wetted-wall perimeter of the inner and outer tubes.

"Sweep" and "Slippage" Studies

In the concurrent flow of gas and liquid through pipes in various positions, it has been found that the gas generally flows at a higher linear velocity than the liquid. This fact can be proved experimentally by shutting in the flow section during a run and measuring the amount of each phase *in place* or *in situ*. In Figures 4 and 5, graphs present a comparison of the *in place* vs the flowing ratios of liquid to gas by weight.

Petroleum engineers make these comparisons in order to obtain *slip velocity* or the velocity of gas compared to that of the liquid. Other investigators have termed these flow phenomena as sweep efficiency curves by stating that the fractional sweep efficiency is the flowing over the *in place* ratio of liquid to gas. For example in Figure 4 the sweep efficiency for water flowing at 10 lbs./sec./ft.^{2} has a fractional sweep efficiency of 0.05 when the flow ratio is 2.5 and the corresponding *in place* ratio is 50. At higher liquid flow rates, the sweep efficiency is considerably greater for the same flowing ratio.

In the case of the annulus (Figure 5), the sweep efficiency is considerably higher, especially at the higher water rate of 40 lbs./sec./ft.^{2} where the two ratios approach each other at the no-slippage line or equal linear velocities of gas and liquid.

"Lift" Efficiencies

The engineer is primarily interested in the conservation of energy in all industrial operations. For this reason Figures 6 and 7 were prepared in order to show the lift efficiency or the

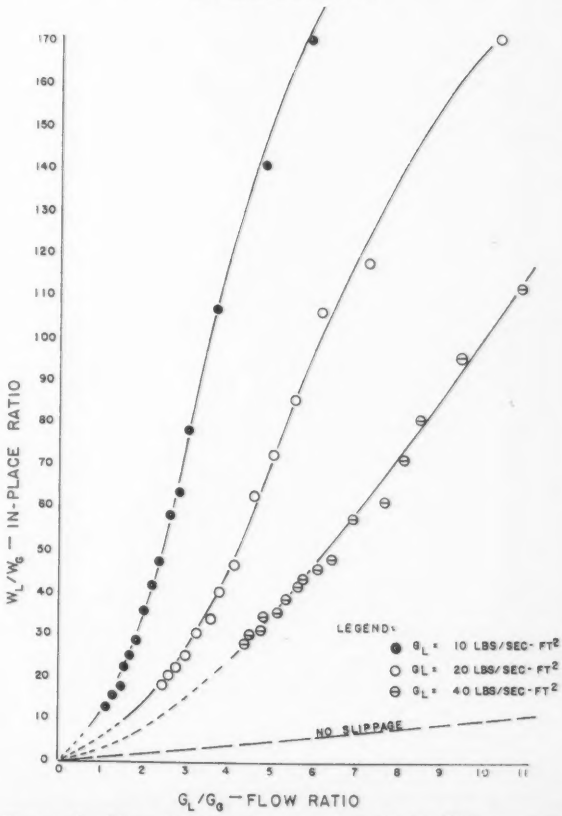

Figure 4—Flow of air and water through the 2⅛-in. open tube.

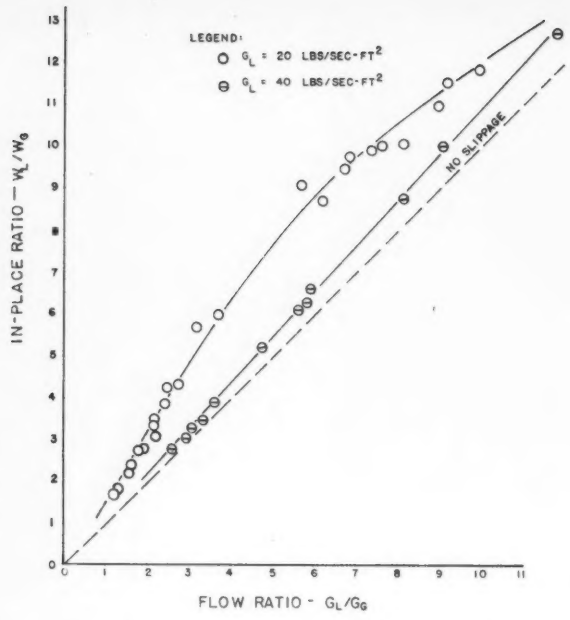

Figure 5—Flow of air and water through the 2⅛-in. x 1 5/16-in. annulus.

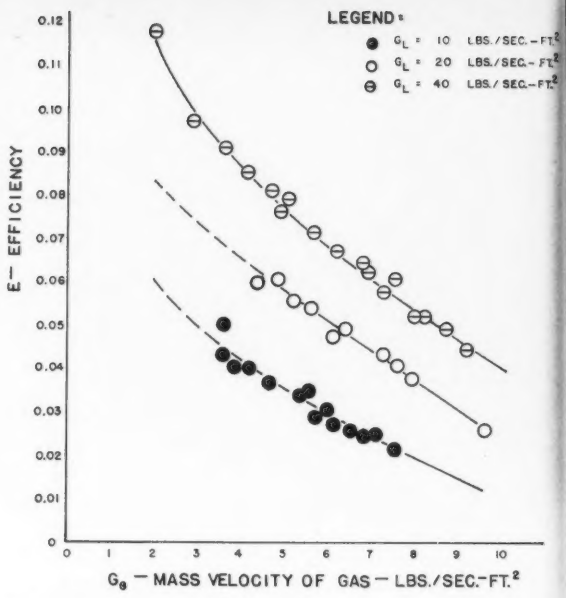

Figure 6—Flow of air and water through the 2⅛-in. open tube.

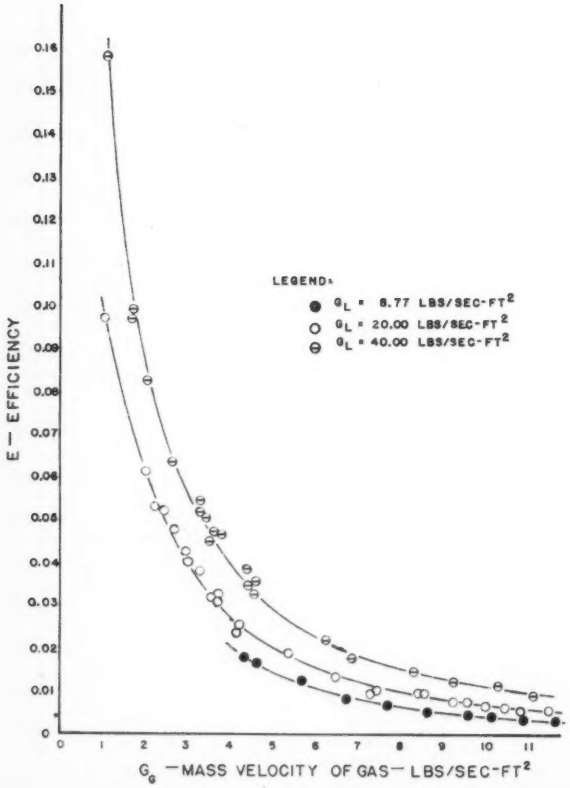

Figure 7—Flow of air and water through the 2⅛-in. x 1 5/16-in. annulus.

ratio of the actual work of lifting the liquid vertically compared to the work done by the air in expanding isothermally from the base to the top of the pipe section.

Over the range of ratios and flow rates which were studied in this experimental investigation, the efficiencies proved to be higher in the open tube than they were in the annulus. These efficiencies varied inversely with the gas-liquid ratios in these ranges; however, an earlier study[4] showed that the lift efficiency curve went through a maximum of 0.42 at a low ratio of gas to liquid and then fell off to zero with no flow of gas.

Strange as it may seem, the lift efficiency runs inversely proportional to the sweep efficiency values. In other words the lift efficiency was high when slugging was taking place and the liquid was making numerous trips up and down the tube; however, the air was being recompressed intermittently by the downward slippage of the water giving the air more than one chance to push upward against the water.

On the spray-annular side of the picture, better sweep-outs were being obtained; however, much of the air was flowing upward between the droplets in the spray without doing any actual lifting of the water, hence the lower lift efficiencies with the higher gas-liquid flowing ratios.

Motion-picture Studies

One of the principal objectives of these vertical flow studies has been that of obtaining a clear picture of the flow types or patterns which take place in the tube or annulus with various flow rates and ratios of gas to liquid. Unfortunately the written word or even a series of "still" photographs cannot convey adequately the visual story to the reader of the published page. Neither can the naked eye see what is taking place when rapid changes are taking place under certain flow regimes. For this reason during each "normal motion" flow, a second camera took a concurrent motion picture record of the flow at 800 frames/sec., thereby stretching out by time a factor of 33 when displayed to the viewer at the normal rate of 24 frames/sec. High-speed film and intensive lighting were required in order to give the required visibility on the movie screen.

Description of Flow Types in Open Tube

For the benefit of the reader who will not have the opportunity of seeing the film, an attempt will be made to present a

Figure 8a—(Air-Water) slug flow in open 2⅛-in. tube. Water rate — 20 lb./sec./ft.²; Air rate 0.5 lb./sec./ft.². White strip is one foot in height.

Figure 8b—(Air-Water) spray-annular flow is open in 2⅛-in. tube. Water rate 20 lb./sec./ft.²; Air rate 10 lb./sec./ft.². White strip is one foot in height.

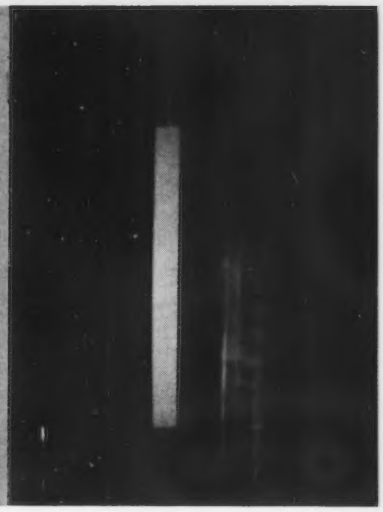

Figure 8c—(Air-Water) spray-annular flow through 1 5/16-in. x 2⅛-in. annulus. Water rate 20 lb./sec./ft.²; Air rate 16.67 lb./sec./ft.². White strip is one foot in height.

word picture of the flow types which took place in an open 2⅛-in. I.D. tube, as water was moving vertically upward at 20 lbs./sec./ft.² of open tubing. Air was first passed through the tube with the water, at a very slow rate, appearing as dispersed bubbles with an occasional bullet-shaped piston, the round nose being at the top of the slow-moving piston. A normal motion view with the naked eye gives one an adequate concept of this flow type.

Holding the water rate constant at 20 lbs./sec./ft.²., the air rate was increased to 0.5 lbs./sec./ft.² causing pronounced slugging as shown in Figure 8A. In the top half of the tube in the left-hand side of the photograph, the upward moving frothy slug can be seen, whereas the water in the bottom half of the section is slipping downward along the wall of the tube soon to meet a frothy slug moving upward in the center of the tube where the linear velocity is higher. Thus one can observe under slow motion, downward slippage of water along the inner tube wall and simultaneously upward movement of the frothy mixture of air and water in the center of the tube. The one-foot white strip has been placed to the right of the tube, so as to make it possible to time the period for the slug to move one foot under slow motion.

With the same water rate (20 lbs./sec./ft.²), the air rate is again increased to 10 lbs./sec./ft.² causing spray-annular flow as shown in Figure 8B. The water droplets in the spray are moving upward at an estimated velocity of 100 ft./sec. through the center of the tube, whereas a small fraction of the total water stream is moving along the inner wall of the pipe as annular frothy rings at linear velocities, ranging from 5-10 ft./sec.

Flow Types in Annular Flow

Let us maintain the same mass velocity of water in the annulus, namely 20 lbs./sec./ft.², as we did in the open tube. As air is flowed upward at a very slow rate, dispersed bubbles work their way upward through the water but the central inner tube (plugged at both ends) prevents the formation of bullet-shaped pistons. Referring to Figure 3, slugging takes place up to 2.5 lbs./sec./ft.² for the air flow rate, with frothy air-water slugs moving upward in the center of the annulus, while downward slippage of water occurs simultaneously along the wetted walls of the inner and outer tubes, especially at the trailing end of each slug.

With the same fixed-mass velocity of water, the air rate is increased to 16.67 lbs./sec./ft.² with the result that spray-annular flow takes place as it did with a high air rate in the open tube (Figure 8C).

Acknowledgement

The authors wish to express their appreciation to undergraduate seniors, namely Byron Capita, Robert LaFon, Eugene Wood, and R. C. Robinson, for their assistance in constructing the apparatus and in taking data. G. O. Kimmell of Kimray Inc., Oklahoma City, supplied pressure regulators gratis. A. R. Baldwin of Hughes Tool Company took the high-speed motion pictures without any charges for his services. Maloney-Crawford Tank and Manufacturing Company and the Natural Gas Supply Men's Association provided financial assistance in the form of scholarships and fellowships.

References

(1) Baxendell, P. B., Trans. Am. Inst. Mining, Met. Petrol. Engrs. T.P8027, 213 (1958).

(2) Bergelin, O. P., et al. Co-Current Gas-Liquid Flow in Vertical Tubes, Heat Transfer and Fluid Mechanics Inst., Berkeley, Calif. (1940).

(3) Brown, R. A. S., Sullivan, G. A., and Govier, G. W., Can. J. Chem. Eng. **38,** 62 (1960).

(4) Cromer, S., et al. Visual Studies of Air-Water Flow in a Vertical Pipe, AIME Tech. Pub. No. 1080, 136 (1940).

(5) Gosline, J. W., Expts on the Vertical Flow of Gas-Liquid Mixtures in Glass Pipes, ASME Trans. **118** (1936).

(6) Govier, G. W., Radford, B. A., and Dunn, J. S. C., Can. J. Chem. Eng. **35,** 58 (1957).

(7) Govier, G. W., and Short, W. Leigh, Can. J. Chem. Eng. **36,** 195 (1958).

(8) Poettman, F. H., et al. The Multiphase Flow of Gas, Oil and Water through Vertical Flow Strings, API Division of Production, March (1952).

(9) Uren, L. C., Flow Resistance of Gas-Oil Mixtures, etc. AIME Trans. (1930).

(10) Versluys, J., Math. Dev. in Theory of Flowing Oil Wells, AIME Trans. 118 (1930).

★ ★ ★

Analysis of the Radiant Heat Absorption in the Boundary Layer Surrounding an Evaporating Drop[1]

T. W. HOFFMAN[2] and W. H. GAUVIN[3]

An approximate analysis is made of the effect of the absorption of thermal radiation on the temperature gradients surrounding an evaporating droplet which is suspended in a high temperature environment. The Hottel-Cohen method for calculating the radiant heat flux distribution in an enclosure containing an absorbing medium of non-uniform temperature, has been applied to the spherical symmetrical model of the system. Conduction and radial movement of the cold vapor from the droplet have been included.

The analysis shows that, at atmospheric pressure, the absorption of radiant energy in the boundary layer is very small and hence does not affect the temperature gradient nor the rate of heat transfer at the droplet surface.

This method of analysis, with the associated solution of the equations describing the reception factors, is quite general and can be applied to any spherical enclosure containing an absorbing medium whether it be one of concentric or hollow spheres.

Les auteurs recherchent l'influence de l'absorption de l'énergie rayonnante sur les gradients de température au voisinage d'une gouttelette qui s'évapore dans un milieu à température élevée. On applique à un modèle à la fois sphérique et symétrique de ce système la méthode Hottel-Cohen pour le calcul de la distribution du flux d'énergie rayonnante dans une enceinte contenant un milieu absorbant de température non uniforme. On a tenu compte de la condition de la vapeur froide ainsi que de son déplacement radial à partir de la gouttelette.

L'étude montre qu'à la pression atmosphérique l'absorption de l'énergie rayonnante dans la couche limite est très faible et par suite n'affecte pas le gradient de température ni le taux de transport de chaleur à la surface de la gouttelette.

Cette méthode d'analyse, qui inclut la solution des équations décrivant les facteurs de réception, est assez générale et peut s'appliquer à toute enceinte sphérique contenant un milieu absorbant, qu'il soit formé de sphères concentriques ou vides.

In a previous study[1], the evaporating rate of a stationary liquid droplet suspended in a high temperature atmosphere was shown to be affected by the evolution of the cold vapor. An additional heat load in the boundary layer was imposed by the sensible heat requirements of the evolved vapor and, as a result, the temperature profile was changed from what would be expected if there were no mass transfer. This effect is most important under free convection conditions, since the flow pattern around the drop is dictated largely by the buoyancy forces, which in turn arise by virtue of the different densities or temperatures in the boundary layer. Any change in temperature distribution is therefore expected to change the evaporation rate.

Since in many cases the vapors in the boundary layer of an evaporating drop are partially opaque to thermal radiation, it might be advanced that the absorption of radiant energy by these vapors might change the temperature profile in the boundary layer and thus affect the evaporation rate.

Filippov[2] has shown that the absorption of radiant heat by a nondiathermanous (or heteropolar) gas will seriously affect the heat transfer processes, especially at high temperatures and pressures. Under certain conditions, heat transfer rates may change much more rapidly than the temperature gradients. Smith[3] recognized that absorption of radiation in the boundary layer may affect the skin temperature of bodies in high speed flow. He proceeded to solve the Fourier-Poisson conduction equation, with a radiation absorption term included, but found, however, that the effect was small under his chosen conditions.

It is the purpose of the present analysis to determine the magnitude and distribution of the radiant energy absorbed in the boundary layer surrounding an evaporating droplet.

Analysis of Problem

In formulating the equations and boundary conditions describing the flow and temperature distribution around a droplet evaporating in high-temperature surroundings, the absorption of radiant energy in the boundary layer cannot be assumed to be negligible. The complete energy equation can thus be written in spherical co-ordinates:

$$(1/r^2)(\partial/\partial r)(kr^2\partial T/\partial r) + (1/r^2\sin^2\Psi)(\partial/\partial\Phi)(k\partial T/d\Phi) + (1/r^2\sin\Psi)(\partial/\partial\Psi)(k\sin\Psi\partial T/\partial\Psi) + (q_R)_G = (c_p\rho)\{(dr/d\theta)(\partial T/\partial r) + (d\Psi/d\theta)(\partial T/\partial\Psi)(1/r) + (d\Phi/d\theta)(\partial T/\partial\Phi)(1/r\sin\Psi)\} \quad (1)$$

where $(q_R)_G$ is the heat absorbed per unit gas volume. Equation (1) implies steady-state conditions. Because of its non-linearity

[1]*Manuscript received January 24; accepted July 25, 1961.*
[2]*Department of Chemical Engineering, McMaster University, Hamilton, Ont.*
[3]*Pulp and Paper Research Institute of Canada and McGill University, Montreal, Que.*
Contribution from the Pulp and Paper Research Institute of Canada and McGill University, Montreal, Que.

and that of the other boundary layer equations, a direct solution is impossible and certain simplifications must be made. The usual procedure is to neglect convection effects; this implies a spherical symmetrical model which allows radial flow of vapor and radial temperature gradients only. The spherical model leads to a relatively simple solution, which can be used to justify any assumptions concerning the absorption of radiation in the boundary layer, a posteriori.

Goldsmith and Penner[4] have shown that this model allows Equation (1) to be written in the integral form:

$$4\pi r^2 k(dT/dr) + (q_R)_G = (dm/d\theta)\lambda - q_R + (dm/d\theta)\int_{T_d}^{T} c_p\,dT \quad \ldots(2)$$

the solution of which is more convenient, particularly when the gas properties are not taken at mean film conditions but are considered to change with temperature.

The simplest solution is obtained when the absorption of radiation in the gas is neglected, the heat capacity of the gas is assigned an average value and the thermal conductivity is assumed to vary linearly with temperature, i.e., $k = k_o + \gamma T$.* Under these conditions, it has already been shown[1] that Equation (2) can be integrated from the drop radius to any point r (which may be the effective radius of the boundary layer r_b) to yield:

$$(1/r_d - 1/r) = [4\pi k_o \ln(1 + c_p\Delta T/\lambda')]/c_p(dm/d\theta) + \{(4\pi\gamma\lambda')/[(dm/d\theta)\,c_p^2]\}\{[\ln(1 + c_p\Delta T)/\lambda'] - [c_p\Delta T/(\lambda' + c_p\Delta T)]\} \quad \ldots(3)$$

where $\lambda' = \lambda - |q_R/(dm/d\theta)|$ and $\Delta T = T - T_d$.

Equation (3) allows the temperature distribution to be calculated for any given set of conditions and evaporation rate.

To calculate the effect of absorption of radiant heat in the boundary layer, it is not enough to know only the overall amount of heat which is transferred to the gas by radiation, but it is necessary to know also the distribution of this absorption in the boundary layer. The net transfer of heat to any spherical gas shell surrounding the drop will depend not only on the temperature of this shell, but also on its volume.

Since the temperature varies continuously throughout the boundary layer, gas shells of differential thickness should be considered. However, because of the integral character of radiation,** finite thickness must be considered.

The method of solution adapted here is an extension of the method presented by Hottel and Cohen[5] for calculating the radiant heat flux and distribution in an enclosure which contains a temperature-varying absorbing gas.

Briefly this method consists of dividing the system into a number of surface-gas zones, the size of which depends primarily on the temperature variation throughout the system. Although each zone should be isothermal, some variation in temperature can be tolerated as long as a representative temperature can be assigned to it. The procedure then is to write heat and material balances for each zone in turn. This requires a knowledge of the radiant interchange view-factors or reception factors (using Hottel and Cohen's terminology), for each of the zones, making due allowance for the absorption of radiation by the intervening gas.

*The latter two assumptions are reasonable since for water vapor, the heat capacity varies from 0.455 at 100°C. to 0.510 (cal.)/(g.)(°C.) at 500°C. and the thermal conductivity over this same temperature interval is satisfactorily represented by the Equation $k = (57 \times 10^{-6}) + (19.5 \times 10^{-8})(T - 100) + (2 \times 10^{-11})(T - 100)^2$ (cal.)/(sec.)(cm.)(°C.).

**The heat transferred by radiation to any one point is the sum of all radiation to that point from all radiators in the system. Therefore, any change at one point influences the heat transfer in the whole system.

Specifically, the problem under consideration involves the evaporation of a droplet in a high-temperature gas enclosed in a container which is very large compared to the size of the droplet. Moreover, the temperature of the wall is the same as that of the gas. Under these conditions, the following two facts are immediately apparent:

(1) All radiation absorbed in the gas outside of the boundary layer must be re-emitted, so that no attenuation of radiation results in this medium. As a consequence of this, the radiation reaching the drop and its immediate environment is the same as that transmitted to this region if it were suspended in a non-absorbing medium;

(2) since the area of the container walls is very much larger than that of the droplet, the radiation reaching the droplet is independent of the wall emissivity.

Hence the droplet and the boundary layer "see" only a black environment. The model now takes the form of an inner droplet surrounded by a concentric sphere with radius equal to r_b and with absorptivity (emissivity) equal to one. The outer surface is completely pervious to the radial flow of vapors from the evaporating drop.

The intervening gas volume between the drop and the outer imaginary surface, which constitutes the boundary layer of the drop, was divided into a number of spherical gas shells according to Figure 1. A surface zone, s, located at r is described by the subscript number equal to its radius relative to the radius of the drop. Similarly any gas zone g is indicated by the subscript number equal to its inner radius relative to the droplet radius. Thus gas zone g_2 is the spherical shell volume contained between r/r_d equal to 2 and 2.5. This nomenclature is shown on Figure 1. The inner volumes are of smaller thickness, since the temperature variations are most extreme in these regions.

In formulating the reception factors for the system in this method of solution, the key parameter is the absorption coefficient k of the gas, which is a measure of the absorption strength of the absorbing medium. For a grey gas, $\underline{k}$ is constant over the full wave-length spectrum and the expression relating the emissivity and absorptivity of a gas to the absorption coefficient is

$$a = \epsilon = 1 - e^{-\underline{k}l} \quad \ldots(4)$$

where l is the thickness of the gas.

Absorption and emission of thermal radiation by a real gas occur only over part of the wave-length spectrum. Hottel[6] has thus proposed that an actual real gas can be replaced by a grey and a clear gas. The grey gas, with absorption coefficient $\underline{k}$, can be thought of as occupying fraction a of the spectrum, and the clear gas ($\underline{k} = 0$) as occupying the fraction $(1 - a)$. In essence, this scheme is one of fitting an emissivity-versus-path length curve to an exponential equation of the form:

$$\epsilon_L = a(1 - e^{-\underline{k}l}) \quad \ldots(5)$$

The parameters a and $\underline{k}$ depend on the conditions and dimensions of the system under consideration. In most industrial systems in which the surface reflectivity is low, these variables can be found, by fitting Equation (5) to the gas emissivity data at L, equal to the mean beam length,* and at $2L$ such that:

$$\underline{k}L = \ln[\epsilon_L/(\epsilon_{2L} - \epsilon_L)] \quad \ldots(6)$$

$$a = (\epsilon_L)^2/(2\epsilon_L - \epsilon_{2L}) \quad \ldots(7)$$

Hottel[6] has shown that the mean beam length for any enclosure is $4V/A_s$ as $P_G L$ approaches zero. In the system under considera-

*The mean beam length is the radius of a hemisphere of gas which absorbs the same radiant flux from a surface located at the centre of its base, as the gas in the enclosure absorbs from the radiating surfaces.

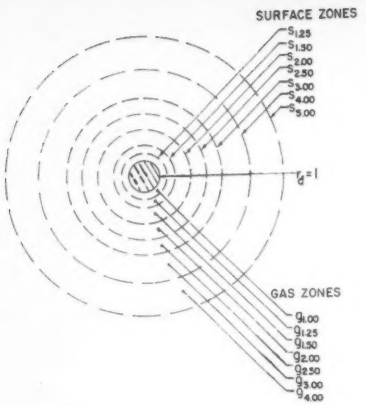

Figure 1—Diagram showing spherical surfaces and gas zones upon which reception factors are based.

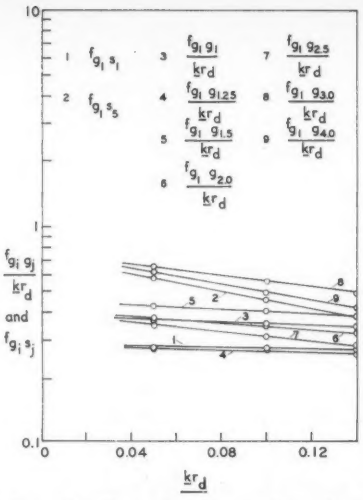

Figure 2—Reception factors for spherical system of Figure 1 for $g_{1.0}$.

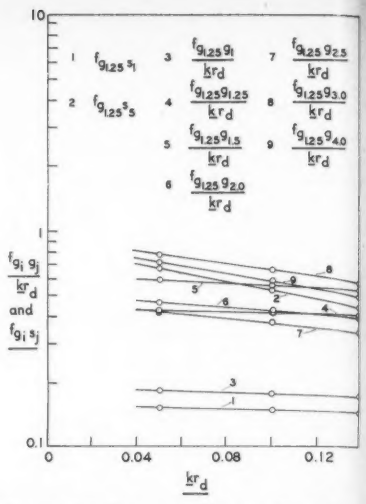

Figure 3—Reception factors for spherical system of Figure 1 for $g_{1.25}$.

tion the P_GL product is very small and hence $L = 0.667\ D_b$, where D_b is the diameter of the effective boundary layer*. Hence Equation (6) becomes

$$\underline{k}r_d = (3/2)\,(r_d/D_b)\,ln[\epsilon_L/(\epsilon_{2L} - \epsilon_L)] \quad \ldots\ldots\ldots\ldots (8)$$

The effective diameter of the boundary layer can be calculated from Equation (3), since all other variables are known from the experimental data.

The emissivity and absorptivity of a gas depends on the temperature of the gas and moreover the absorptivity depends on the temperature of the radiating source. Hottel[6] has shown that both the absorptivity and emissivity of a gas can be approximated by

$$\epsilon_G = \epsilon_{ave}[(4 + d + b - c)/4] \quad \ldots\ldots\ldots\ldots (9)$$

where d and b are the slope of the $(ln\ \epsilon_G)$ — vs. — $(ln\ P_GL)$ and $(ln\ \epsilon_G)$ — vs. — $(ln\ T)$ curves, respectively, and c is an empirical constant (equal to 0.45) used in evaluating gas absorptivity from gas emissivity data. ϵ_{ave} is found from the available emissivity plots[6] at the average of the surface and gas temperatures (this procedure is not recommended when the surface and gas temperature differ by more than a factor of two). Using these average values of gas emissivity, the absorption coefficient and the fraction a may be calculated for this case from Equations (6) and (7).

Cohen(7) has shown that the emissivity of a gas may also be expressed on a volume basis and that it is equal to $4\underline{k}$. Hence the emission rate of a gas volume dV** is

$$E = 4\underline{k}dV\,\sigma\,T_G{}^4 \quad \ldots\ldots\ldots\ldots (10)$$

Returning to the main problem, the reception factors between any two zones in the model must be known as a function of the gas absorption strength before a solution can be attempted. In general, these factors express the fraction of the energy originating in or at any zone which reaches and is absorbed in or at another zone. Surfaces are considered to be completely absorbing. The formulation of these factors is given in Appendix A and the resulting plots of these factors as a function of $\underline{k}r_d$ are given in Figures 2 to 9.

By definition, the one-way flux from surface s_i to s_j is given by

$$A_{s_i} \cdot f_{s_i s_j}\,\sigma\,T_{s_i}{}^4 = q_{s_i \to s_j} \quad \ldots\ldots\ldots\ldots (11)$$

$A_{s_i}\,f_{s_i s_j}$ has been termed a direct-interchange area[5] and is designated by $\overline{s_i s_j}$. Similarly be definition

$$\overline{s_i g_j} = A_{s_i} \cdot f_{s_i g_j} \quad \ldots\ldots\ldots\ldots (12)$$

and

$$\overline{s_i g_j} = \overline{g_j s_i} = 4\underline{k}V_{g_j} \cdot f_{s_j s_i} \quad \ldots\ldots\ldots\ldots (13)$$

since, from the first two laws of thermodynamics, the net interchange must be zero when the temperatures of these zones are the same. For gas-to-gas interchange

$$\overline{g_i g_j} = \overline{g_j g_i} = 4\underline{k}V_{g_i} f_{g_i g_j} \quad \ldots\ldots\ldots\ldots (14)$$

When using these interchange areas, each must be multiplied by the fraction a, since the gas is capable of radiating and absorbing energy only over a fraction of the wave-length. Over the remainder of the spectrum the gas-to-gas and gas-to-surface factors are zero.

These factors are applicable to a black-walled system; in those cases where the droplet does not have a high absorptivity, some consideration must be given to the transmitted and reflected part of the radiation striking the drop. These effects can be accounted for approximately by the methods described in Appendix B.

Since sharp temperature variations occur in the boundary layer, an effective temperature must be assigned to each gas zone. The effective temperature of any gas zone must account for the increasing volume of gas at points furthest removed from the drop, as well as for the changing temperature over the given zone. By definition, the effective temperature must be such that:

$$\begin{aligned} q_{g_i} &= 4\underline{k}a\ V_{g_i}\,\sigma\,T_{eff}{}^4 \\ &= 4\underline{k}a\ [(4/3)\,\pi\,(r_2{}^3 - r_1{}^3)]\,\sigma\,T_{eff}{}^4 \\ &= 4\underline{k}a\,\sigma \int_{r_1}^{r_2} 4\pi r^2 \cdot T_r{}^4\,dr \quad \ldots\ldots\ldots\ldots (15) \end{aligned}$$

The subscripts 1 and 2 indicate the inner and outer limits of the gas zone. Over the small radial distances in question, T may be considered to vary linearly with r, such that:

$$(T - T_1)/(T_2 - T_1) = (r - r_1)/(r_2 - r_1) \quad \ldots\ldots\ldots\ldots (16)$$

*If a more accurate estimate of the mean beam length of a spherical enclosure is required, use may be made of the following relationship (based on an analysis presented in a recent paper(12)):

$$[\Phi_i = \sum_{i,j} (1 - f_{g_i g_j})\ V_{g_i}/V_i]$$

where i, j = 1.0, 1.25, 1.5, 2.0, 2.5, 3.0, 4.0.
and the mean beam length, L, is defined by the equation:

$$4\underline{k}\ V_i\,\Phi_i/A_i = 1 - e^{-\underline{k}l}$$

The correction in the present case is negligible.

**Simpson (8) has indicated that $\sigma\,T_G{}^4$ is the emission rate per unit area of black surface into a vacuum and that this should be modified for other media by multiplying by the square of the refractive index. Since the refractive index of most gases is near one, this factor can be ignored.

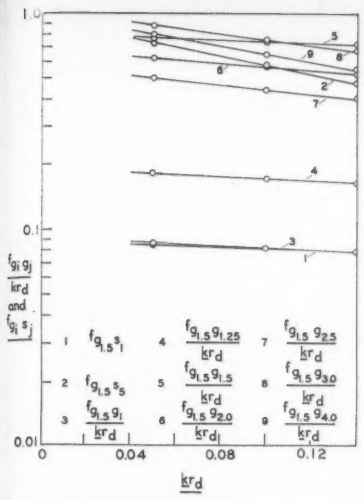

Figure 4—Reception factors for spherical system of Figure 1 for $g_{1.5}$.

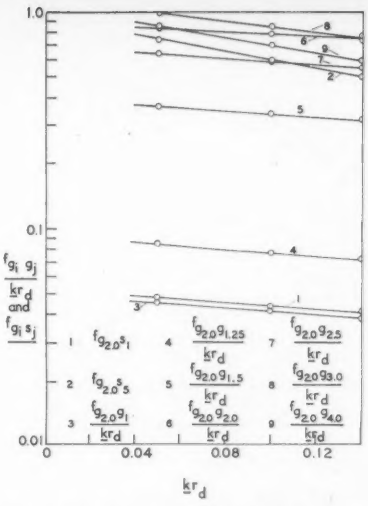

Figure 5—Reception factors for spherical system of Figure 1 for $g_{2.0}$.

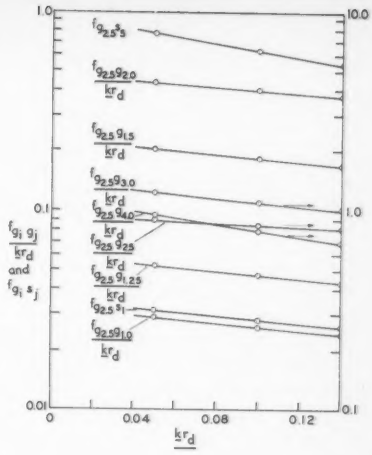

Figure 6—Reception factors for spherical system of Figure 1 for $g_{2.5}$.

This allows Equation (15) to be integrated to yield:

$$T_{\text{eff}}^4 = \left(\frac{3}{r_2^3 - r_1^3}\right)\left(\frac{r_2 - r_1}{T_2 - T_1}\right)^3 \left[T_2^5\left(\frac{T_2^2}{7} + \frac{\eta T_2}{3} + \frac{\eta^2}{5}\right) - T_1^5\left(\frac{T_1^2}{7} + \frac{\eta T_1}{3} + \frac{\eta^2}{5}\right)\right] \quad \ldots\ldots(17)$$

where

$$\eta = \{[(T_2 - T_1)/(r_2 - r_1)]r_1\} - T_1 \quad \ldots\ldots(18)$$

The heat and material balances on each gas zone, g_j, thus take the form:

Heat conducted into zone g_j from the outer adjacent zone.	=	Heat conducted out of zone g_j into the adjacent inner zone.
+ Sensible heat associated with vapor flow into g_j from the inner adjacent zone.	=	+ Sensible heat associated with the vapor flow out of g_j.
+ Radiation into g_j from all other surface and gas zones.	=	+ Radiation leaving g_j to all other surface and gas zones.

Expressed mathematically:

$$X_2 + [(dm/d\theta)c_pT]_{r_2} + \sum_i \overline{s_i g_j}\,\sigma\, T_{s_i}{}^4 + \sum_i \overline{g_i g_j}\,\sigma\, T_{g_i}{}^4 = X_1 + [(dm/d\theta)c_pT]_{r_1} + [\sum_i \overline{g_j s_i} + \sum_i \overline{g_j g_i}]\,\sigma\, T_{g_j}{}^4 \quad \ldots\ldots(19)$$

where

$$X_i = [k\,A\,(dT/dr)]_{r_i} \quad \ldots\ldots(20)$$

Equation (3) can be used to calculate an approximate temperature profile in the boundary layer, which provides a convenient starting point. In this way, temperatures may be assigned to the boundaries of each zone and the effective temperatures calculated from Equation (17). The conduction terms[2] appear as unknowns in the balance equation. However, the evaporation rate at the drop surface (subtracting the direct radiation contribution) is a boundary condition which enables these terms to be evaluated at every point in the boundary layer (Equation (19)). Substituting the values of the thermal conductivity and area at the respective boundary allows a calculation of the temperature gradient at each point. The resulting curve of $(dT/dr)_{r_i}$ versus r_i can be graphically integrated to yield the temperature distribution which accounts for

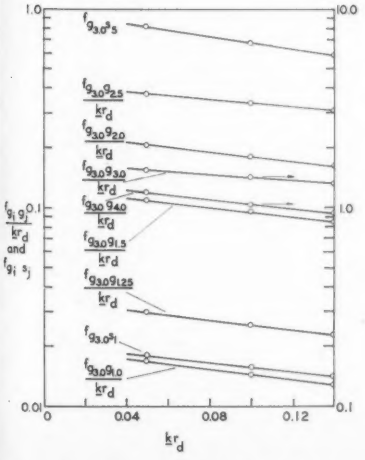

Figure 7—Reception factors for spherical system of Figure 1 for $g_{3.0}$.

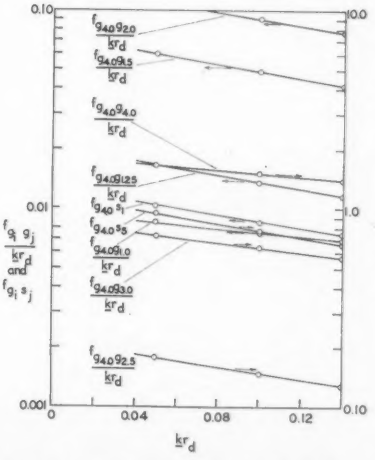

Figure 8—Reception factors for spherical system of Figure 1 for $g_{4.0}$.

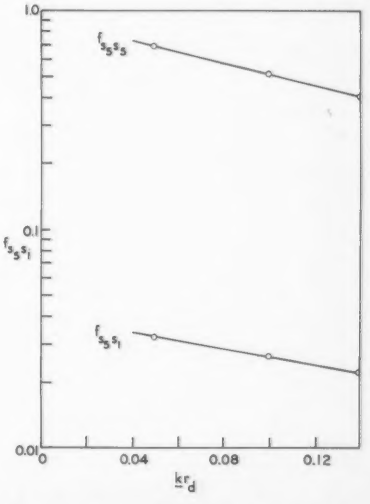

Figure 9—Reception factors for spherical system of Figure 1 for s_5.

TABLE 1

RESULTS OF CALCULATED TEMPERATURE PROFILE IN BOUNDARY LAYER WITH AND WITHOUT RADIATION TO THE GAS

Gas Zone i	$X_{i+1} - X_i$ (No Radiation to Gas) $\times 10^4$	$X_{i+1} - X_i$ (Radiation to Gas) $\times 10^4$	dT/dr $\times 10^{-4}$ °C./cm. (With and Without Radiation)	T_{G_i} (inner boundary) °C. (With and Without Radiation)
1.00	48.8	48.5	1.497	100
1.25	30.3	29.9	0.772	235
1.50	38.8	37.7	0.493	313
2.00	26.1	25.4	0.256	402
2.50	10.6	11.9	0.158	453
3.00			0.110	487

the radiation absorption phenomenon and changing gas properties in the boundary layer. This iterative procedure is repeated until the calculated temperature profile coincides with the assumed one. In those cases where the gas absorbs an appreciable amount of radiation, the direct radiation to the drop will have to be reduced accordingly, which in turn results in a higher temperature gradient at the drop surface to effect the same evaporation. This calculation can also be performed excluding the adsorption/emission of radiation by the gas, but including the effect of temperature on thermal conductivity and heat capacity. The difference then is a measure of the effect of radiation

It must be pointed out that this calculation is not intended to show the effect of radiation on the boundary conditions, i.e., evaporation rate and boundary layer thickness. It merely gives an appreciation of the magnitude of this phenomenon and its effect on the temperature profile under a given set of conditions and for the assumed model:

Example

Diameter of water droplet	1000 microns
Temperature of gas and wall	500°C.
Evaporation rate	73.5×10^{-6} g./sec.
Direct radiation to the droplet without attenuation by the boundary layer ($a_p = 0.90$)	12.9×10^{-3} cal./sec.
r_b/r_d [Equation (3)]	2.75

The boundary layer was assumed to extend to three times the droplet diameter for the calculation of the mean beam length for the system. By the methods already described, a and $\underline{k}r_d$ were calculated to be 0.065 and 0.10 respectively. The initial assumed temperature profile, as shown on Figure 10, was calculated with $(k)_{r_d} = 57 \times 10^{-6}$ (cal.)/(sec.) (°C.) (cm.); $\gamma = 19.5 \times 10^{-6}$ and $(c_p) = 0.480$ (cal.)/(g.) (°C.). The results of the calculations are shown in Table 1 and Figure 10 illustrates the comparison of the temperature profiles with and without radiation to the gas.

Discussion of Results

The absorption of radiation in the boundary layer is very small and has a negligible effect on the temperature profile around the drop, and hence does not influence the droplet evaporation rate. In other words, the gas is not sufficiently opaque at atmospheric pressure to absorb an appreciable amount of radiation. Increasing the pressure of the gas is known to broaden the absorption bands[9] and in general to increase the absorption power of a gas considerably. Under these conditions of higher pressures and possibly at higher temperatures, the radiation energy absorbed in the boundary layer might become appreciable[2], in which case the temperature gradients around the drop would be different. This would in fact result, since the radiant heat transfer direct to the drop would be reduced, and for any given evaporation rate this would necessitate a sharper temperature gradient at the drop surface. At points removed from the drop surface, the gradients would be smaller than expected because part of the heat load would be supplied by radiation, as Equation (19) shows.

Conclusions

An analysis based on a spherical symmetrical boundary layer model and neglecting any convection effects has been presented for an evaporating droplet in high temperature surroundings. An iterative method of solution was adopted, based on mass and energy balances which took into account heat transfer by conduction and radiation as well as the sensible heat transfer associated with radial vapor flow, under conditions of changing gas properties with temperature. The gas was considered to be real, but its absorption strength was assumed to be constant throughout the spherical shell. It should be noted that this method of solution is quite general and its application to a cylindrical system has been discussed in a recent paper[12].

Calculations showed that for a drop of about one millimeter in diameter, the temperature profiles with and without absorption of radiation by the boundary layer are practically identical. These findings substantiate the assumption of negligible absorption of radiation in the boundary layer which was made in a previous investigation[1]. It is impossible, in the present state of knowledge, to extend this analysis to take into account the convection currents set up by the cold vapor in the boundary layer of an evaporating droplet. Although these convective effects will undoubtedly modify the temperature profiles calculated in the present analysis, they could not conceivably cause greater absorption of radiation by the boundary layer.

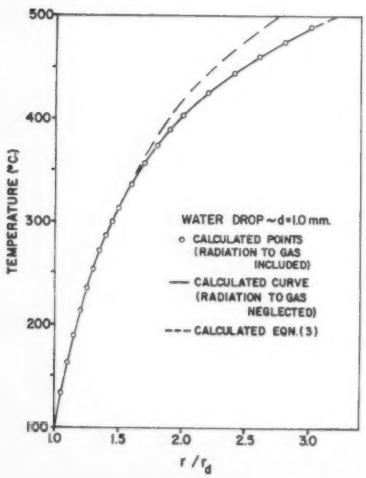

Figure 10—Comparison of calculated results.

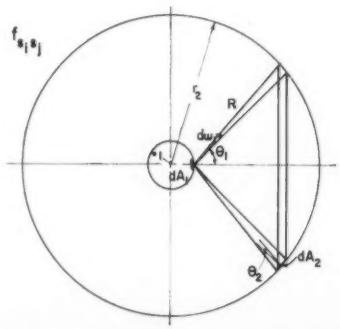

Figure 11 — Spherical system upon which the formulation of f_{s1s2} is based.

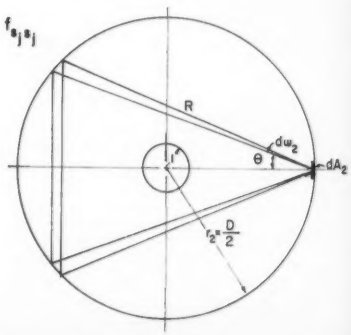

Figure 12 — Spherical system upon which the formulation f_{s2s2} is based.

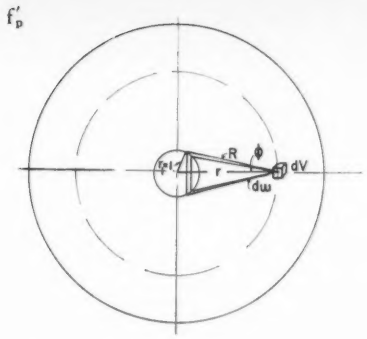

Figure 13—Spherical system upon which the formulation of f_p' is based.

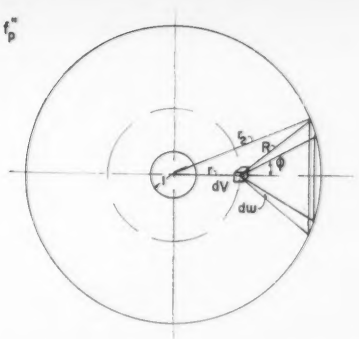

Figure 14—Spherical system upon which the formulation of f_p'' is based.

An important aspect of this study was the calculations of accurate reception factors for spherical systems up to a radius ratio (r/r_d) of 5, which are presented in Figures 2 to 9. Total interchange areas have also been worked out (see Appendix B) which allow for reflection at the surface of the inner sphere. It is believed that this information will become increasingly useful, in view of the growing number of high-temperature processes and applications in which radiant heat transmission plays an important part. With slight modifications, the analysis and method of solution presented in this paper could be applied to the evaporation and combustion of sprays of liquid fuels, the reduction of particles of metallic oxides, and various other chemical reactions in particulate systems. Although based on a simplified model, the information thus obtained would provide a better understanding of the actual, more complex situation.

It is interesting to note that very recently an analysis involving a heat-generating gas in a spherical system similar to the one discussed in this paper was presented by Sparrow, Usiskin and Hubbard[10]. By neglecting conduction and convection, and by assuming that the internal rate of heat generation was uniform, that the gas was grey and of uniform absorption coefficient (independent of temperature), and that the spherical enclosure was black-walled, an energy balance on an infinitesimal spherical volume dV was established, which permitted the ingenious formulation of a governing integral equation. The latter was solved by numerical means using an iterative method and the results for enclosing surfaces of equal temperature were given in the form of plots of the gas emissive power distribution (or temperature distribution) in the enclosure, as a function of the geometry or size of the system and for a wide variation in the value of the absorption coefficient. It is believed that the general method of solution discussed in the present paper could have been applied to this special case; its use would probably be required for the solution of the more general case, where the two enclosing surfaces are at different temperatures.

Acknowledgement

This paper is based on T. W. Hoffman's Ph.D. thesis (McGill University, 1959). Assistance from the Pulp and Paper Research Institute of Canada and from the National Research Council in the form of equipment grants is gratefully acknowledged. Recognition is due also to Dupont of Canada Ltd. for the use of their computing facilities and to H. H. Hearne, of the same company, for his assistance in the preparation of the computer program.

Nomenclature

Roman Symbols

a = weighting factor in Equation (5)
A_i = surface area, cm.^{2}
A_t = total surface of boundaries enclosing a volume of gas
b = slope, $\partial\ ln\ \epsilon_G/\partial\ lnT$
c = exponent on temperature ratio which allows the gas absorptivity to be evaluated from emissivity data
c_p = heat capacity, cal./(g.) (°C.)
D_b = diameter of effective spherical boundary layer, cm.
d = slope, $\partial\ ln\ \epsilon_G/\partial\ ln\ (P_GL)$
$-Ei(-y)$ = exponential integral of y
E = radiant energy emission rate, (cal.)/(sec.)
F = direct geometric view factor for black-walled system containing a non-absorbing medium = fraction of radiation leaving one zone which reaches and is absorbed by another (subscripts denote sender and receiver)
f_{ss},f_{sg},f_{gs} = reception factor for a black-walled enclosure containing an absorbing medium = fraction of radiation leaving one zone which reaches and is absorbed by another (subscripts denote sender, first, and receiver, second).
f_p' = fraction of radiation leaving an elemental volume of gas which reaches and is absorbed by an inner spherical black surface
f_p'' = fraction of radiation leaving an elemental volume of gas which reaches and is absorbed by an outer spherical black surface
G,g = gas zones
$\overline{GG},\overline{GS},\overline{SS}$ = total interchange areas for a grey-walled system containing an absorbing medium = area regulates the amount of radiation leaving any zone (first letter) which reaches and is absorbed by another zone (second letter), including the reflection at surface zones, cm.^{2}
$\overline{\overline{gg}},\overline{\overline{gs}},\overline{\overline{ss}}$ = direct interchange areas for a black-walled system containing an absorbing medium, calculated from f-factors, cm.^{2}
i,j = subscripts denoting any zone
k = absorption coefficient for the gas, cm.$^{-1}$
k = thermal conductivity, (cal.)/(sec.)(cm.)(°C.); k_o: at 0°C.
L = mean beam length, cm.
l = thickness of absorbing medium, cm.
m,n = subscripts denoting any zone
m = mass evaporated, g
P_G = partial pressure of absorbing gas, atm.
q_R = radiant heat transfer rate to droplet, cal./sec.
$(q_R)_G$ = radiant heat transfer rate to gas between droplet surface and radius r, cal./(sec.) (unit volume)
R = separating distance, cm., unless normalized
r = radius at any point in effective boundary layer, cm., unless normalized
r_b = radius of effective spherical boundary layer, cm.
r_d = droplet radius, cm.
S_i,S_j = surface zones
T = absolute temperature, °K.
T_d = droplet temperature, °K.
T_G = gas temperature, °K.
V = gas volume, cm.^{3} (V_t = total gas volume; V_{g_i} = volume of gas in zone i)
X_1,X_2 = defined by Equation (20)

Greek Symbols

α = absorptivity
α_p = absorptivity of particle
α_s = absorptivity of surface
γ = constant in thermal conductivity equation
ϵ = emissivity
ϵ_G = emissivity of gas
ϵ_L,ϵ_{2L} = emissivity evaluated at one and two mean beam lengths, respectively
ϵ_s = emissivity of surface
η = defined by Equation (18)
θ = time, sec.
θ_1,θ_2 = angles on Figure 11, 12
λ = latent heat of vaporization, cal./g.
λ' = $\lambda - [q_R/(dm/d\theta)]$
μ = absolute viscosity, g./(sec.) (cm.)
π = total pressure, atm.

ρ = reflectivity
σ = Stefan-Boltzmann constant: 1.355×10^{-12} (cal.)/(sec.)(cm.^{2})(°K.^{4})
Φ = spherical co-ordinate, Equation (1); also angles on Figures 13 and 14
Φ_t = escape factor
Ψ = spherical co-ordinate, Equation (1)
Ψ = factor by which characteristic length is multiplied to give the mean beam-length of the system
ω = solid angle, Figures 11, 12, 13 and 14

References

(1) Hoffman, T. W., and Gauvin, W. H., Can. J. Chem. Eng., **38:** 129 (1960).
(2) Filippov, L. P., Vestnik Moskov. Univ., 9, No. 2, Ser. Fiz.-Mat. Estestven Nauk, No. **1:** 51-6 (1954).
(3) Smith, J. W., J. Aero. Sc. Readers' Forum, 579 (1953).
(4) Goldsmith, M., and Penner, S. S., Jet. Prop., **24:** 245 (1954).
(5) Hottel, H. C., and Cohen, E. S., A.I.Ch.E. Journal, **4:** 3 (1958).
(6) Hottel, H. C., in McAdams' "Heat Transmission", Chap. IV, McGraw-Hill Co. Inc., New York, 3rd ed. (1955).
(7) Cohen, E. S., Sc.D. Thesis, M.I.T. (1955).
(8) Simpson, H. C., Sc.D. Thesis, M.I.T. (1955).
(9) Penner, S. S., J. App. Mechanics, **18:** 53 (1951).
(10) Sparrow, E. M., Usiskin, C. M., and Hubbard, H. A., presented at the ASME-AIChE Heat Transfer Conference, Buffalo, N.Y., August 15-17 (1960).
(11) Lowan, A. N., (Director) "Tables of Sine, Cosine and Exponential Integrals" Vol. I, Federal Works Agency, City of New York (1940).
(12) Hoffman, T. W., and Gauvin, W. H., Can. J. Chem. Eng., **39:** 179 (1961).

APPENDIX A

Formulation of the Reception Factors for a Spherical System

In the analysis of the radiation absorbed in the boundary layer of an evaporating drop, a spherical symmetrical model was postulated. The region around the drop in which the temperature gradients exist was divided into a number of spherical gas shells, so that the distribution of absorbed radiation in each gas shell could be calculated (see Figure 1).

To formulate the reception factors for this system, two assumptions must be made:

(1) the surfaces are black
(2) the absorption strength of the gas is uniform throughout

The latter assumption has been discussed in detail by Hottel and Cohen[6].

The following types of reception factors are considered:

(1) surface-to-surface
(2) gas-to-inner and -outer surfaces
(3) gas-to-gas

To make the solution completely general, all length terms are normalized with respect to the droplet radius (inner sphere) $= r_d$.

(1) *Surface-to-surface.*

(a) Inner to outer surface.

Referring to Figure 11, consider the radiation leaving dA_1 at an angle θ_1 to the normal of dA_1. The quantity of radiation received by dA_2 located at a distance R is proportional to the relative area of each as seen by the other and inversely proportional to the square of the separating distance. Moreover this radiation will be reduced as a result of absorption in the intervening gas. Introducing the proportionality constant $(1/\pi)$, the one way radiation from dA_1 to dA_2 becomes:

$$dq_{dA_1 \to dA_2} = [(dA_1 \cos\theta_1)(dA_2 \cos\theta_2)\, e^{-\underline{k} r_d R}](\sigma T_{s_1}^4)/\pi(r_d R^2) \quad \text{(A1)}$$

By definition

$$q_{s_1 \to s_2} = A_{s_1} f_{s_1 s_2} \sigma\, T_{s_1}^4 \quad \text{(A2)}$$

Equating (A1) and (A2), and since $d\omega_1 = dA_2 \cos\theta_2/(r_d R^2)$:

$$f_{s_1 s_2} = \frac{1}{\pi A_{s_1}} \int_{A_1} dA_1 \int_{\omega} \cos\theta_1\, e^{-\underline{k} r_d R}\, d\omega_1 \quad \text{(A3)}$$

Since every part of A_{s_1} sees the same relative portion of A_{s_2}, $f_{s_1 s_2}$ must be independent of where dA_1 is located and hence:

$$f_{s_1 s_2} = (1/\pi) \int_{\omega} \cos\theta_1 d\omega_1\, e^{-\underline{k} r_d R} \quad \text{(A4)}$$

Expressing $\cos\theta_1$ and $d\omega_1$ in terms of r_1^*, r_2 and R (see Figure 11), Equation (A4) becomes:

$$f_{s_1 s_2} = (1/2) \int_{R_1}^{R_2} \{[(r_2^2 - r_1^2)/r_1]^2 (1/R^3) - (R/r_1^2)\}\, e^{-\underline{k} r_d R} dR \quad \text{(A5)}$$

where the limits of integration are

$$R_1 = r_2 - r_1 \text{ and } R_2 = (r_2^2 - r_1^2)^{1/2*} \quad \text{(A6)}$$

Then

$$f_{s_1 s_2} = (1/2)[I_1 - I_2] \quad \text{(A7)}$$

where

$$I_1 = \int_{R_1}^{R_2} [(r_2^2 - r_1^2)/r_1]^2 (1/R^3)\, e^{-\underline{k} r_d R}\, dR \quad \text{(A8)}$$

and

$$I_2 = \int_{R_1}^{R_2} (R/r_1^2)\, e^{-\underline{k} r_d R} dR \quad \text{(A9)}$$

Both integrals can be evaluated by integrating by parts, hence:

$$\begin{aligned} f_{s_1 s_2} = (1/4)[(r_2^2 - r_1^2)/r_1]^2 \Bigg\{ & \left[\frac{e^{-\underline{k} r_d R_1}}{R_1^2} - \frac{e^{-\underline{k} r_d R_2}}{R_2^2}\right] - \\ & - \underline{k} r_d \left[\frac{e^{-\underline{k} r_d R_1}}{R_1} - \frac{e^{-\underline{k} r_d R_2}}{R_2}\right] \\ & - (\underline{k} r_d)^2 [-Ei(-\underline{k} r_d R_1) - [-Ei(-\underline{k} r_d R_2)]] \Bigg\} \\ & - 1/2 r_1^2 \{[(1/\underline{k} r_d)(R_1 e^{-\underline{k} r_d R_1} - R_2 e^{-\underline{k} r_d R_2})] \\ & - (1/\underline{k} r_d)^2 [e^{-\underline{k} r_d R_1} - e^{-\underline{k} r_d R_2}]\} \end{aligned} \quad \text{(A10)}$$

where $[-Ei(-\underline{k} r_d R_1)] = \int_{\infty}^{R_1} e^{-\underline{k} r_d R}\, d\, R/R$ is the familiar exponential integral, which has been tabulated[11], and R_1 and R_2 are given by (A6).

(b) Outer surface to outer surface.

Referring to Figure 12, the relation which describes the fraction of the radiation leaving dA_2 in the solid angle $d\omega_2$ and intercepted by the outer sphere is given by:

$$f_{s_2 s_2} = 1/\pi \int_{\omega} \cos\theta\, d\omega_2\, e^{-\underline{k} r_d R} \quad \text{(A11)}$$

which can be written (since $d\omega_2 = 2\pi \sin\theta\, d\theta$, and $\cos\theta = R/D$):

$$f_{s_2 s_2} = (-2/D^2) \int_{o}^{R_2} R e^{-\underline{k} r_d R}\, dR \quad \text{(A12)}$$

Integrating by parts:

$$f_{s_2 s_2} = [2/(\underline{k} r_d D)^2] \{[\underline{k} r_d R_2\, e^{-\underline{k} r_d R_2}] - e^{-\underline{k} r_d R_2} + 1\} \quad \text{(A13)}$$

where $R_2 = 2(r_2^2 - r_1^2)^{1/2}$. In the system considered, $r_1 = 1$

(2) *Gas-to-surface factors.*

(a) Gas to the inner surface sphere surface.

Referring to Figure 13, a volume element dV, located at point r, is radiating over the total solid angle 4π steradians. The radiation reaching dA_1 located at a distance R from dV is contained in the differential solid angle $d\omega$. This radiation must be reduced by the transmissivity of the gas over the separating distance. Hence, the one way flux is expressed by:

$$dq_{dV \to dA_1} = 4\underline{k} dV (\sigma\, T_G^4)\, e^{-\underline{k} r_d R} \cdot (d\omega/4\pi) \quad \text{(A14)}$$

Substituting for $d\omega = 2\pi \sin\Phi\, d\Phi$ from Figure 13, dividing by the total emission from volume element dV and integrating over the solid angle which includes the inner surface, the result is the

*In the system considered $r_1 = 1$.

fraction of the radiation originating in dV which reaches and is absorbed at the inner spherical surface. This fraction is defined as f_p' at point r and is given by:

$$(f_p')_r = (1/4r)\int_{R_1}^{R_2}[(r^2 - r_1^2/R^2) - 1] \cdot e^{-kr_dR}\, dR \quad \text{.....(A15)}$$

Equation (A15) can be integrated by parts, twice, to yield:

$$(f_p')_r = (1/4r)\left((r^2 - r_1^2)\{[(e^{-kr_dR_1}/R_1) - e^{-kr_dR_2}/R_2] - kr_d[-Ei(-kr_dR_1) - (-Ei(-kr_dR_2))]\} - (1/kr_d)[e^{-kr_dR_1} - e^{-kr_dR_2}]\right) \quad \text{.....(A16)}$$

where $R_1 = r - r_1$ and $R_2 = (r^2 - r_1^2)^{1/2}$. In the system considered,

$$r_1 = 1 \quad \text{.....(A17)}$$

(b) **Gas to any outer surface.**

Referring to Figure 14, the equation describing the radiation from volume element dV contained in a differential solid angle $d\omega$ which reaches and is absorbed at the outer sphere located at a distance R is:

$$dq_{dV \to dA_2} = 4kdV(\sigma T_G^4)\, e^{-kr_dR}\, d\omega/4\pi \quad \text{.....(A18)}$$

Dividing by the total emission by volume element dV and integrating over that portion of the outer surface which dV "sees", yields the following expression for the fraction of the energy originating in dV which is absorbed by the outer surface:

$$(f_p'')_r = \int_\omega e^{-kr_dR}\,(d\omega/4\pi) \quad \text{.....(A19)}$$

Substituting for $d\omega = 2\pi \sin\Phi\, d\Phi$ from Figure 14, and integrating:

$$(f_p'')_r = (1/4r)\left((r_2^2 - r^2)\{[(e^{-kr_dR_1}/R_1) - (e^{-kr_dR_2}/R_2)] - kr_d[-Ei(-kr_dR_1) - (-Ei(-kr_dR_2))]\} + (1/kr_d)[e^{-kr_dR_1} - e^{-kr_2R_2}]\right) \quad \text{.....(A20)}$$

where $R_1 = r_2 - r_1$ and $R_2 = (r_2^2 - r_1^2)^{1/2} + (r^2 - r_1^2)^{1/2}$ ....(A21)

In the system considered, $r_1 = 1$.

The gas-to-surface factors can be found from the f_p-factors (whether f_p' or f_p'') since:

$$4kV_G f_{gs}(\sigma T_G^4) = \int_V 4kdV f_p(\sigma T_G^4) \quad \text{.....(A22)}$$

Since f_p is the same for all points at a given radius

$$f_{g,s} = \frac{\int_V 4\pi r^2 (f_p)_r}{V_{G_i}}\, dr \quad \text{.....(A23)}$$

The numerator of (A23) is conveniently integrated by numerical methods.

(3) *Gas-to-gas factors.*

The reception factors for any two gas zones may be obtained from the f_p'' expressions. The difference between the factors for any two imaginary surfaces bounding the gas zone will yield the fraction of the radiation originating in dV which is absorbed in the given volume. Integrating over the emitting zone volume and dividing by the total emission from that gas zone yields the desired gas-to-gas reception factor, f_{gg}.

Thus

$$f_{g_ig_j} = \frac{\int_{V_{G_i}} 4\pi r^2 (f_{p_m}'' - f_{p_n}'')_r}{V_{G_i}}\, dr \quad \text{.....(A24)}$$

The integral can be evaluated by numerical methods.

Evaluation of the Factors

The expressions for the f_p factors were evaluated by means of an I.B.M. 650 digital computer. The numerical integrations were carried out on the computer, by employing Simpson's Rule.

The f_{gg} integrals were evaluated on a desk calculator. In all cases, eight place accuracy was maintained throughout.

The final factors are indicated in Figures 2 to 9 and Table 2.*

APPENDIX B

Allowance for Reflection at the Drop Surface

The direct interchange areas are obtained from the reception factors. However, these areas are applicable only to a black system. An imaginary black surface can be postulated at the outer edge of the boundary layer; the inner drop, however, may be only partially absorbing and some of the radiation striking this surface may be reflected and some transmitted. The problem becomes even more complicated if an attempt is made to trace the transmitted beam. However, if one assumes the transmissivity to be equal to zero, i.e., $\rho + \alpha_p = 1$, the error introduced will be small, since the radiation which is not absorbed by the drop is still being considered. If, moreover, the surface is assumed to act as a grey body, the absorption of the reflected beam can easily be calculated from the direct interchange areas. To account for this reflected flux, another interchange area is introduced, which corresponds to (AF) of the old nomenclature[6]. These terms are known as total interchange areas and are defined as follows:

$\overline{S_iS_j}$ $\overline{S_iG_j}$ $\overline{G_iG_j}$ — the fraction of the energy originating at s_i (s_i, g_i respectively) which is absorbed at s_j (g_j, g_j respectively) taking into account the direct radiation, as well as the multiple reflections at all surfaces in the enclosure, and the absorption by the intervening gas.

The determinant method for formulating these total interchange areas from the direct interchange areas was discussed in a recent paper[5]. Applying this method to the present case, the following total interchange areas result:

$$(1)\quad \overline{S_1S_5} = \alpha_{s_1}\,\overline{s_1s_5} \quad \text{.....(B1)}$$

$$(2)\quad \overline{G_1S_1} = \alpha_{s_1}\,\overline{g_is_1} \quad \text{.....(B2)}$$

$$(3)\quad \overline{G_iS_5} = \overline{g_is_5} + [(\overline{s_1s_5})\,(g_is_1)\,(1 - \alpha_{s_1})/A_{s_1}] \quad \text{.....(B3)}$$

$$(4)\quad \overline{S_5S_5} = \overline{s_5s_5} + [\overline{s_1s_5}\,(1 - \epsilon_{s_1})\,(\overline{s_5s_1})/A_{s_1}] \quad \text{.....(B4)}$$

$$(5)\quad \overline{G_iG_j} = \overline{g_ig_j} + [(\overline{g_ig_1})\,(1 - \alpha_{s_1})\,(\overline{s_ig_j})/A_{s_1}] \quad \text{.....(B5)}$$

When the absorptivity of the droplet is high ($\alpha_{s_1} > 0.90$), the increased absorption in the gas, arising as a result of reflection at the drop surface, is small and may be neglected without seriously affecting the result.

*Table 2 of this paper has been deposited as Document No. 6878 with the ADI Auxiliary Publications Project, Photoduplication Service, Library of Congress, Washington 25, D.C. A copy may be obtained by citing the Document No. and by remitting $1.25 for photoprints, or $1.25 for 35 mm. microfilm. Advance payment is required. Make cheques or money orders payable to: Chief, Photoduplication Service, Library of Congress.

★ ★ ★

Sulphur and Sulphur Dioxide for Separating Copper from Nickel-Cobalt-Copper Sulphate Solutions[1]

W. KUNDA[2] and V. N. MACKIW[2]

In hydro-metallurgical processes for the production of nickel and cobalt, the leach solutions usually contains salts of nickel, cobalt and copper. To recover high purity nickel and cobalt metals from such solutions, the copper is removed prior to the nickel-cobalt separation.

During the course of extensive investigations to determine the most economical and efficient methods for separating the copper, it was established that copper in solution reacts with elemental sulphur in the presence of sulphur dioxide forming a copper sulphide precipitate. This reaction permits a simple and quantitative separation of copper from nickel and cobalt leach solutions.

The variables affecting this reaction were studied and the results are presented in this paper. Studies were conducted on: the sulphur concentration between 0 to 2.0/1 molar ratio of sulphur to copper, the sulphur dioxide concentration 0 to 17 gpl., the temperature in the range from 100°F. to 325°F., the copper concentration from 1 to 30 gpl. and pH from 1.0 to 9.0.

The results are correlated and a tentative mechanism for the reaction is discussed.

Nickel and cobalt concentrates or mattes prepared from nickel-cobalt-sulphide ores usually contain a significant quantity of copper. Among a number of conventional methods for processing these materials are oxidizing leaches in either ammoniacal ammonium sulphate solutions or sulphuric acid.

During the above leach treatment, the nickel, cobalt and copper sulphides are converted to water soluble sulphates and are separated from the leach residue by filtration.[1,2]

The compositions of the leach solutions, in each case are dependent upon the composition of the treated material.

The compositions of typical leach solutions are shown below:

Type of Solution	Ni gpl.	Co gpl.	Cu gpl.	NH_4F gpl.	$(NH_4)_2SO_4$ gpl.	H_2SO_4 gpl.	pH
Ammoniacal	50	0.5–2.0	5–10	30–100	100–300	0	7–9
Acid	60–120	0.5–5.0	6–20	0	0–30	2–5	1–4

[1]*Manuscript received March 27; accepted July 27, 1961.*
[2]*Research and Development Division, Sherritt Gordon Mines Limited, Fort Saskatchewan, Alta.*
Based on a paper presented to the Joint A.I.Ch.E.-C.I.C. Chemical Engineering Conference, Cleveland, Ohio, May 7-10, 1961.

Copper must be removed from these solutions before the recovery of nickel and cobalt by reduction with hydrogen at elevated temperature and pressure[3,4,5,6,7,8,9,10].

It has been discovered that this removal of copper can be achieved by the addition of elemental sulphur to the leach solutions thereby causing the precipitation of copper sulphide. This reaction proceeds only in the presence of sulphite, thiosulphate and polythionate ions.

The ammoniacal leach solutions may contain a sufficient amount of these compounds for the precipitation of copper sulphide to be accomplished by the addition of sulphur alone. However, the concentrations of thionates in acid leach solutions are too small for a reasonable rate of precipitation and it is therefore advantageous to add sulphur dioxide as a source of sulphite, thiosulphate and thionate ions.

This paper describes the conditions under which copper can be precipitated from sulphate solutions as copper sulphide by the addition of sulphur and sulphur dioxide.

Experimental Procedure and Results

The solutions used in this work were either actual acid or ammoniacal leach solutions obtained from concentrates or synthetic solutions with the same general composition as leach solutions.

The experiments were carried out in a 1 gallon stainless steel autoclave equipped with a mechanical agitator and heated or cooled externally by gas or water respectively.

The autoclave was charged with 2 litres of solution and a calculated quantity of sulphur powder. Sulphur dioxide or ammonium sulphite solution was added usually at the reaction temperature either directly through the charging port or by means of a pressure bomb if the temperature was above 212°F.

Sulphur dioxide in aqueous solution (sulphurous acid) was determined in the head solution by titration with a 0.008 N $KBrO_3$ solution. The same titration was used during the reaction to determine combined sulphide, thiosulphate and polythionate concentrations. However in certain specific tests the sulphite, thiosulphate, polythionate and sulphate concentration were determined separately (see Figure 14). The sulphite concentrations were determined from the differences in titration of equal volumes of the sample in acetic acid and formaldehyde solutions using a standard iodine solution. The thiosulphate concentration was determined from the direct titration with iodine in the formaldehyde solution. The polythionates were determined from the differences between the iodine titration in the acetic acid solution and a third sample in hydrochloric acid solution using a standard potassium bromate solution. Starch was used as the indicator for the iodine titrations and methyl-orange for the $KBrO_3$ titration.

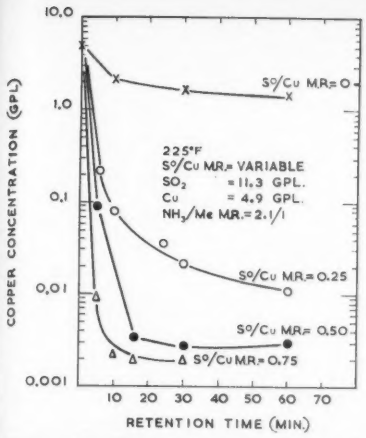

Figure 1—Effect of varying the sulphur addition on the rate of copper precipitation from an ammoniacal Ni-Co-Cu sulphate solution.

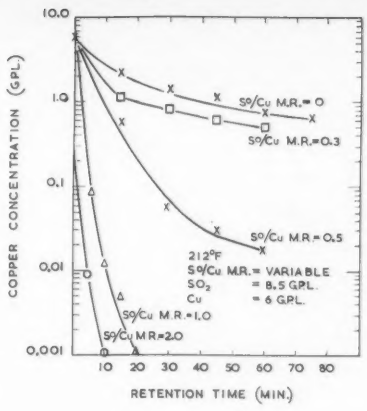

Figure 2—Effect of varying the sulphur addition on the rate of copper precipitation from an acid Ni-Co-Cu sulphate solution.

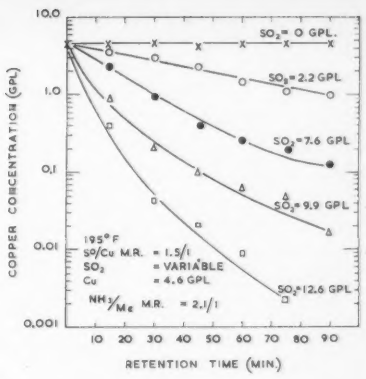

Figure 3—Effect of sulphur dioxide concentration on the rate of copper precipitation from an ammoniacal Ni-Co-Cu sulphate solution.

The sulphate ion concentration was determined gravimetrically by direct precipitation of barium sulphate using barium chloride. The copper concentration in solution was followed by taking samples at suitable intervals and analyzing for copper by electroplating or colorimetrically.

After completion of the test the precipitated copper sulphide was recovered, washed and analyzed.

During the preliminary experiments it was observed that the extent and rate of copper sulphide precipitation was influenced by the concentrations of sulphur, sulphur dioxide and copper and also by the temperature and the hydrogen ion concentration of the reaction system.

The concentration of nickel was found to be without effect in the range 60-120 gpl. in acid solutions and 40-50 gpl. in ammoniacal solutions. The same holds true for the ammonium sulphate concentration up to 100 gpl. in acid, and between 200 and 300 gpl. in ammoniacal, leach solutions.

The Effect of Sulphur Concentration

The reaction between sulphur and copper sulphate in solutions is a heterogeneous reaction and therefore the physical characteristics of the solid phase are very important. Decreasing particle size of sulphur and treatment of the sulphur with wetting agents accelerate the reaction rate.

Technical or reagent grade sulphur passing 200 mesh and treated with Aerosol OT was found to be very effective for the precipitation of copper.

The quantity of sulphur added to the solution was expressed as the sulphur to copper molar ratio. The relationship between the S°/Cu molar ratio and the rate of copper precipitation under the conditions specified in Figures 1 and 2 showed that the rate of copper precipitation increased, and copper content in the purified solution decreased, with an increase of sulphur concentration. The minimum quantity of sulphur required for copper precipitation is between 0.5 to 1.0 mols of sulphur per mol of copper in solution.

Effect of Sulphur Dioxide Concentration

The reaction between elemental sulphur and copper ions in sulphate solutions leading to the precipitation of copper sulphide are complex and involve sulphite, thiosulphate and thionate species, which may act as carriers and reductants of the sulphur.

Leach solutions obtained by the extraction of sulphide concentrates with highly ammoniacal solutions of ammonium sulphate usually contain sufficient concentration of these intermediate species to give an acceptable rate of copper sulphide precipitation when elemental sulphur is added to the leach solutions. However, the concentration of these sulphur carriers in acid leach solutions, and in some ammonium sulphate leach solutions containing relatively small amounts of ammonia, is too low to give acceptable rates of copper sulphide precipitation when sulphur powder is added to these solutions. In these cases an external source of sulphite, thiosulphate or thionate ions must be added with the elemental sulphur. This addition is most easily accomplished by the addition of sulphur dioxide, or ammonium sulphite.

The effect of the amount of sulphur dioxide added is shown in Figures 3 and 4 from which it can be seen that the rate of copper sulphide precipitation is a function of the sulphur dioxide concentration.

The Effect of Temperature

The effect of temperature was investigated between 100° and 325°F. Figures 5 and 6 show that the temperature has a very pronounced effect upon the rate of copper sulphide precipitation.

Because of this marked temperature-dependence the quantity of sulphur dioxide required to achieve a certain rate of copper sulphide precipitation could be decreased by increasing the reaction temperature. This is shown in Figures 7 and 8. The lowest temperature for a satisfactory rate of copper sulphide precipitation appears to be 125°F. while above 325°F. copper sulphide precipitation occurs even when sulphur dioxide is not added to the solution.

The Effect of Copper Concentration

The copper concentration of leach solutions may vary widely depending upon the composition of the treated material, but usually the copper concentration in solution is between 5 and 10 gpl. These investigations however, were extended beyond this limit and the copper precipitation was carried out on solutions containing 1 to 30 gpl. of copper. The results illustrated in Figures 9 and 10 show that below 212°F. the initial copper concentration has a negative effect upon the copper sulphide precipitation and more sulphur dioxide is required to precipitate the copper to the specification level. The relationship between initial copper concentration and sulphur dioxide concentration at 212°F. is shown in Figures 10 and 11.

At higher temperatures the effect of the sulphur dioxide concentration is less pronounced and at 270°F. (Figure 9)

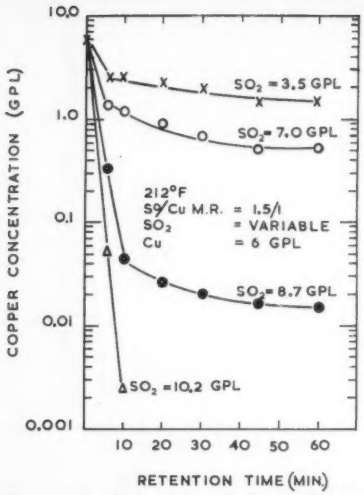

Figure 4—Effect of sulphur dioxide concentration on the rate of copper precipitation from an acid Ni-Co-Cu sulphate solution.

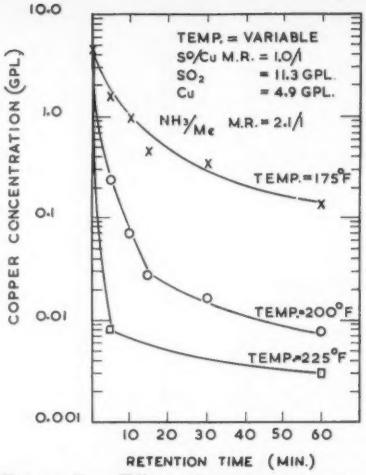

Figure 5 — Effect of temperature on the rate of copper precipitation from an ammoniacal Ni-Co-Cu sulphate solution.

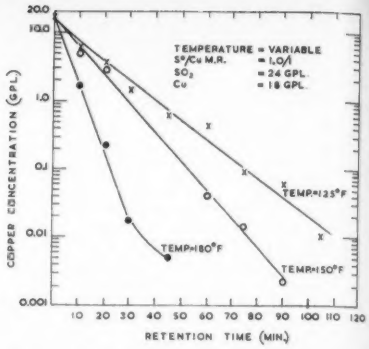

Figure 6 — Effect of temperature on the rate of copper precipitation from an acid Ni-Co-Cu sulphate solution.

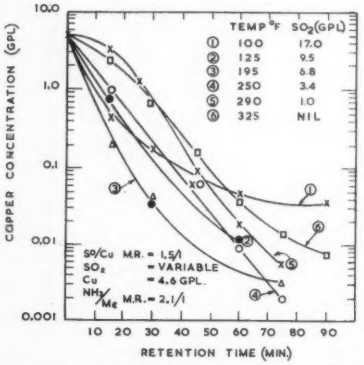

Figure 7—Rate of copper precipitation from ammoniacal Ni-Co-Cu sulphate solution at various temperatures and corresponding sulphur dioxide concentrations.

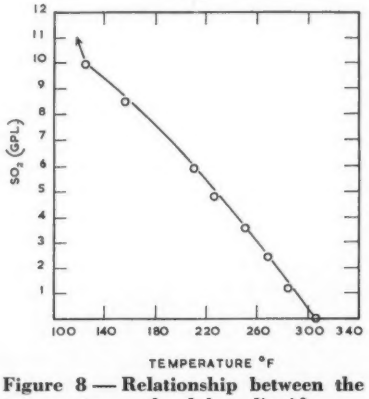

Figure 8 — Relationship between the temperature and sulphur dioxide concentration necessary to remove the copper from an ammoniacal Ni-Co-Cu sulphate solution containing 4.6 gpl. to less than 0.02 gpl. Cu. within one hour; the other conditions were: S°/Cu M.R. = 1.5/1, NH_3/Me M.R. = 2./1.

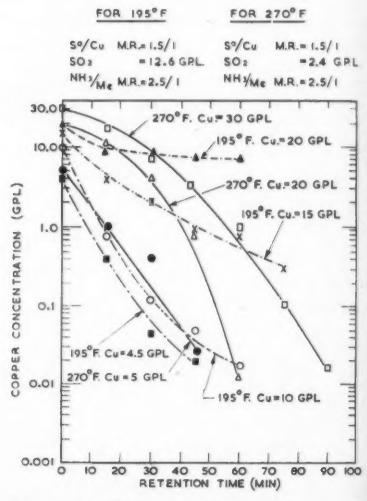

Figure 9—Effect of the initial copper concentration on the rate of copper precipitation from an ammoniacal Ni-Co-Cu sulphate solution at 195°F. and 270°F.

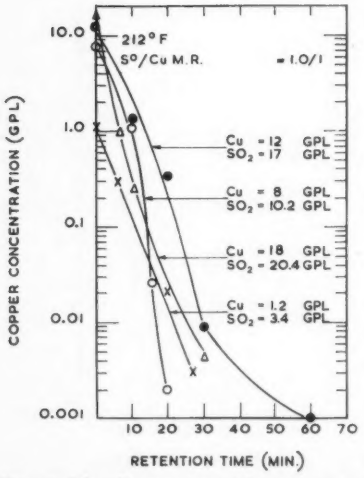

Figure 10—Copper precipitation rate-curves for various copper and sulphur dioxide concentrations in acid Ni-Co-Cu sulphate solutions. Conditions: SO_2 & Cu variable.

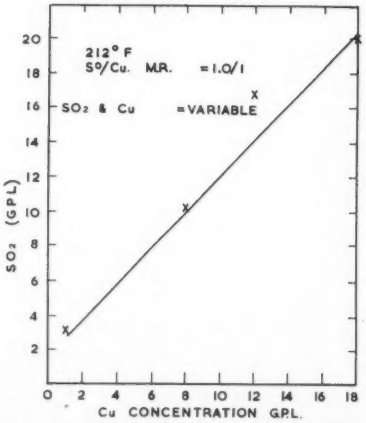

Figure 11—Sulphur dioxide requirements to lower various copper concentrations to less than 0.02 gpl. Cu in 30 mins. from acid Ni-Co-Cu sulphate solutions.

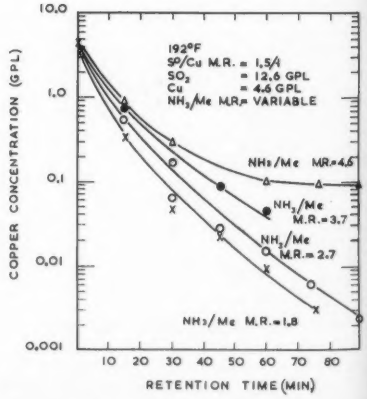

Figure 12 — Effect of free ammonia concentration on the precipitation of copper from an ammoniacal Ni-Co-Cu sulphate solution.

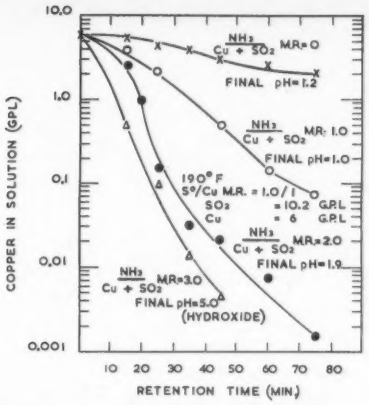

Figure 13—Effect of ammonia addition on the precipitation of copper from an acid Ni-Co-Cu sulphate solution (pH-1.7).

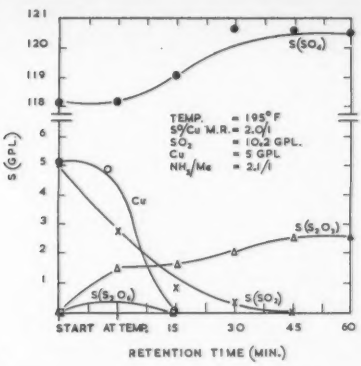

Figure 14—Changes of concentration of copper and sulphur-dioxide-thiosulphates-trithionates and sulphate ions during precipitation of copper from ammoniacal Ni-Co-Cu sulphate solution with sulphur and sulphur dioxide.

ceases completely. This can be explained by the fact that at low temperatures the reaction is affected by the presence of thionates. Increasing the copper concentration in the solution, then causes the thionates to be used more rapidly than they are produced and the rate of copper precipitation decreases. At higher temperatures however, the direct reactivity of the elemental sulphur increases and the reaction proceeds to completion as soon as the required quantity of elemental sulphur is available.

The Effect of Hydrogen Ion Concentration

The effect of pH was studied in both the ammoniacal and the acid leach solutions.

Figure 12 illustrates the effect of increasing amounts of ammonia on the precipitation of copper sulphide from an ammoniacal leach solution. The amount of ammonia present is expressed as a molar ratio which is the ratio of the number of mols of ammonia which can be titrated with sulphuric acid to the number of mols of metal (Ni, Co and Cu) present in solution. It can be seen that an increase of this $NH_3/Ni+Co+Cu$ molar ratio increases the final equilibrium concentration of copper and prevents complete precipitation of the copper as copper sulphide. This is another example of complex-formation exhibiting a pronounced effect on metal ion reaction in aqueous solution.

Figure 13 shows the effect of ammonia upon the precipitation of copper sulphide from the acid leach solutions. In this case the amount of ammonia added is expressed as a $NH_3/Cu + SO_2$ molar ratio. The theoretical quantity required is determined from the following equation:

$$CuSO_4 + S + SO_2 + 4\ NH_4OH \rightarrow CuS + 2(NH_4)_2SO_4 + 2\ H_2O \quad \ldots\ldots\ldots (1)$$

From this equation it can be seen that two mols of ammonia must be added for each mol of SO_2 consumed and two mols of ammonia for each mol of precipitated copper sulphide in order to neutralize the acid produced in these reactions. The $NH_3/Cu + SO_2$ molar ratios in Figure 13 calculated according to Equation (1) using a solution with an initial pH of 1.7 are in good agreement with this conclusion. The SO_2 concentration used in calculating the $NH_3/Cu + SO_2$ molar ratio was the amount of SO_2 consumed in the reaction and not the SO_2 concentration present in the initial solution. The addition of less than the theoretical amount of ammonia caused a drop in pH which prevented the complete precipitation of copper sulphide. The use of the theoretical amount of ammonia allows the precipitation to proceed to completion while the pH remains essentially unchanged. If excess ammonia is added the pH rises rapidly and above about pH 4.5 the copper precipitates out as the hydroxide rather than the sulphide.

THE REACTION PRODUCTS AND REACTION MECHANISM

The Nature of the Precipitated Copper Sulphide

The material precipitated during the reaction is a high grade copper sulphide contaminated with a small quantity of elemental sulphur and nickel sulphide.

Typical analyses of the residues precipitated from the two types of solution are:

Solution	Cu %	Total S %	Elemental S %	Ni %	Co %	$S_T - S^\circ/Cu$
Ammoniacal	68	32	3	0.8	<0.01	0.8
Acid	63	35	3	0.1	<0.01	1.0

The copper sulphide precipitated from ammoniacal solution is characterized by a higher contamination with nickel sulphide. This is explained by the fact that sulphide ions will precipitate both metals above pH 7. However, the copper is preferentially precipitated and only a small amount of nickel sulphide is present in it.

In acid solution sulphide ions do not precipitate nickel and the copper sulphide therefore contains very little nickel when precipitated under these conditions.

The sulphide sulphur, which was calculated by difference between total sulphur and elemental sulphur, to copper ratio in the copper sulphide indicates that in ammoniacal solutions copper precipitates as a mixture of CuS and Cu_2S, whereas in acid solution the precipitate is cupric sulphide.

The elemental sulphur in the copper sulphide may deviate widely from the typical analysis depending upon the precipitation conditions.

The Reaction Mechanism

The mechanism of the reaction between copper ions and elemental sulphur to produce copper sulphide is a complex one and involves many competing, simultaneous and consecutive reactions, all with their own rate of temperature-dependence.

The postulated sequence of reactions is as follows:

(a) Dissolution of sulphur:

$$SO_2 + H_2O \rightarrow SO_3^{--} + 2H^+ \quad \ldots\ldots\ldots (2)$$

$$SO_3^{--} + S \rightarrow S_2O_3^{--} \quad \ldots\ldots\ldots (3)$$

(b) Formation of thionic acids:

$$4SO_3^{--} + S_2O_3^{--} + 6H^+ \rightarrow 2S_3O_6^{--} + 3H_2O \quad \ldots\ldots\ldots (4)$$

$$2S_2O_3^{--} + 8Cu^{++} + 4H_2O \rightarrow S_4O_6^{--} + 8Cu^+ + SO_4^{--} + 8H^+ \quad \ldots\ldots (5)$$

(Reaction (5) only possible in alkaline solution)

(c) Precipitation of copper sulphide:

$$2Cu^{+} + S_3O_6^{--} + 2H_2O \rightarrow Cu_2S + 2SO_4^{--} + 4H^{+} \quad (6)$$

$$Cu^{++} + S_3O_6^{--} + 2H_2O \rightarrow CuS + 2SO_4^{--} + 4H^{+} \quad (7)$$

$$Cu^{++} + S_2O_3^{--} + H_2O \rightarrow CuS + SO_4^{--} + 2H^{+} \quad (8)$$

The order and rate of these reactions depends on the pH, temperature and concentrations of the various intermediate ionic species.

The net result of these reactions is that at low temperature elemental sulphur is reduced to sulphide while SO_2 is oxidized to sulphate, and at high temperature the elemental sulphur is both reduced to sulphide and oxidized to sulphite.

The sulphide ion is produced gradually and reacts with the copper in solution to produce copper sulphide. Since the solubility products of NiS, CuS and Cu_2S are 1.4×10^{-24}, 8.5×10^{-45} and 2×10^{-47} respectively it follows from the lack of nickel sulphide in the precipitate that the concentration of sulphide ions in solution does not normally exceed 10^{-24} moles/litre, under the reaction conditions.

During the reaction shown in Figure 14 the concentrations of sulphate and thiosulphate rose while the concentration of sulphur dioxide fell. The decomposition of trithionate ions was so rapid that if could be detected only in the initial stages of the reaction. However both these species could be demonstrated in similar solutions in the absence of metals.

As the temperature is increased all these various reactions are accelerated until at 325°F. and above the copper and elemental sulphur can react directly without the intermediary of thionate ions and the following reaction appears to take place.

$$4S^{\circ} + 4H_2O \rightarrow 3H_2S + H_2SO_4 \quad (9)$$

Conclusion

The separation of copper from leach solutions containing nickel, cobalt and copper sulphates can be achieved by adding elemental sulphur and sulphur dioxide which cause the precipitation of copper sulphide.

This reaction involves sulphite, thiosulphate and thionate ions as intermediates and the primary purpose of the sulphur dioxide addition is to generate these ionic species. Above 325°F. these intermediaries, and sulphur dioxide, are unnecessary and the addition of elemental sulphur is sufficient to bring about the precipitation of copper sulphide.

The reaction can be carried out over a wide temperature range, the lowest practical temperature being 125°F. The dependence of rate upon temperature is very great.

The reaction can be carried out over the pH range of 1 to 9 although the rate is slower at these extremes and the small pH range about neutrality cannot be used because of the precipitation of copper hydroxide.

The acid produced in the reaction can be neutralized by the base most suitable for the subsequent steps in the process. It may include Na_2CO_3, NaOH, KOH, CaO, MgO, NH_4OH, $Ni(OH)_2$, $Co(OH)_2$ and also metals such as cobalt and nickel can be used for acid neutralization.

Under properly controlled conditions the rate of copper removal is very rapid and copper can be removed to less than 0.02 gpl. within a few minutes. The precipitated copper sulphide is a high grade material containing less than 1% nickel and cobalt.

This method of copper separation is very flexible and can be adapted to various hydrometallurgical processes, where the main reagents, SO_2 and sulphur, are readily available.

Acknowledgements

The authors wish to thank Sherritt Gordon Mines Limited, for permission to present this paper. The assistance of B. Rudyk and other colleagues during the experimental work and B. Meddings in preparation of the paper are gratefully acknowledged.

References

(1) Forward, F. A. and Mackiw, V. N., J. Metals, **7,** 457-63 (1955).

(2) Pearce, R. F., Warner, J. P. and Mackiw, V. N., J. Metals, **12,** No. 1, 28-32 (1960).

(3) Mackiw, V. N., Can. Patent No. 518,834 (1955).

(4) Mackiw, V. N. and Nashner, S., Can. Patent No. 518,835 (1955).

(5) Mackiw, V. N., Kunda, W. and Benoit, R. L., Can. Patent No. 586,406 (1959).

(6) Mackiw, V. N., Benoit, R. L., Loree, R. J. and Yoshida, N., Chem. Eng. Progr. **54,** No. 3, 79-85 (1958).

(7) Mackiw, V. N., Lin, W. C. and Kunda, W., J. Metals, Trans. AIME, **209,** 786-793 (1957).

(8) Mackiw, V. N., Lin, W. C., Benoit, R. L. and Benz, T. W., AIME Meeting, Feb. 1958, published in part in J. Metals, **10,** No. 12, 800-802 (1958).

(9) Kunda, W., Warner, J. P. and Mackiw, V. N., Symposium on "The Chemistry of the Liberation of Metals from their Compounds" co-sponsored by The Chemical Inst. of Canada and the Dep. Mines Tech. Surveys, Ottawa, Sept. 9-11, 1959.

(10) Mackiw, V. N., 36th Annual Conference, The Chemical Inst. of Canada, Windsor, Ont., June 1953.

★ ★ ★

Research at the McGill Hypersonic Propulsion Research Laboratory[1]

J. SWITHENBANK[2] and S. MOLDER[2]

Research on supersonic combustion ramjets started in 1958. Theoretical studies show that the performance is good up to Mach 25; they are thus suitable for satellite boosting[1,2].

Facilities which have been constructed for experimental work are:

(1) Zirconia pebble bed to heat 0.1 lb/sec. air up to 2000°C. at 100 p.s.i.

(2) Vacuum system 0.1 lb./sec. at 0.5 p.s.i.a. connected to various test facilities.

(3) Hypersonic shock tunnel, Mach 12 upwards.

(4) Fuel mixing study facility providing two supersonic dissimilar gas streams.

(5) Nozzle recombination test facility using nitrogen dioxide diluted.

(6) Thrust measuring test facility.

(7) High temperature 1500°C. electric furnace.

Most of the combustion research to date has been carried out using air heated by the zirconia pebble bed, and has been directed at obtaining information on or relevant to shock free supersonic combustion.

The following experiments have been carried out.

(1) Spontaneous combustion of hydrogen up to Mach 1.

This experiment was simply to give the lower ignition limit of hydrogen in a flow system. This temperature was found to be about 600°C.

(2) Ignition delay of hydrogen/air mixtures at high temperatures.

This data was acquired to extend the data currently available to 1300°K. at sub-atmospheric pressures. The results are shown in Figure 1.

(3) Boundary layer injection of hydrogen at $M = 2.1$ and 2.6.

These experiments were carried out to determine the possibility of supersonic combustion with porous wall fuel injection. Difficulties were encountered due to separation of the boundary layer caused by combustion heat release. This is considered to be inherent with this type of fuel injection, and it has been discontinued.

(4) Downstream injection of hydrogen at $M = 1.2$ using a slotted nozzle.

Satisfactory combustion was obtained with no change of flame character as the Mach No. went through 1. The length/diameter ratio of the flame retained its classical relationship throughout. Higher Mach Numbers and/or lower heat release was required for shock combustion.

(5) Downstream and cross-stream injection of tri-ethyl aluminum (T.E.A.) at $M = 4$.

Using air with reduced oxygen content to decrease the maximum heat release showed that combustion could easily be obtained, although certain precautions had to be taken with the injector to prevent plugging due to decomposition of the T.E.A.

(6) Constant area combustion of T.E.A. at $M = 4$, using cross-stream injection.

This experiment used 3 radial stub jets to penetrate the boundary layer; the combustion was carried out in an instrumented constant area tube. The results showed that a shock formed near the fuel injector station and great difficulty was caused by the aluminum oxide deposit fouling the instrumentation lines.

(7) Constant area combusion of hydrogen at $M = 4$ using cross-stream injection.

These experiments are at present underway, using air total temperatures of 2500°C. obtained by vitiating the air.

Future supersonic combustion research requires even higher temperatures. However, since the ignition delays are less than 10^{-4} seconds, we believe that satisfactory results will be obtained in intermittent type facilities with running times of a few milliseconds. The proposals are discussed as follows:

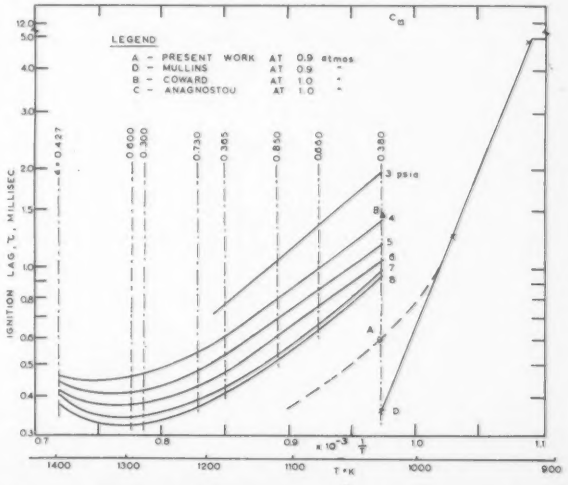

Figure 1—Relation of $\log_e \tau$ versus $\frac{1}{T}$ at constant pressure.

[1]*Manuscript received September 7, 1961.*
[2]*Mechanical Engineering Department, McGill University, Montreal, Que.*

Studies of Hypersonic Air-Breathing Engines in the Shock Tunnel

Combustion Research

A high pressure (80,000 p.s.i.) shock tunnel is being constructed to study combustion phenomena at conditions occurring in a supersonic combustion ramjet —

Total temperature	3,800°K.
Total pressure	76,000 p.s.i.
Mach Number	4 +

These conditions will be simulated at the nozzle exit of the shock tunnel. The initial experiments will involve downstream injection through an axial injector through the main shock tunnel nozzle. Subsequent tests will show the effectiveness of cross-stream injection. The fuel, hydrogen in most cases, will be injected into the main airflow by means of an auxiliary shock tube, driven either by its own driver or from the main testing air driver.

Intake Research

Experimentation and theoretical work is in progress to study the effects of shock waves and boundary layers on the efficient deceleration of hypersonic flow to supersonic speeds. Straight wedges and oblique shock models are presently being tested a $M = 12$. Future experiments will involve curved intake surface with controlled boundary layers.

Nozzle Research

Both the high and the low pressure shock tube will be used for nozzle flow studies. Combustion products in the driven tube will be shock heated/compressed and blown into a propulsion nozzle. Pressure and thrust measurements will then determine the performance.

Connected Tests

After completion of the above tests together with the present intake tests it is planned to run experiments on complete configurations, i.e., intake, combustion and exhaust. Subsequent experiments will then be conducted with gun-launched hypersonic free-flight models.

*References**

(1) S.C.S. 24. Hypersonic Ramjet–Zurich Conference Report, September 1960. D. L. Mordell and Swithenbank, J.

(2) S.C.S. 21. An Air-Breathing Satellite Booster. S. Molder and Wu, J. H. T.

Other reports are generally available on request from the Group.

*References S.C.S. 1-42, and Technical Notes H2 and H3, have been deposited as Document No. 6894 with the ADI Auxiliary Publications Project, Photoduplication Service, Library of Congress, Washington 25, D.C. A copy may be obtained by citing the Document No. and by remitting $1.25 for photoprints, or $1.25 for 35 mm. microfilm. Advance payment is required. Make cheques or money orders payable to: Chief, Photoduplication Service, Library of Congress.

★ ★ ★

The Design and Operation of a High Pressure Reforming Pilot Plant[1]

J. A. BICHARD[2], *J. BUMBULIS*[2] *and R. M. BUTLER*[2]

A pilot plant has been designed and constructed for the exploration of reforming processes at temperatures up to 1200°F. and pressures up to 1500 p.s.i.g. The components of the pilot plant are described, as well as the calculation of material balances and product yields by an IBM 650 computer.

When catalytic reforming was introduced at Imperial Oil's refineries, it was decided to build a reforming pilot plant. The pilot plant was to evaluate the effects of new feeds, catalysts and changes in the operating conditions, as well as assist the refineries on any problems that may develop. This paper presents a brief outline of the final design, incorporating some modifications carried out following the initial start-up operation.

Design Basis

The first problem to be solved was the size of the pilot unit. For simplicity of operation, and to minimize catalyst and feed requirements, the unit had to be as small as possible, consistent with obtaining an adequate sample for quality evaluation in a reasonable time. But another factor had to be taken into account. Many reformer feeds contain more sulphur than can be tolerated by the reforming catalyst, and they have to be hydrogen treated or hydrofined before reforming. Normally this would not be important, since the feed could be obtained from the refinery, after hydrofining. However, the discovery of new oil fields presents new naphthas, not processed by a refinery, for evaluation. These would have to be hydrofined in the laboratory before reforming. Since the hydrofining flow plan is not very different from that of reforming, the same pilot plant could be used, but it should have a relatively large capacity, so that too much time would not be spent on feed preparation. In the final design, this problem was solved by the use of interchangeable reactors of different capacity. The rest of the system was sized to process the expected maximum feed rate.

Catalytic reforming is carried out at 850-950°F. and 300-500 p.s.i.g. over platinum catalyst to improve the octane rating of gasoline by conversion of low octane components. Figure 1 shows the principal reactions involved. The most desirable reactions are the conversion of naphthenes and paraffins to aromatics. Both of these reactions produce high octane material from relatively low octane components, and are endothermic. Isomerization of straight chain paraffins is slightly exothermic, while hydrocracking of paraffins is fairly exothermic. The overall reaction usually is quite endothermic, causing an appreciable temperature drop in the reactor.

In its simplest form, the catalytic reforming pilot plant flow plan can be represented by the scheme shown in Figure 2. The feed, consisting mainly of naphthenes and paraffins is taken from storage, mixed with hydrogen or recycle gas, and passed into the reactor. The product enters a separator, where a hydrogen rich gas is removed from the hydrocarbons, and then the aromatics rich reformate is stabilized by removing the light hydrocarbons—ethane, propane and butanes. The hydrogen rich gas is recycled. Provision has been made to introduce other gases — hydrogen, nitrogen or air into the system, as shown by the dotted section of Figure 2.

Reactor Design

The heart of the entire system is the reactor section. Here the incoming feed has to be heated to the reaction temperature, and contacted with the catalyst.

There are two possible ways of operating the reactor — isothermally or adiabatically. In the isothermal operation enough heat is supplied to the reactor to maintain constant temperature throughout the catalyst bed. This method would be preferable, since it simplifies the evaluation of the reaction mechanisms involved. In adiabatic operation, only enough heat is supplied to the reactor to balance heat losses. Here a temperature gradient may exist along the reactor. This approximates a commercial reactor, and thus may be more indicative of the performance to be expected. Figure 3 shows the large difference in the temperature profile between an adiabatic and isothermal reactor, using the same feed, catalyst and inlet temperature. The isothermal system was not truly isothermal with a 75°F. temperature drop in the first part of the reactor, where most of the highly endothermic naphthene dehydrogenation occurred. The temperature of the sandbath, used to heat the isothermal reactor, is shown for comparison.

It was decided to use both methods of reactor heating, and two parallel reactor systems were designed. The isothermal system is shown in Figure 4. It consists of a single reactor, suspended in a fluidized sandbath. The outside of the sandbath is heated by resistance wire heater, and the sand acts as the heat transfer medium. The fluidizing air is preheated in an aluminum block heater, while the feed is preheated in the coiled part of the inlet pipe. Two reactors were built, of identical dimensions, except for the diameter of the catalyst chamber. This permits easy change of the reactor capacity. The temperature of the

[1]*Manuscript received November 15, 1960; accepted July 28, 1961.*
[2]*Research Department, Imperial Oil Limited, Sarnia, Ont.*

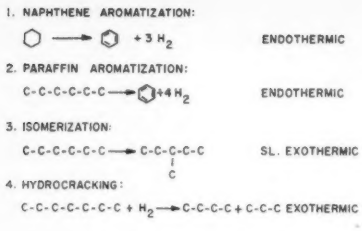

Figure 1—Typical reforming reactions.

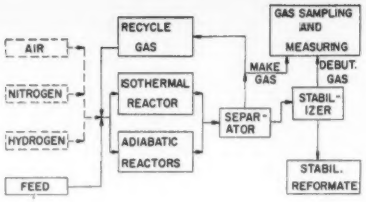

Figure 2—General flow plan.

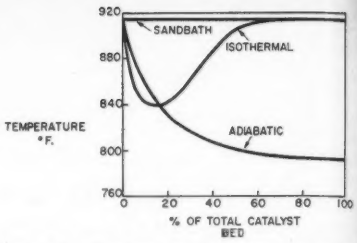

Figure 3—Reactor temperature profile.

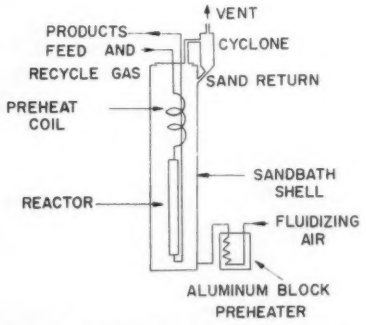

Figure 4—Isothermal reactor system.

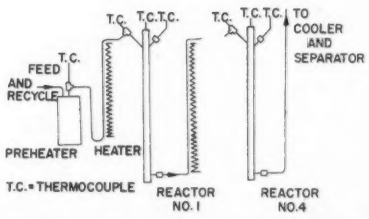

Figure 5—Arrangement of the adiabatic system.

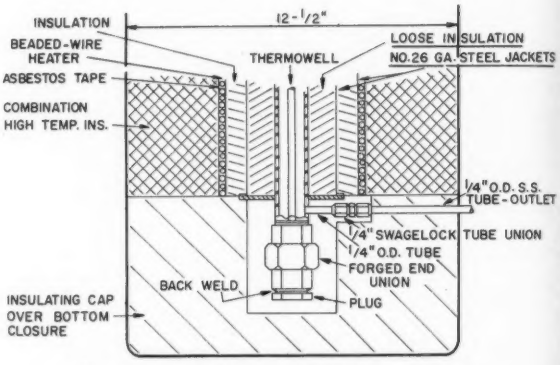

Figure 6—Insulation of adiabatic reactors.

reactor is controlled by a thermocouple immersed in the sandbath, connected to a controller set to hold a given temperature.

The adiabatic system, shown in Figure 5, consists of four reactors connected in series. The feed passes through an aluminum block preheater, and is heated in the transfer lines between the reactors. The line heaters are made up of two "Calrod" heating elements placed alongside the connecting pipe, with all three encased in a pipe filled with copper shot for better heat transfer.

To maintain adiabatic conditions, the reactors are well insulated, and heaters are also provided. These heaters supply only enough heat to prevent heat loss. Therefore, the temperature controllers are set to maintain a given temperature difference between the catalyst bed and the insulation, rather than to hold a given temperature. Usually the insulation is held at the same temperature as the catalyst bed, but occasionally may be higher to compensate for heat transfer along the reactor wall. As Figure 3 showed, there is a large temperature drop along the reactor. If a single heater were used to compensate the heat losses, too much heat would be supplied to the bottom part, and not enough to the top. Therefore, several heaters were provided, three for the first reactor, with the largest temperature drop, and two for each of the others, each with a separate differential temperature controller.

Figure 6 shows the method of insulating the adiabatic reactors. There are three layers of insulation. The inner layer is loose insulation, contained in a sheet metal jacket with a removable bottom cover plate. This insulation can be dumped, to remove the reactor. The middle layer of insulation is covered by another sheet metal jacket, which supports the wire heaters, and thermowells for measurement of the insulation temperature. The heaters are covered with a layer of asbestos tape, and a layer of high temperature insulation.

To change catalyst in the reactor, the insulating cap can be removed, and catalyst discharged by opening the end union. A similar closure at the top permits loading of catalyst without removal of the reactor from the system. The same closure is also used on the isothermal reactors. It permits a rapid change of the catalyst charge.

The reactors operate at rather severe conditions — up to 1200°F. and 1500 p.s.i.g. in an atmosphere consisting mainly of hydrogen. Type 347 stainless steel stabilized with columbium was chosen for the reactors, to avoid carbide precipitation, particularly when back welding fittings. Subsequent experience in other units has shown that carbide precipitation apparently is not serious, and type 316 stainless steel is suitable for this service. Another problem found with these conditions is to find a valve that will stay pressure tight for any length of time at high temperatures. As a result, the reactor outlet block valve had to be placed after the product cooler.

Of these two systems, the isothermal is simpler to operate, and has been used more frequently than the adiabatic system, since at equivalent temperature the nature of the reactor seems to have little effect. The maximum catalyst capacity is 2000 cc. for each system, and smaller loads can be obtained by dilution of the catalyst with inert material.

Feed and Product Recovery

The feed system is shown in Figure 7. It consists of three parts — a container for the feed, means of measuring the feed rate, and a way of getting the feed into the reactor. The critical point of this system is accurate measurement of the feed rate. There are two ways of measuring the feed rate — by weight or by volume. As finally adopted, the volume of feed is measured by determining the change in the level of a calibrated blowcase. Two pairs of blowcases are used, of 4 and 16 liter capacity, because of the range of required feed rates. Two diaphragm pumps driven by a common motor were chosen. One pump is normally used for feed rates up to about 1500 cc./hr., and the other is used at higher feed rates, up to 8000 cc./hr. While the pumps are of the constant displacement type, the flow has been

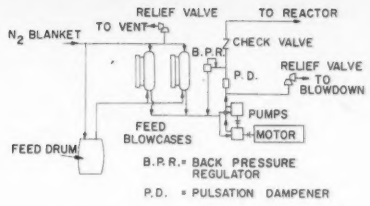

Figure 7—Feed system.

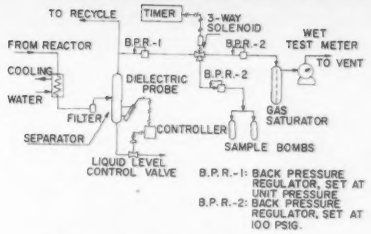

Figure 8—Make gas system.

too variable for their use as directly calibrated metering pumps. All the feed tanks are nitrogen blanketed and nitrogen pressure is used to transfer the feed from the drum to the blowcases.

If a gas feed is used, as for example once-through hydrogen, it is taken from a compressed cylinder, measured by a rotameter, and passed into the reactor. If recycle gas is used, it is taken from the separator, the flow rate is measured by a rotameter, it is compressed and returned to the reactor. To handle the wide range of recycle gas flow rates, a diaphragm compressor with three pumping heads driven by a common motor was chosen. The heads are connected in parallel, and can be bypassed to vary the capacity. Usually two heads are used, with the third bypassed, and used if one of the others fails.

Figure 8 shows the make gas system, including the gas sampling. The reaction products pass through the cooler into a high pressure separator. The liquid from the separator is withdrawn through a pneumatic control valve to the debutanizer. Some of the hydrogen rich gas is taken for recycle, and the rest is passed through two back pressure regulators in series. The first regulator lowers the gas pressure from operating pressure to 100 p.s.i.g. At this point, the gas enters a timer-controlled 3-way solenoid valve, which can pass the gas into sample bombs, or to a wet test meter. Each of these lines has another back pressure regulator, reducing the pressure to sample bomb pressure in the one case, and atmospheric pressure in the other. This arrangement permits a maximum sample bomb pressure of 100 p.s.i.g. The gas going to the wet test meter passes through a saturator, to prevent evaporation of water in the meter.

The debutanizer system is similar to the make gas system, but without a high-pressure back pressure regulator. The debutanizer consists of an electrically heated bottom section, and a steel pipe filled with stainless steel packing for the distillation column. The bottoms product is withdrawn through a control valve and cooler into a tared sample can.

Instrumentation and General

Type 316 stainless steel was used for all vessels operating at unit pressure, and stainless steel tubing was used for all the lines carrying feed and products, regardless of pressure. Stainless steel was used to provide high temperature strength and corrosion resistance, avoiding contamination of products. Carbon steel was used for low pressure service, such as feed blowcases and the stabilizer.

The capacity of the pilot plant has presented problems in the selection of control instruments. There is no serious problem with the temperature control. Conventional controllers can be used, with thermocouples as the sensing elements. The liquid levels in the separator and stabilizer are maintained by pneumatic control valves, using dielectric probes as the sensing elements, and pressures by back-pressure regulators. However, the flows have to be controlled manually by adjustment of feed pump for liquid flow and needle valves on rotameter inlets for gas flows.

Since the materials processed — hydrogen and hydrocarbons — can form explosive mixtures very readily, the entire pilot plant had to be of explosion-proof construction. Explosion-proof motors, solenoids and conduits for the electrical wiring were used, but the use of explosion-proof housings on the temperature controllers, electrical switches, timers and auto-transformers would have been very costly. Therefore, all these instruments were housed in two air-purged, fully enclosed panel boards. These boards are maintained under a positive air pressure at all times while the electrical circuits are energized. An explosivity meter is used to monitor the unit at selected points, and give warning if flammable vapors escape to the atmosphere.

All the high pressure sections are protected by safety valves connected to the vent, and several vent valves are provided for the other sections. All pressure vessels have been hydraulically pressure-tested to 8300 p.s.i.g. To shut down the unit, in the case of an emergency, such as fire, controls have been installed outside the building housing the pilot plant. These consist of two switches to cut off the electricity, and a blow-down tank and valves to dump the contents of the unit and purge it with nitrogen. While this installation has not been used for an actual emergency, it is used at intervals to shut down the pilot plant at the end of a run, to test the equipment and familiarize the operators.

When the actual assembly of the equipment was considered, there were two choices. One was to group all the vessels as closely as possible, to minimize the connecting tubing, and thus the hold-up in the unit. The other alternative, and the one actually chosen was to place all the vessels in a line, with easy access from both sides. The equipment is supported on "Unistrut" framing in two parallel structures. The front of the unit contains the feed and product recovery sections, all the pressure gauges, regulators and most of the controlling valves. The back section contains the reactors. While this assembly involves some long runs of piping, it has been compensated by the ease with which maintenance and addition of new equipment can be carried out.

Figure 9 shows an overall view of the pilot plant. The top of the isothermal reactor and sandbath can be seen in the centre of the right-hand window. The adiabatic reactors are located under the hood to the left of the isothermal reactor, at the back of the unit. The instrument panel in the middle contains most of the pressure gauges, control valves and pressure regulators.

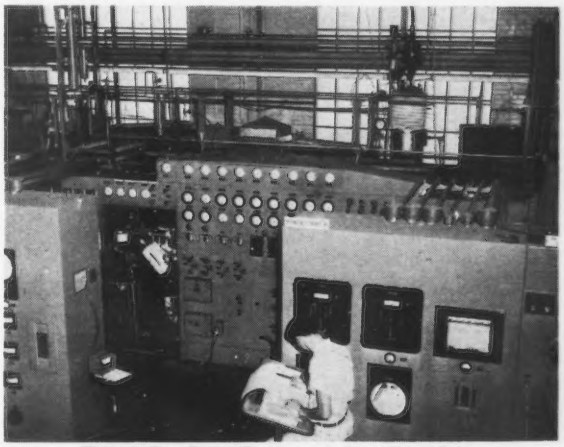

Figure 9—Overall view of the pilot plant.

The stabilizer level control sight-glass and probe can be seen to the left of this panel. In the foreground are the two air purged control panels housing the electrical equipment.

Material Balance

The catalyst performance is measured by the yield and quality of the desired products in this case of hydrogen and C_5+ reformate.

Usually there is one feed stream, and three product streams — make gas, debutanizer gas and stabilized reformate. The recycle gas does not appear in the material balance, but its composition is the same as that of the make gas. These streams are all measured, and the product streams are analyzed.

The composition of the make gas and debutanizer gas is determined by mass spectroscopy, and expressed in mole % or volume %. The composition of the stabilized reformate is measured by Vapor Liquid Partition Chromatography, and expressed in weight %. Other inspections of the reformate are the specific gravity, ASTM distillation curve, vapor pressure and octane number.

An IBM 650 digital computer is used to calculate the yields of the products, and the quality of the C_5+ reformate. The latter cannot be obtained by direct measurements, because there is not a perfect separation in the stabilizer.

Table 1 summarizes the input data to the computer. They consist of the analyses of the individual streams, their quantities, conditions at which they were measured and the operating conditions.

Table 2 shows the items calculated by the computer. The yield of the C_5+ reformate is calculated by adding the amount of pentanes and heavier in the make gas and debutanizer gas, and subtracting the amount of butanes in the reformate from the yield of stabilized reformate. It is checked by summing the individual component yields as calculated from the analyses. The 7 lb. RVP reformate is calculated by adding butanes to the C_5+ reformate.

The last item in this figure — the number of moles hydrocracked may require some explanation. Because of the large number of components in the naphtha, and the variety of possible reactions, it is very difficult, if not impossible, to calculate the extent of any one reaction. But every time a molecule is cracked, two molecules are produced. Therefore, the difference between the moles of hydrocarbons in the products and in the feed represents the net number of individual cracking steps, or C-C bonds broken.

Table 3 shows the basis of this calculation. The amount of aromatics formation can be expressed as the number of moles of hydrogen produced by adding the number of moles of hydrocracking to the measured production of hydrogen. The extent of naphthene dehydrogenation and paraffin dehydrocyclization cannot be differentiated by these data, but this can be done from analysis of feed and products.

The results of the individual calculations are printed out, and a summary table is also printed at the same time, suitable for inclusion in reports as shown in Tables 4 and 5.* The IBM program has been a real time-saver, cutting the computing time from about 6 man-hours/weight balance by hand calculation to a few minutes of machine time, thus speeding the evaluation of the experimental results.

Unit Performance

The pilot plant has been in service for about 3 years, and has performed quite satisfactorily. It has shown good reproducibility, and the results have agreed well with actual plant performance. Normally, the overall material balances have been within 98-102%, and frequently within 99-101%. The main problem in this respect has been the maintenance of leak-proof joints with frequent heating and cooling.

This pilot plant is not restricted to catalytic reforming, and could be used to study any reaction involving a fixed bed catalyst and liquid or gaseous feeds at elevated temperatures and pressures. Minor modifications may be required, such as steam tracing, if high melting point materials were used, such as tars or waxes.

★ ★ ★

TABLE 1

IBM 650 PROGRAM — INPUT DATA

1. Feed:
   - Volume and blowcase temperature
   - Gravity and distillation curve
2. Gases:
   - Wet test meter volume and temperature
   - Sample bomb volume and pressure
   - Analyses and atmospheric pressure
3. Reformate:
   - Weight of reformate
   - Gravity and distillation curve
   - Octane number and vapor pressure
   - Analysis
4. Miscellaneous:
   - Weight of catalyst
   - Hours in weight balance
   - Reactor pressure
   - Recycle gas rate

TABLE 2

IBM 650 PROGRAM — CALCULATED RESULTS

1. Weight Balance:
   - Molecular weight and wt. % on feed of the three streams
   - Material loss
2. Yield of Individual Components:
   - Wt. %, Vol. % and Mole % on feed
3. C_5 + Reformate:
   - Yield in Wt. %, Vol. % and Mole % on feed
   - Octane number, density and vapor pressure
4. 7 lb. RVP Reformate:
   - Yield — Vol. % on feed
   - Octane number
5. Miscellaneous:
   - Recycle gas rate — MSCF/B
   - Feed rate — W/W. hr.
   - Hydrogen partial pressure
   - Moles hydrocracked/100 moles feed

TABLE 3

METHOD FOR CALCULATION OF TOTAL HYDROGEN PRODUCED FROM AROMATIC FORMATION AND HYDROGEN CONSUMED IN HYDROCRACKING

	No. of Moles Increase	
A. Aromatic Formation	Hydrogen	Hydrocarbon
Naphthene → Aromatic + $3H_2$	3	0
Paraffin → Aromatic + $4H_2$	4	0
B. Hydrocracking		
Hydrocarbon + H_2 → 2 Hydrocarbons	−1	1

C. Data required from material balance

Feed	(a) Wt.	(b) Gravity	(c) ASTM distillation
Make gas	(a) Vol.	(b) M. Wt.	(c) H_2 content
Stabilizer gas	(a) Vol.	(b) M. Wt.	(c) H_2 content
As made reformate	(a) Wt.	(b) Gravity	(c) ASTM distillation

*Tables 4 and 5 of this paper have been deposited as Document No. 6877 with the ADI Auxiliary Publications Project, Photoduplication Service, Library of Congress, Washington 25, D.C. A copy may be obtained by citing the Document No. and by remitting $1.25 for photoprints, or $1.25 for 35 mm. microfilm. Advance payment is required. Make cheques or money orders payable to: Chief, Photoduplication Service, Library of Congress.

Contents of Volume 39

The Canadian Journal of Chemical Engineering

INDEX OF AUTHORS

INDEX OF PAPERS

* * *

The Canadian Journal of Chemical Engineering

Published by The Chemical Institute of Canada

GUIDE TO AUTHORS IN PREPARING THEIR DRAWINGS FOR REPRODUCTION

Original drawings or clean glossy photographs are acceptable. Drawings should be carefully made with India ink on white drawing paper or tracing linen. Letters (capitals preferred) and numerals should be neatly made, with a stencil or lettering set. No grid lines should appear, but rather mark-offs along the scales. Whenever possible, drawings should be about 10 inches wide by 8 inches deep, although different sizes are also acceptable when the ordinary size is awkward to produce. In order to reduce the number of engravings required, it is advisable to group, when possible, two or more drawings.

In most cases, engravings are made either 3¼ or 7 inches wide. If all curves, dots, letters and numerals are to reproduce well they should be made of thick enough lines to take into account the reductions in size which usually take place when engravings are made. As a guide, one should aim at having letters or numerals no smaller than 1/16th of an inch tall, after reproduction. As an author usually knows whether a particular drawing will reduce to 3¼ or 7 inches in width, he is aware of the reduction factor applicable and should use the appropriate template and pen combination. For a reduction factor of 3, for instance, a Leroy template No. 200 and pen No. 3 should be used.

Here are actual examples of satisfactory reductions of original drawings made to these standard widths.

Portion of Original Drawing—Actual Size
22″ wide x 9″ deep

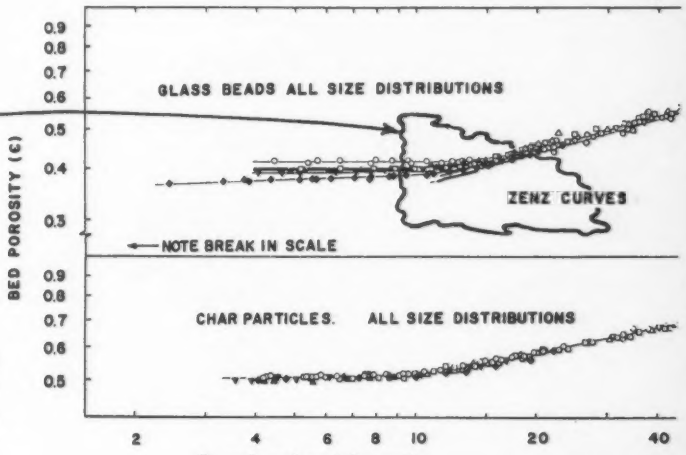

It reduced satisfactorily to make an engraving 7″ wide x 2 13/16″ deep, part of which is shown here.

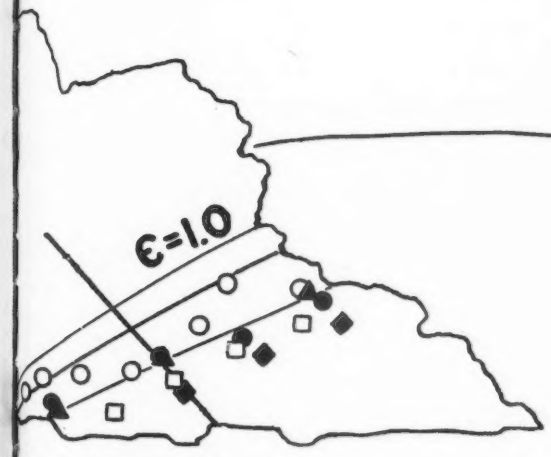

Portion of Original Drawing—Actual Size
10″ wide x 8″ deep

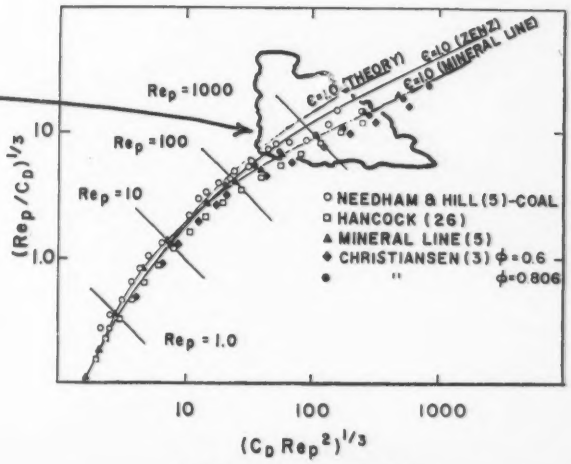

It reduced satisfactorily to make this engraving 3¼″ wide x 2⅝″ deep.

CALL FOR PAPERS

MAY 27-30, 1962

At the Annual Conference of The Chemical Institute of Canada, Edmonton, Alberta, the Chemical Engineering Division is planning five special sessions. Submit titles of proposed papers to D. B. Robinson, head, department of chemical and petroleum engineering, University of Alberta, Edmonton, Alberta.

C.I

Sunday,

8.00 p.r

Monday

8.30 a.r
9.15 a.r

9.20 a.r
9.40 a.r

10.05 a.r

10.40 a.r
10.50 a.r

11.25 a.r

12.15 p.r
2.00 p.r

2.50 p.r
3.00 p.r

5.00 p.r
6.30 p.r

.....

For comp
and plant
p. 106.

C.I.C. Canadian Chemical Engineering Conference

Chateau Frontenac
Quebec, Que.

November 7, 8, 9, 1960

Sunday, November 6

8.00 p.m.-10.00 p.m. Registration and Mixer.

Monday, November 7

8.30 a.m. Registration.

9.15 a.m. Welcome to Quebec by General Conference Chairman, P. Grenier, Laval University, Quebec, Que.

CHEMICAL ENGINEERING AND COMPUTERS SYMPOSIUM

Chairman: P. H. Sterling, Canadian Industries Limited, McMasterville, Que.

9.20 a.m. Introductory Remarks—P. H. Sterling.

9.40 a.m. Film—An Introduction to Electronic Analog Computation in Chemical Engineering, produced by A. I. Johnson and W. G. MacElhinney, University of Toronto, Toronto, Ont.

10.05 a.m. Application of a Bi-variant Function Generator to an Analogue Solution of a Reactor Design Problem—H. Kubota, National Research Council, Ottawa, Ont.

10.40 a.m. Break.

10.50 a.m. Some Aspects of the Design of Heat Exchangers on a Digital Computer — G. A. Sullivan and N. E. Cooke, Canadian Industries Limited, Montreal, Que.

11.25 a.m. Using the Arrhenius Function in Analogue Computation—P. H. Sterling and D. C. West, Canadian Industries Limited, McMasterville, Que.

12.15 p.m. Luncheon.

2.00 p.m. Chemical Engineers and Computers—Keynote Speaker: T. J. Williams, Monsanto Chemical Company, St. Louis, Mo.

2.50 p.m. Break.

3.00 p.m. Panel Discussion: Computers and Control.
Moderator: S. W. Churchill, University of Michigan, Ann Arbor, Mich.
Panelists: T. J. Williams, Monsanto Chemical Company, St. Louis, Mo.
J. H. Milsum, National Research Council, Ottawa, Ont.
J. M. Andrews, Computers Systems Inc., Trenton, N.J.

5.00 p.m. Annual General Meeting.

6.30 p.m. Oyster Party.

For complete details of the program including abstracts and plant tours, see *Chemistry in Canada*, September issue, p. 106.

Tuesday, November 8

EXPLOSIVES TECHNOLOGY SYMPOSIUM

Chairman: L. A. Dickinson, C.A.R.D.E., Quebec

9.00 a.m. Solid Rocket Propellants — The Control of Oxidizer Particle Size — B. J. Holsgrove, C.A.R.D.E., Valcartier, Que.

9.35 a.m. Safety of Materials of Construction used in Explosives Manufacture — F. van Zeggeren, Canadian Industries Limited, McMasterville, Que.

10.10 a.m. Solid Rocket Propellants — An Advanced Vacuum Processing System—B. J. Holsgrove, C.A.R.D.E., Valcartier, Que.

10.40 a.m. Break.

10.50 a.m. Microwave Hazards Associated with Commercial Electric Blasting Caps—J. A. Darling and D. A. B. Stevenson, Dept. of Mines and Technical Surveys, Ottawa, Ont.

11.25 a.m. Unusual Applications of Commercial Explosives—R. F. Knott and G. G. Goyer, Canadian Industries Limited, McMasterville, Que.

GENERAL PAPERS SESSION

Chairman: W. J. M. Douglas, McGill University

9.00 a.m. Reactions in a Fluidized Coke Bed with Self-resistive Electric Heating — H. S. Johnson, Shawinigan Chemicals Limited, Shawinigan, Que.

9.30 a.m. The Electrical Properties of Fluidized Coke and Graphite Particles—E. A. Harvey and W. Graham, National Research Council, Ottawa, Ont.

10.00 a.m. Use of the Nagiev Method for Calculating Material Balances in Recycle Systems—P. M. Reilly and J. J. Klauke, Polymer Corporation, Sarnia, Ont.

10.30 a.m. Break.

10.40 a.m. Optimum Performance of Combined Flow Reactors under Adiabatic Conditions—A. Cholette and J. L. Blanchet, Laval University, Quebec, Que.

11.10 a.m. Effect of Various Factors on Mixing Efficiency in Continuous Flow Systems—L. Cloutier and A. Cholette, Laval University, Quebec, Que.

11.35 a.m. Highway Transportation of Liquid Ethylene—C. P. Warkentin, Imperial Oil Ltd., Sarnia, Ont.

12.15 p.m. Organized luncheon options for small groups.

2.00 p.m. Plant tours.
Tour A.: Canadian Armament Research and Development Establishment (C.A.R.D.E.).
Tour B: Quebec Department of Mines Pilot Plant and Lignosol Chemicals Limited.

6.00 p.m. Cocktail hour.

7.00 p.m. Annual Dinner.
Guest Speaker:

(over)

Wednesday, November 9

9.00 a.m. Chemical Engineering Education Subcommittee.

Chairman: A. I. Johnson, University of Toronto, Toronto, Ont.

Topic: Graduate Study of Chemical Engineering in Canada.

11.00 a.m. R. S. Jane Award Lecture.

Chairman: J. R. Donald, J. T. Donald & Co. Limited, Montreal, Que.

Award Lecture: E. R. Rowzee, Polymer Corporation, Sarnia, Ont.

12.15 p.m. Organized luncheon options for small groups.

PROCESS INVESTIGATIONS SESSION

Chairman: E. Christensen, Polymer Corporation, Sarnia, Ont.

2.00 p.m. Disposal of Hydrogen Sulphide from an Ammonia Plant Off-Gas—N. E. Cooke, H. Ho, R. H. Dick and R. Wood, Canadian Industries Limited, Montreal, Que.

2.35 p.m. Design and Operation of a High Pressure Reforming Pilot Plant, J. A. Bichard, J. Bumbulis, and R. M. Butler, Imperial Oil Ltd., Sarnia, Ont.

3.10 p.m. Effects of Water Vapor Content on the Inflammable Limits of Ammonia-Oxygen-Nitrogen Mixtures—W. J. DeCoursey and N. Yoshida, Sherritt Gordon Mines Limited, Fort Saskatchewan, Alta.

3.45 p.m. Break.

3.55 p.m. The Disposal of the By-product Carbon from an Oil Fired Texaco Generator in a Spray Furnace — N. E. Cooke, Canadian Industries Limited, Montreal, Que.

4.30 p.m. Electrical Power Supplies for Spacecraft—V. Srepel, Northrup Corp., Hawthorne, California.

FLUID MECHANICS—HEAT TRANSFER SESSION

Chairman: W. H. Gauvin, Pulp and Paper Research Institute of Canada and McGill University, Montreal, Que.

2.00 p.m. Heat Transfer to a Surface Reacting Fluid in Turbulent Flow—R. I. Rothenburg and J. M. Smith, Northwestern University, Evanston, Illinois.

2.30 p.m. Heat Transfer to High Quality Stream-Water Mixtures Flowing in a Horizontal Rectangular Duct—E. J. Davis and M. M. David, University of Washington, Seattle, Wash.

3.00 p.m. An Analysis of Spray Evaporation in a High-Temperature Environment — T. W. Hoffman and W. H. Gauvin, McMaster University, Hamilton, Ont., and McGill University, Montreal, Que.

3.30 p.m. Break.

3.40 p.m. Viscous Flow Around Fluid Spheres at Intermediate Reynolds Numbers — A. E. Hamielec and A. I. Johnson, University of Toronto, Toronto, Ont.

4.10 p.m. A Study of Aggregative Fluidization — D. B. Robinson and G. Davies, University of Alberta, Edmonton, Alta.

4.35 p.m. Coalescence of Liquid Drops — A. R. Smith, J. E. Casell, P. P. Larson and S. D. Cavers, University of British Columbia, Vancouver, B.C.

* * *

CHEMICAL ENGINEERS ESTABLISH AWARDS

Commencing this autumn, the Chemical Engineering Division of the C.I.C. will present two awards–the first for the best paper published in *The Canadian Journal of Chemical Engineering* during the year immediately preceding the Fall Conference, and the second for the best oral presentation of a technical paper at the C.I.C. Annual Conference (Chemical Engineering Session) and at the Fall Conference of the Chemical Engineering Division. The awards will take the form of an engraved certificate and silver tankard with the proper inscription.

For the first award, the winning paper will be selected from the October '59 issue through to August '60 issue of C.J.Ch.E. No restrictions are placed on the nature of the paper (whether of a research, industrial development or review type), nor on the nationality, and affiliation of the author or authors. In case of joint authorship, each of the authors would receive identical certificates and tankards. Three judges have been set to represent academic circles, industry, and government, so as to have a fair representation of the three major areas of chemical engineering activity in Canada.

For the second award, on oral presentation, the program chairman is to appoint three judges to rate the various papers, if only single sessions are held. These judges are to represent industry, academic circles, and government, or alternately research and development organizations which do not properly fit in the first two categories. A uniform method of scoring will be used and the winner will be announced at the end of the meeting. Formal presentation will then be made at the next C.I.C. Conference. If simultaneous sessions are held it will be necessary to appoint one or more judges in order that all sessions will be screened carefully.